Copyright is owned by the Author of the thesis. Permission is given for a copy to be downloaded by an individual for the purpose of research and private study only. The thesis may not be reproduced elsewhere without the permission of the Author.

Rate Controlling Mechanisms in Atmospheric Freeze Drying

A thesis presented in partial fulfilment of the

requirements for the degree of

Doctor of Philosophy

in

Chemical and Bioprocess Engineering

at Massey University, Manawatū, New Zealand.

MASSEY UNIVERSITY
TE KUNENGA KI PŪREHUROA
UNIVERSITY OF NEW ZEALAND

Merit Mathew

2023

[intentionally blank]

Abstract

Atmospheric freeze drying (AFD) can be considered a cost-effective alternative to vacuum freeze drying (VFD) but the very slow drying rate associated with it limits industrial scale adoption. Nevertheless, there are applications, particularly with thin sections such as sliced fruit or leaves, for which hops is an example, where the rate of AFD is relatively high. Therefore, it is important to understand the rate-controlling mechanisms in AFD and how it is affected by the structure of the fruit or leaf. Such understanding will help identify the bottlenecks of the process and thus the steps that may be taken to overcome them. This project has developed a mathematical model for AFD by considering the intrinsic material properties and the theoretical principles of heat and mass transfer. This could help the end-users to run simulations of AFD for different products and arrive at the best drying strategies to achieve faster drying rates before doing time-consuming and expensive experiments.

In this work, hops are considered as the model system for the model development. The study needed high-quality experimental data for continuous in-situ weight loss measurements during AFD and there was a lack of such data in the literature reviewed. To deliver this, part of the project has developed a new experimental apparatus. The experimental apparatus developed is capable of continuous weight-loss measurement and data logging temperature and RH of the air in the drying chamber. Temporal weight-loss trial data are used to fit parameters and predict the drying rate and product weight loss.

During the study it was found that AFD of hops is a mass transfer limited process. The drying rate was found to increase with process temperature and the adsorbent to hops ratio. Air circulation also helped in increasing the drying rate. The one-dimensional model developed to simulate AFD of hops was able to predict the drying behaviour based on the process parameters and the fitting factors for the hops.

Ice sublimation was also studied in this project, based on the hypothesis that the AFD of hops is a type of pure ice sublimation with an additional layer of resistance to mass transfer. This hypothesis was found to be true for the present case and the model was development based on this.

Acknowledgements

I would like to first acknowledge my supervisors Prof. Richard Archer, Prof. Jim Jones, and Dr. Qun Chen for seeing a potential in me to do this doctoral study. I am really grateful for the support they gave me throughout this project. Their mentoring and guidance helped me not only complete this work but also helped me evolve into a better researcher and instil confidence in me to face my research career ahead with my new research role in the industry. I still remember the evening I first landed in Palmerston North, when Prof. Richard Archer had come to pick me up at the airport; I was unsure of my decision and uncertain of my future, but the past three and a half years have been a wonderful time and I thank them for being my guides. I thank them for the emotional support when I required it, as it was really hard not being able to visit family back home due to covid travel restrictions, there was the financial strain of living on the stipend, the visa requirements, etc, but they were always available to have a chat and I greatly appreciate their open door policy which always made me felt welcome and cared for. I would miss the regular meetings and the walk-ins but would love to continue being in touch throughout my life.

I thank the FIET programme from MBIE which sponsored my research work and made this doctoral study possible for me and to come to New Zealand. I would like to thank Prof. John Bronlund for teaching me a structured way to develop a model which greatly helped me in developing the model in the current work.

I would like to acknowledge the work done by the engineering and electronics workshop technicians in helping me fabricate the experimental system, the lab managers, and the IT team for helping me out during the project when required.

I would like to thank my parents and brother and for the love and care they gave me and the support they gave throughout my life and during the PhD. I would always be indebted to my parents for all the sacrifices they made and for my upbringing that has shaped me into what I am today. I thank my in-laws and siblings for the support when I made my decision to go for and during the project.

I would like to thank my wife who has been a constant believer in me and supported and motivated me throughout the PhD. Her support helped me get through some hard times and I am thankful and indebted to her for being there with me throughout journey and for the sacrifices she made.

Last but not the least, I thank the Almighty for being the source of my hope.

Table of Contents

Abstract i

Acknowledgements ii

Table of Contents iv

List of Figures ix

List of Tables xiv

List of Symbols xv

Chapter 1 Introduction 1

1.1 Rationale 1

1.2 Objectives of the study 4

1.3 Thesis Overview 5

Chapter 2 Literature Review 6

2.1 Introduction 6

2.2 Freeze drying 7

2.3 AFD of biological materials 12

2.4 Rate limiting mechanism and debottlenecking 13

2.5 Current models for AFD 16

2.6 Experimental Set-up 19

2.7 Research gaps 20

Chapter 3 Materials and Methods 23

3.1 Materials 23

3.1.1 Hops 23

3.1.2 Ice 23

3.1.3 Silica gel 24

3.2 Methods 24

3.2.1 Measurement of weight loss during AFD 24

3.2.2 Measurement of temperature and RH of air 24
3.2.3 Measurement of temperature of ice 25
3.2.4 Measurement of air velocity 25
3.2.5 Measurement of RH and temperature of air near hops 25
3.2.6 Area of Hops 26
3.2.7 The thickness of hops petals 26
3.2.8 The density of hops – pycnometer 26
3.2.9 Moisture content hops 26
3.2.10 Water activity of hops 27
Chapter 4 Development of Experiment Apparatus 28
4.1 Introduction 28
4.2 Maintaining freezing conditions 28
4.3 Weight loss measurement 29
4.4 Air RH and temperature measurement 31
4.5 Design and sizing of the two-box unit 31
Chapter 5 Model Development 35
5.1 Ice sublimation in the AFD apparatus 36
5.1.1 Assumptions and Parameters 39
5.2 AFD of Hops in the AFD apparatus 46
5.2.1 Assumptions: 50
5.3 Conclusions 57
Chapter 6 Ice Experiment System and Discussion 58
6.1 Introduction 58
6.2 Experimental procedure 58
6.2.1 Constant ice surface area experiments 61
6.2.1.1 Case I 61

6.2.1.2 Case II 62
6.2.2 Ice temperature 62
6.2.2.1 Case III 62
6.2.3 Changing ice surface area 62
6.2.3.1 Case IV 62
6.3 Results & discussion 63
6.3.1 Ice sublimation experiment for constant surface area 63
6.3.1.1 Weight loss by sublimation 63
6.3.1.2 Air humidity in the AFD apparatus drying chamber 67
6.3.1.3 Air temperature in the AFD apparatus drying chamber 70
6.3.2 Comparing the ice and air temperatures during sublimation 71
6.3.3 Ice sublimation experiment for changing surface area 74
6.3.3.1 Weight loss by sublimation 74
6.3.3.2 Sublimation flux and rate 75
6.4 Comparison of experiment results - model fitting & predictions 77
6.4.1 Weight loss during sublimation 78
6.4.2 Air RH during sublimation 79
6.4.3 Silica gel moisture content during sublimation 79
6.5 Conclusions 80
Chapter 7 Hops Experiment System and Discussion 81
7.1 Introduction 81
7.2 Experiment procedure 81
7.2.1 Effect of temperature on AFD of hops kinetics 82
7.2.1.1 Case I 83
7.2.1.2 Case II 83
7.2.2 Effect of ratio of mass of the adsorbent to hops on AFD kinetics 83

7.2.2.1 Case III 83
7.2.3 Effect of air circulation on AFD kinetics 84
7.2.3.1 Case IV 84
7.3 Results & discussion 84
7.3.1 Effect of temperature on AFD of hops kinetics 84
7.3.1.1 Air temperature in the AFD apparatus drying chamber 84
7.3.1.2 Weight loss by sublimation 85
7.3.1.3 Air humidity in the AFD apparatus drying chamber 86
7.3.1.4 AFD hops sublimation flux 87
7.3.2 Effect of ratio of mass of the adsorbent to hops on AFD kinetics 89
7.3.2.1 Weight loss by sublimation 89
7.3.2.2 Air humidity in the AFD apparatus drying chamber 89
7.3.2.3 AFD hops sublimation flux 90
7.3.3 Effect of air circulation on AFD of hops kinetics 92
7.3.3.1 Weight loss by sublimation 92
7.3.3.2 Air humidity in the AFD apparatus drying chamber 92
7.3.3.3 AFD hops sublimation flux 93
7.4 Comparison of experiment results with the model predictions 94
7.4.1 Calculation of fitting parameters – RF_I & RF_II 94
7.4.1.1 Weight loss during sublimation 94
7.4.1.2 Air RH during sublimation 95
7.4.2 AFD of Hops – Case II 96
7.4.2.1 Weight loss during sublimation 96
7.4.2.2 Air RH during sublimation 97
7.4.3 AFD of Hops – Case I 98
7.4.3.1 Weight loss during sublimation 98

7.4.3.2 Air RH during sublimation 98
7.4.4 AFD of Hops – Case III 99
7.4.4.1 Weight loss during sublimation 99
7.4.4.2 Air RH during sublimation 100
7.4.5 AFD of Hops – Case IV 101
7.4.5.1 Weight loss during sublimation 101
7.4.5.2 Air RH during sublimation 101
7.5 Conclusions 102
Chapter 8 Overall Discussion and Future Work 104
8.1 Overall conclusions 104
8.2 Suggested future works 106
References 107
A. Appendices 115
I. Derivation for the ODE for heat balance in Ice 115
II. Fitting of constants for the model 116
Fitting of the initial boundary layer thickness for the ice sublimation – case I 116
Fitting of the RF_I and RF_II for the AFD of hops – case 0 118
III. Biot Number calculation 120
IV. MATLAB codes -Pure ice sublimation – Case II 120
V. MATLAB codes -AFD Hops – Case II 125

List of Figures

Figure 2-1 Mass transfer steps and the partial pressure gradient 9

Figure 2-2 Heat transfer steps and the temperature gradient 10

Figure 3-1 Hops sample used during the AFD experiment 23

Figure 3-2 Ice cube holder with ice 24

Figure 4-1 Side view of the experiment set-up with the polycarbonate set-up inside the chest freezer (376L, Fisher & Paykel) 29

Figure 4-2 Front view of the experiment set-up 30

Figure 4-3 Side view of the experiment set-up 30

Figure 4-4 Top view of the experiment set-up top box 30

Figure 4-5 Supressed view of the experiment set-up 32

Figure 4-6 Dimetric view of the experiment set-up 32

Figure 4-7 Fabricated two box unit for the experiment 33

Figure 4-8 Exploded view of the experiment set-up 34

Figure 5-1 Diagram of the ice sublimation in the AFD drying chamber 36

Figure 5-2 Diagram of the ice sublimation in the AFD drying chamber with resistances 39

Figure 5-3 Diagram of the AFD of hops in the AFD drying chamber. 47

Figure 5-4 Diagram of the AFD of hops in the AFD drying chamber with resistances. 50

Figure 6-1 Ice in the 3D-printed ice cube holder with iButton 59

Figure 6-2 Constant ice surface experiments- case I & case II 61

Figure 6-3 Changing ice surface area experiment- case IV 63

Figure 6-4 Weight loss comparison during the ice sublimation – no air circulation region -case I (ice surface deeper inside the 3D printed ice holder) & case II (ice surface near the outer edge of the 3D printed ice holder) 64

Figure 6-5 Sublimation flux comparison during the ice sublimation – no air circulation region -case I (ice surface deeper inside the 3D printed ice holder) & case II (ice surface near the outer edge of the 3D printed ice holder) 64

Figure 6-6 Weight loss comparison during the ice sublimation experiments–case I (no air circulation) & case II (no air circulation for 120 hrs and then with air circulation) 65

Figure 6-7 Sublimation flux & Moving average of ice sublimation flux for experiment-case II (no air circulation for 120 hrs and then with air circulation) 65

Figure 6-8 Ice sublimation flux comparison for same 120 hours duration– plot of mass transfer path length in the 3D printed holder for -case I (ice surface deeper inside the 3D printed ice holder) & no air circulation region -case II (ice surface near the outer edge of the 3D printed ice holder) 66

Figure 6-9 Ice sublimation flux comparison for same pathlength change– plot of mass transfer path length in the 3D printed holder for -case I (ice surface deeper inside the 3D printed ice holder) & no air circulation region -case II (ice surface near the outer edge of the 3D printed ice holder) 67

Figure 6-10 Air RH in the drying chamber of the AFD apparatus - case I (no air circulation) & case II (no air circulation for 120 hrs and then with air circulation) 68

Figure 6-11 Pseudo equilibrium adsorption curve for case I and case II (Moisture content in air versus moisture content in silica gel) 69

Figure 6-12 Air temperature in the drying chamber of the AFD apparatus- case I (no air circulation) & case II (no air circulation for 120 hrs and then with air circulation) 70

Figure 6-13 Temperature of ice and air during the experiment – case III 71

Figure 6-14 Temperature of ice and air - No air circulation period – case II 71

Figure 6-15 Temperature of ice and air - full experiment - case II 72

Figure 6-16 Temperature of ice versus air for case II for the first 200 hours without air circulation. The dashed line is the x=y line. 73

Figure 6-17 Comparison of weight loss by sublimation - case IV (changing area) & case I (constant area) 74

Figure 6-18 Rate of weight loss by sublimation – case IV (changing area) & case I (constant area) 75

Figure 6-19 Ice sublimation flux comparison – case IV (changing area) & case I (constant area) 76

Figure 6-20 Ice sublimation flux comparison - mass of ice remaining in ice holder – case IV (changing area) & case I (constant area) 76

Figure 6-21 Comparison of weight loss during sublimation – Model prediction (no air circulation for 120 hrs and then with air circulation) vs case II (no air circulation for 120 hrs and then with air circulation) 78

Figure 6-22 Comparison of Air RH (%) - Model with experiment 79

Figure 6-23 Moisture content increase in the silica gel 80

Figure 7-1 Air temperature in the drying chamber of the AFD apparatus - AFD of Hops - Exp VI – case I (-15 °C) & case II (-12 °C) 85

Figure 7-2 Weight loss comparison during AFD of Hops – case I (-15 °C) & case II (-12 °C) 86

Figure 7-3 Comparison of air RH in the drying chamber of AFD apparatus– case I (-15 °C) & case II (-12 °C) 86

Figure 7-4 AFD hops sublimation flux comparison - AFD of Hops– case I (-15 °C) & case II (-12 °C) 87

Figure 7-5 AFD hops sublimation flux comparison based on ice content remaining- AFD of Hops- case I (-15 °C) & case II (-12 °C) 88

Figure 7-6 Specific weight loss during AFD of Hops - case III (-15 °C, High adsorbent ratio), I (-15 °C, Low adsorbent ratio) & II (-12 °C, Low adsorbent ratio). Vertical axis is plotted in grams of ice/gram of dry matter. 89

Figure 7-7 Air RH in the drying chamber of AFD apparatus- case III (-15 °C, High adsorbent ratio) & I (-15 °C, Low adsorbent ratio) 90

Figure 7-8 AFD hops sublimation flux comparison - case III (-15 °C, High adsorbent ratio), I (-15 °C, Low adsorbent ratio) & II (-12 °C, Low adsorbent ratio) 91

Figure 7-9 AFD hops sublimation flux comparison - case III (-15 °C, High adsorbent ratio), I (-15 °C, Low adsorbent ratio) & II (-12 °C, Low adsorbent ratio) 91

Figure 7-10 Weight loss during AFD of Hops - case IV (-12 °C, Fan ON)& case II (-12 °C, Fan OFF)..... 92

Figure 7-11 Air RH in the drying chamber of AFD apparatus- case IV (-12 °C, Fan ON)& case II (-12 °C, Fan OFF)..... 93

Figure 7-12 AFD hops sublimation flux comparison - case IV & II..... 94

Figure 7-13 Comparison of weight loss during sublimation – AFD Hops case 0 (-12 °C, Fan OFF, Low adsorbent ratio)..... 95

Figure 7-14 Comparison of Air RH (%) - Model vs AFD Hops case 0 (-12 °C, Fan OFF, Low adsorbent ratio)..... 95

Figure 7-15 Comparison of weight loss during sublimation – AFD Hops case II (-12 °C, Fan OFF, Low adsorbent ratio)..... 97

Figure 7-16 Comparison of Air RH (%) - Model vs AFD Hops case II (-12 °C, Fan OFF, Low adsorbent ratio)..... 97

Figure 7-17 Comparison of weight loss during sublimation – AFD Hops case I (-15 °C, Fan OFF, Low adsorbent ratio)..... 98

Figure 7-18 Comparison of Air RH (%) - Model vs AFD Hops case I (-15 °C, Fan OFF, Low adsorbent ratio)..... 99

Figure 7-19 Comparison of weight loss during sublimation – AFD Hops case III (-15 °C, Fan OFF, High adsorbent ratio)..... 100

Figure 7-20 Comparison of Air RH (%) - Model vs AFD Hops case III (-15 °C, Fan OFF, High adsorbent ratio)..... 100

Figure 7-21 Comparison of weight loss during sublimation – AFD Hops case IV (-12 °C, Fan ON, Low adsorbent ratio)..... 101

Figure 7-22 Comparison of Air RH (%) - Model vs AFD Hops case IV (-12 °C, Fan ON, Low adsorbent ratio)..... 102

Figure A-1 Fitted value for the boundary layer thickness – case I..... 117

Figure A-2 Fitted value for the boundary layer thickness – case I (+2%)..... 117

Figure A-3 Fitted value for the boundary layer thickness – case I (-2%)..... 118

Figure A-4 Fitted value for RF_I and RF_II – case 0..... 119

Figure A-5 Fitted value for RF_I and RF_II – case 0 (+2%).....119

Figure A-6 Fitted value for RF_I and RF_II – case 0 (-2%).....120

List of Tables

Table 4-1 Bill of materials of the experiment set-up 34

Table 5-1 Material thermal properties 38

Table 5-2 System nomenclature with units and parameter classes 40

Table 5-3 Defining the number of equations 42

Table 5-4 List of ODEs..... 42

Table 5-5 List of constitutive equations for ice 43

Table 5-6 Initial conditions 46

Table 5-7 List of system inputs..... 46

Table 5-8 System nomenclature with units and parameter classes - AFD of hops..... 51

Table 5-9 Defining the number of equations. 52

Table 5-10 List of ODEs – AFD of Hops..... 53

Table 5-11 List of constitutive equations for hops (cf Table 5-5 for ice)..... 53

Table 5-12 Initial conditions 56

Table 5-13 List of system inputs for AFD of hops..... 56

Table 6-1 Ice sublimation experiments 60

Table 7-1 Hops AFD experiments 82

Table 7-2 Resistance factor values for model prediction and fitting..... 96

Table A-1 Biot number for ice and hops 120

List of Symbols

Symbol	Description	Units
A_{ice}	Area of ice in hops for sublimation	m^2
b_{box}	width of box	m
d_{cell}	Average diameter of a cell	m
$D_{H2O\text{-}air}$	Effective diffusivity of water vapour of air	m^2/s
$D_{H2O\text{-}eff\text{-}silicagel}$	Effective diffusivity of water vapour in silica gel	m^2/s
$D_{H2O\text{-}silicagel}$	Diffusivity of water vapour in silica gel	m^2/s
d_{ice}	Diameter of ice crystal	m
$d_{ice,o}$	Initial diameter of ice crystal	m
$K_{MT\text{-}silicagel}$	Mass transfer coefficient of H2O for silica gel	m/s
l_{box}	Length of box	m
$l_{hops\text{-}air}$	Boundary layer thickness for hops	m
$l_{hops\text{-}cell}$	Path length for diffusion in cell	m
$l_{hops\text{-}inter}$	Average intercellular path length	m
$l_{ice\text{-}air}$	Effective path length for diffusion in Ice sublimation	m
$l_{ice\text{-}air,o}$	Initial effective path length for diffusion in Ice sublimation	m
$M_{hops\text{-}dry}$	Mass of hops dry (dry)	kg
M_{ice}	Mass of ice in hops	kg
$M_{ice,o}$	Initial mass of ice in hops	kg
$M_{silicagel}$	Mass of silica gel (dry)	kg
N_{ice}	Number of ice crystals	
P_{air}	Vapour pressure of H2O in air	Pa
$P_{air\text{-}sat}$	Saturated vapour pressure of H2O in air	Pa
P_{ice}	Vapour pressure of ice near the ice surface in hops	Pa
P_{total}	Total system pressure	Pa
$r_{silicagel}$	Average radius of silica gel	m
RF_1	Resistance factor for resistance in cell	
RF_2	Resistance factor for resistance in intercellular region	
RH_{air}	RH of air	Pa
t	Time	s
T_{air}	Temperature of air	K
T_{hops}	Temperature of hops	K
$T_{silicagel}$	Temperature of silica gel	K
u_{air}	Air velocity	m/s
V_{box}	Volume of air in box	m^3

V_{cell}	Volume of a cell	m^3
V_{hops}	Volume of hops	m^3
V_{ice}	Total volume of ice in hops	m^3
$V_{ice,o}$	Volume of ice	m^3
X_{air}	Moisture content in air (dry basis)	kg/kg
$X_{air,o}$	Initial moisture content in air (dry basis)	kg/kg
X_{hops}	Moisture content in hops (dry basis)	kg/kg
$X_{hops,o}$	Initial moisture content in hops (dry basis)	kg/kg
X_{ice}	Moisture content at ice surface (dry basis)	kg/kg
$X_{silicagel}$	Moisture content in silica gel (dry basis)	kg/kg
$X_{silicagel,equil}$	Moisture content of silica gel in equilibrium with air (dry basis)	kg/kg
$X_{silicagel,o}$	Initial moisture content silica gel (dry basis)	kg/kg
z_{box}	height of box	m

Symbol	Description	Units
ρ_{air}	Density of air	kg/m^3
$\rho_{hops\text{-}dry}$	Density of dry hops	kg/m^3
ρ_{ice}	density of ice	kg/m^3

Chapter 1 Introduction

1.1 Rationale

Atmospheric freeze drying (AFD) has many features in common with the better-known vacuum freeze drying (VFD). Both remove moisture from heat sensitive products, or those that assume an undesirable shrivelled texture if dried at higher temperatures (Rahman & Mujumdar, 2012), where the shrivelled texture is due to the surface tension of the evaporating water interface drawing the product in upon itself. The advantage with both AFD and VFD is that shrinkage can be avoided by first freezing the product, then subliming the water away leaving the original structure intact. However, in all other respects the two processes are quite different.

VFD is an energy-intensive process due to the use of a vacuum, the supply of heat energy required for sublimation, the cooling required in the freeze condenser, and the heat for the subsequent melting of the ice from the condenser coil. Furthermore, vacuum pumps are precision-engineered devices with close tolerances and so have a high capital cost. In operation, VFD is also generally a batch-wise process which takes time. These cost and time factors mean that VFD is used mostly for high-value products like pharmaceuticals and other high value food products where the capital cost and operating costs of the drying unit are economical (Claussen et al., 2007; Rahman & Mujumdar, 2012). In New Zealand, some examples of vacuum freeze-dried products are mussels used as an intermediate step before LYPRINOL® extraction, tramping meals, specialty product fruits such as strawberries, and some premium pet food treats.

In contrast, atmospheric freeze drying (AFD) does not require the capital or operating costs of the vacuum and condenser. Some of the main advantages of AFD are the low initial investment cost, its ability to be designed as a continuous system thus increasing productivity and lowering operating cost and, more recently, the possibility of incorporating heat pumps and other heating sources to increase drying rates (Claussen et al., 2007). Furthermore, the product never experiences temperatures greater than the inlet air temperature, *ca*. -5 ^{O}C, because air is the heat transfer medium between the cooling surface and the product surface. It is equally as effective at moisture removal with a lower energy requirement of 5690 kJ/kg to sublime 1 kg of ice in a product with 3 kg water/kg dry matter compared to 7330 kJ/kg for VFD (Rahman & Mujumdar, 2012). Written the

other way around, the moisture extraction rate for AFD is in the range of 4.6-1.5 kg water per kWh of energy expended, and 0.4 kg water per kWh for VFD (Claussen, Ustad, et al., 2007)).

The origin of atmospheric drying is attributed to Dr Harold Meryman (Meryman, 1959), who experimentally showed that the diffusion of water vapour from the subliming surface of ice through the dried layer was due to the gradient of partial pressure of water vapour in the system thus eliminating the requirement of vacuum in the freeze-drying process. This led to active research in atmospheric freeze drying (AFD) as an alternative to VFD. However, despite the advantages mentioned above, industrial uptake of AFD has not occurred. Partly this is because of very slow drying rates compared to VFD and the lack of specific case studies that have been carried out to definitively show its utility and economics (Andrés et al., 2019; Rahman & Mujumdar, 2012).

Conducting case studies is hampered by the long timescales involved in doing experiments and the number of mass and heat transfer related parameters that need to be investigated. Nevertheless, they are essential to raise awareness of the advantages of AFD, and to understand the kinetics of drying so that it can be optimised. One way to drive commercial uptake of AFD is to develop a general purpose mathematical model that can simulate different scenarios in industrial-scale atmospheric and vacuum freeze-drying processes (Santacatalina et al., 2015). The present state of AFD modelling is limited to specific materials which, due to the high variation in physiology of plant and animal products, is reflected in a wide range of mass and heat transfer properties (Claussen, Ustad, et al., 2007). Thus, developing a generalised model which works for all biological samples is difficult and no such approach has been found in the literature. To accommodate material differences, this project develops a micro-process-based model that incorporates the relevant physics in a generic way by focussing on how the resistances to mass and heat transfer are typically arranged and co-designing an experimental methodology that allows these resistances to be defined for a specific case study material, and which should be transferable to any other material.

Before defining how mass and heat transfer resistances are arranged, it is important to understand the factors that affect the rate of sublimation. The most significant of these is the potential. In both AFD and VFD, the driving potential is the vapour pressure

difference between the saturated value at the ice surface and that in the drying chamber (Claussen, Ustad, et al., 2007). The rate of drying in AFD is very slow compared to VFD because principally, by using a vacuum, VFD maximises the potential. The use of high plate temperatures in VFD which are in thermal contact with the product also helps in maintaining the high drying rate.

Another important factor is the surface area of the ice surface from which sublimation occurs. This is essentially an inherent property of the material and will be a function of its initial moisture content. Ice surface area decreases over time.

Then there is the interplay between heat and mass transfer. Sublimation is a solid-to-gas phase change and so requires *ca*. 2800 kJ/kg of heat. Thus, steady-state freeze-drying occurs when the constant removal of subliming vapour is matched by the constant supply of heat to the ice interface. In this way, the mass and heat transfer resistances determine the atmospheric freeze-drying rate (Hua et al., 2010b). Mass transfer resistances includes the resistance to diffusion of water vapour inside the product material and the resistance to vapour transport encountered from the surface of the material to the bulk air. Heat transfer resistances consist of the resistance to convective heat transfer from the air to the surface of the product and the conductive and the mixture of convective heat transfer resistance encountered when heat flows from the surface of the product to the ice crystals inside the product (Claussen, Ustad, et al., 2007; Heldman & Hohner, 1974; Rahman & Mujumdar, 2012).

The dominant mechanism or the rate controlling mechanism in AFD of different products is still unclear although most of the time it is assumed to be mass transfer controlled, due to the long timeframes over which AFD occurs. Therefore, the revelation of the dominant mechanism for AFD is important for developing techniques to improve the drying rate thus facilitate its wide application in food industry. This current project studies the rate controlling mechanisms in AFD.

Leafy or leaf-like products are ideal candidates for atmospheric freeze drying. First, their AFD is relatively fast due to their thin cross section; second, they are not suitable for VFD due to the large volume of the raw product when space is at a premium in VFD; and third, leafy products contain a lot of void space which poses difficulty for conductive heat transfer from the heated shelves to the bulk of the product. Thus, leafy products are

expected to offer the most economic case studies for atmospheric freeze drying. Among these is hops, which has a leaf-like structure along with stomata, which are pore openings to the vascular network inside the plant material. Hops are also a valued product for the beer industry where retention of flavour compounds is enhanced by low temperature drying.

Therefore, this project focuses on AFD, generically of leaf-like products, and specifically with the model material as hops. However, the study of the kinetics of AFD cannot be done without high-quality temporal data. The most important measurement is the weight loss of a specimen undergoing atmospheric freeze-drying along with system temperature and humidity over several hundred hours. To address this, the project has developed an AFD experimental system to generate high-quality data for drying.

1.2 Objectives of the study

The project aims to define the rate-controlling mechanisms in atmospheric freeze-drying and thus guide technological interventions to increase the rate of drying. To achieve these goals the following objectives were considered.

1. Identify the material and system properties that affect the drying rate from literature and formulate relationships between them.
2. Develop a structural model for hops, which is the model material under consideration.
3. Develop an experiment set up to replicate likely industrial AFD conditions with the capability to do *in-situ* continuous weight loss measurements along with measurements of psychrometric variables.
4. Conduct experiments and generate drying curves to generate data for model development.
5. Identify the rate controlling mechanism for AFD of leaf-like products.
6. Develop a theoretical model for atmospheric freeze-drying of leaf-like specimens based on heat and mass transfer principles for predicting drying rates and the time required for achieving any required final moisture content.
7. Propose technological interventions to enhance the drying rate.

1.3 Thesis Overview

The thesis chapters are arranged to address the objectives stated above. This first chapter introduces the project and its objectives. The second chapter details the status of relevant research work reported in the literature. The third chapter provides an account of the materials used for the experiments and the methods of analysis used in the research project. The design, development and validation of the experimental set is described in the fourth chapter. Chapter five describes the model development, including justifying the assumptions and theoretical principles used. The sixth chapter discusses the experiments and results for the atmospheric freeze-drying experiments done with ice, while the seventh chapter discusses those for hops. Based on the insights gained from the experiments and from the model, the technological interventions which can enhance the sublimation rate during atmospheric freeze-drying are described in the final chapter along with discussion on the overall project outcomes and suggestion to guide future research. An appendix is provided at the end of the thesis along with the bibliography.

Chapter 2 Literature Review

2.1 Introduction

Atmospheric freeze drying (AFD) is the process of using cold gas with low partial pressure of water vapour to dry products below their freezing point at atmospheric pressure. Two of the main advantages of AFD over vacuum freeze drying (VFD) are its lower capital cost and lower energy requirement. These savings are due to AFD not requiring a vacuum pump and the associated utilities of heated shelves and manifolds for heating the products and the condenser system that first removes the sublimed water vapour onto frozen coils then is later defrosted to water (Rahman & Mujumdar, 2012). Instead, AFD removes the sublimed water vapour by some form of water vapour trap, the methods of which will be discussed in more detail later. Due to the atmospheric pressure operation, AFD is amenable to operate as a continuous system (Heldman & Hohner, 1974). Another advantage is that AFD can be done as a closed system by circulating an inert gas to avoid oxidative damage to the product and the product temperature can also be elevated using different modes of heat input such as convection, radiation and conduction (Claussen, Ustad, et al., 2007). Furthermore, air, or gas, is a heat carrier and so enhances the heat transfer to the product compared to VFD (Heldman & Hohner, 1974). For leafy products, this convective heat transfer to the leaf surfaces is approximately uniform, with less risk of overheating of the product at the contact surfaces as occurs with conduction-only heat transfer in VFD.

To date AFD has not been adopted industrially. Even though it has the above advantages, its major disadvantage is the low drying rate when compared to VFD, which is an impediment when production rate is constrained by the capacity of the drying plant. For this reason it is not considered an economic alternative to VFD (Claussen, Ustad, et al., 2007; Heldman & Hohner, 1974; Rahman & Mujumdar, 2012). Nevertheless, AFD deserves attention in order to identify products where it can offer economic advantage. For this, we need to understand the rate controlling mechanisms and be able to model the process so that the drying strategies can be optimised. The following sections present the current understanding about AFD as reported in the literature.

2.2 Freeze drying

Freeze drying of a sample, whether by AFD or VFD, starts with the freezing of the sample. During freezing of a biological material, the water in the sample gradually changes phase onto the surfaces of growing ice crystals (Meryman, 1959). As the crystals grow, the residual solute concentration increases which decreases the freezing point (also known as freezing point depression). Thus, some water will remain unfreezable although, as the temperature continues to decrease, this may solidify as an amorphous glass depending on the solutes (Berk, 2018; Oetjen, 2000; Petzold & Aguilera, 2009). The size of the crystal resulting from the initial freezing depends on the rate of freezing defined by the interface velocity and temperature gradient present at the freezing interface, and the temperature and super-cooling achieved in the adjacent solution (Kochs et al., 1991, 1993). The rate of freezing will be also affected by the mass and heat transfer dynamics of the system (Bellissent-Funel et al., 2016; Chaplin, 2019; Kiani & Sun, 2011). During storage, further changes occur. Here, the equilibrium of crystal growth favours large crystals at the expense of small crystals in a process termed Ostwald ripening (Vicent et al., 2019). At the beginning of freeze drying, the crystal size distribution (CSD) in the sample will be the net effect of the initial freezing and the subsequent storage. Some freeze dryer operators favour slow initial freezing to encourage growth of large ice crystals, which ultimately leave large channels for water vapour egress because large crystals rupture the cell walls.

When freeze drying process is analysed, there are two types of water in the product that need to be removed, the free water and the bound water. For a high moisture product, the free water is often about ~90% of the total moisture content (Hua et al., 2010a). In the case of VFD, the removal of this free water is called the sublimation drying or primary drying. To do this, the frozen material is heated inside a chamber which is kept at vacuum using a vacuum pump. Drying starts from the outside of the product and the dried layer grows inwards. The interface between the dried and the frozen layer is called the ice front or the sublimation front (Hua et al., 2010a). The vapour escapes through the dried layer and the heat for sublimation is transferred to the sublimation front by radiation and conduction from the heated shelves on which the products are kept (Duan et al., 2016).

A further consideration is the frozen layer's glass transition temperature above which the frozen layer would collapse. This is at the collapse temperature which is typically a few

degree Celsius above the glass transition temperature and depends on the moisture content and the nature of the material (Farid, 2010). It is important to preserve the original structure of the plant material. For example, if a glassy solid is formed during the freezing or freeze-drying, then the operating temperature for freeze drying must be lower than the glass transition temperature so that the viscous-liquid region is avoided. Also, the dried layer temperature should always be lower than the collapse temperature to prevent the dried structure from collapsing (Hua et al., 2010b, 2010a).

The vapour formed during sublimation drying is voluminous and can increase the pressure in the drying chamber and thus increase the temperature of the subliming surface and melt the frozen layer. To avoid this, a cold trap is used to capture these vapours (Hua et al., 2010a). The cold trap is maintained at very low temperatures like -40 ^{o}C to -50 ^{o}C to provide the driving force required for water vapour movement from the frozen product front. The cold trap also helps in preventing the moisture going into the vacuum pump, as the vacuum pump is mainly used to remove the non-condensable gas from the product and the air leaking into the drying chamber (Hua et al., 2010a).

The secondary drying, or desorption drying, starts when the primary drying is completed, and the free water is removed. This drying removes the bound water and is enhanced by heating the product to elevate its temperature. The final dried product generally has a moisture content lower than 5% (Duan et al., 2016; Hua et al., 2010a).

In the case of AFD, sublimation drying, or primary drying is done by keeping the frozen product in a drying chamber at atmospheric pressure and a cold dry gas is used to remove the moisture from the product as well as provide the heat for sublimation. The moisture from air is removed using an adsorbent or other mechanism (Rahman & Mujumdar, 2012). Like VFD, AFD has two processes going on simultaneously – (1) removal of moisture from the product and (2) supply of heat to the product to facilitate sublimation.

The steps involved in atmospheric freeze drying can be expanded and broadly categorized as mass transfer or heat transfer processes. The mass transfer processes in AFD can be expanded into the following steps:

1. the sublimation of ice crystals to maintain saturation vapour pressure near the ice crystal;

2. transport of water vapour from the water vapour saturated region adjacent to the ice crystal inside the product to the bulk air; and
3. the moisture removal from the bulk air either by a desiccant or a water vapour trap.

The heat transfer processes in AFD can be expanded into the following steps:

1. the decrease in temperature of the ice crystals due to sublimation which is an endothermic process;
2. the heat transfer from the product surface, through the product matrix and to the ice crystal;
3. the heat transfer from the bulk air to the product surface; and
4. additional heat supplied to the bulk air using a heat pump to compensate the heat loss to the product and the heat loss through the cold vapour trap (in the case of a closed system with adsorption of moisture on the desiccant, the heat is released during the exothermic adsorption of moisture on to the adsorbent).

(Claussen et al., 2007; Duan et al., 2016; Heldman & Hohner, 1974; Rahman & Mujumdar, 2012). These steps can be seen in the schematics of atmospheric freeze drying as shown in Figure 2-1 and Figure 2-2.

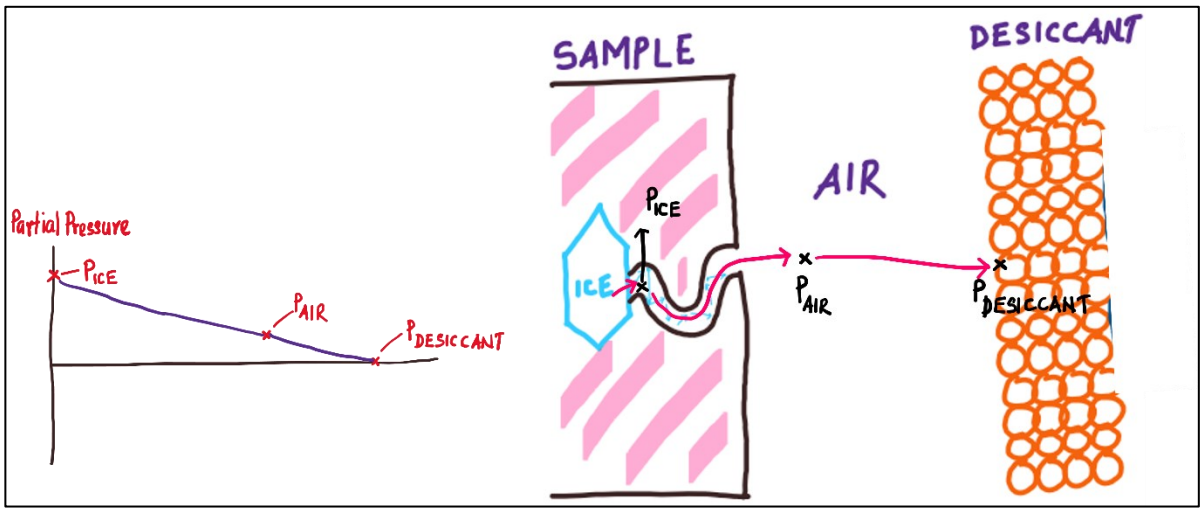

Figure 2-1 Mass transfer steps and the partial pressure gradient

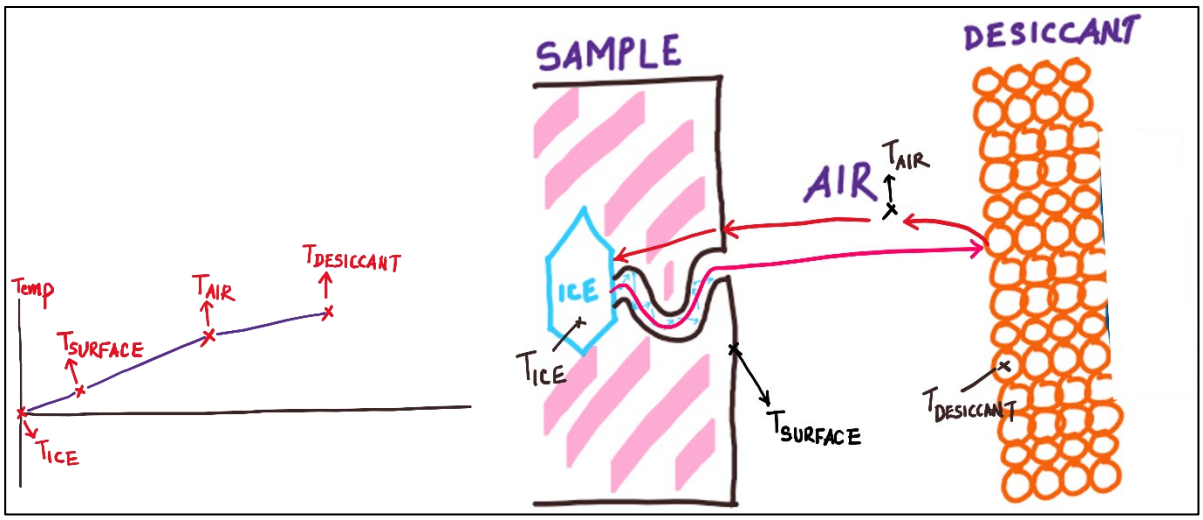

Figure 2-2 Heat transfer steps and the temperature gradient

In AFD, the transfer of moisture from one point to another is driven by the partial pressure gradient of the water vapour (Wolff & Gibert, 1990). The mass transfer steps and the figure show that the mass transfer potential is the water vapour gradient from the surface of the ice crystal to the surface of the desiccant with the highest moisture concentration at the surface of the ice crystal and the lowest moisture concentration at the surface of the desiccant or the water vapour trap (Duan et al., 2016; Rahman & Mujumdar, 2012).

The moisture content at the desiccant side depends on the type and quantity of desiccant used, and its temperature (Chua et al., 2002; Kim et al., 2003; Wolff & Gibert, 1990). The saturation moisture content in the air is a function of the temperature of the air, whereas, the moisture content of air in equilibrium with a desiccant is a function of the desiccant temperature (Wolff & Gibert, 1990). Similarly, the saturation partial pressure of water vapour at the ice surface depends on the temperature of the subliming ice crystal (Haseley & Oetjen, 2018; Wolff & Gibert, 1990).

The rate of mass transfer from the surface of the subliming ice crystals to the adsorbing desiccant also depends on the resistances it encounters along the pathway from the ice surface inside the product to the environment outside the product (Heldman & Hohner, 1974; Rahman & Mujumdar, 2012). The mass transfer resistance inside the product depends on the temperature dependent diffusion coefficient of water vapour both through the plant cell matrix if ice crystals are enclosed or encased, and through the gas filled internal pores, or vascular structure, of the plant material. The internal mass transfer

resistance also depends on the path length over which diffusion occurs which will be a function of the tortuosity of the gas phase diffusion path from the ice to the surface of the product (Di Matteo et al., 2003; Heldman & Hohner, 1974). Thus, a more tortuous pathway implies a longer path length and so a slower mass transfer rate. The mass transfer resistance outside the product can be described by a temperature dependent diffusion coefficient for water vapour in air and a boundary layer thickness, which will be a function of the local mixing of the air (Di Matteo et al., 2003).

While mass transfers out of the product, heat transfers in to supply the heat for sublimation. Therefore, for a closed AFD system, the potential is the temperature difference between the highest temperature, at the desiccant where the exothermic adsorption of the water vapour takes place, and the lowest temperature, is at the subliming ice crystal surface (Claussen, Strømmen, et al., 2007; Di Matteo et al., 2003; Duan et al., 2016; Heldman & Hohner, 1974; Rahman & Mujumdar, 2012). The rate of heat transfer from the bulk air to the product surface is dependent on the convective heat transfer coefficient assuming the air is moving relative to the product, which is a function of the thermal conductivity of the air and the quiescent boundary layer, and the radiative heat transfer if relevant (Rahman & Mujumdar, 2012; Wolff & Gibert, 1990). Most biological materials are anisotropic and so the heat transfer rate will depend on an averaged effective thermal conductivity of the product, which depends on the intrinsic thermal conductivities of the dry product, ice and air, the moisture content and porosity of the product (Claussen, Ustad, et al., 2007; Di Matteo et al., 2003). Sublimation, which is an endothermic process, removes from the ice crystal an amount of heat equal to the heat of sublimation thus cooling the crystal. This heat removal rate depends on the resistances to mass transfer of water vapour inside the product (Duan et al., 2016).

Mass and heat transfer rates depends on the surface area and a higher surface area will enhance sublimation rate in AFD if the potential and the resistances are not limiting. An operator may affect this by choosing a fast initial freezing rate, per the discussion above and create smaller ice crystals for the same quantity of total ice content and thus a higher ice surface area. Also, as the system is in series, so two areas are important, the internal ice area inside the frozen sample and the total external surface area across which heat and mass transfer exchange occurs with the ambient air. Maximising the ratio of product surface area to volume or weight is one controllable factor influencing the rate of freeze

drying. High ratios go hand-in-hand with smaller characteristic distances in solids, and reduced path length associated with reduced resistance to both heat and mass transfers (Heldman & Hohner, 1974).

In summary, the rate of drying in AFD depends on mass and heat transfer which occur simultaneously. However, it is not unexpected that one of them limits the process. As the potential for each is easily measured, and the areas of mass and heat transfer are also estimable, this leaves the challenge of determining the resistances, which will be specific to the products that are dried by AFD.

2.3 AFD of biological materials

Most research on AFD of products of biological origin is on plant-based foods with only a few studies on animal-based products. The most studied plant-based materials are apple cubes, carrot slices, peas, egg plant cubes, and mushroom slices (Bhatta et al., 2020). Animal origin studies have examined beef cubes (Heldman & Hohner, 1974), and cod cubes (Bantle et al., 2011; Rahman & Mujumdar, 2012). As noted in the list, these studies have mostly used cubes of various dimensions in order to study the kinetics of the process and model it.

No study has been found for AFD of leaf or leaf-like products. The structure of leaf or leaf-like products is quite different (Earles et al., 2018; Mathers et al., 2018) to the above reported cubes of solid plant material or frozen solutions where drying was explained as taking place from the outside of the object progressing towards the inner regions (Andrés et al., 2019; Claussen, Ustad, et al., 2007; Nakagawa et al., 2020; Rahman & Mujumdar, 2012; Tolstorebrov et al., 2018). In leaf-like materials, since most of the cells are involved in photosynthesis, they are exposed to an intercellular airspace for exchange of gases when alive (Earles et al., 2018). When a frozen leaf-like product is subjected to AFD, it can be hypothesized that drying can take place simultaneously in all the cells as they are all exposed to a common air pathway unlike the solid products where the internal sites are exposed only when the air pathway associated with the dried region reaches them. This aspect is considered in this thesis.

The internal resistance for mass transfer has a contribution from the cell walls and membranes between unconnected pathways through which the moisture must traverse to

reach the surface of the product. It is also important to note that the cell walls and membranes might be broken depending on the freezing method employed (Kiani & Sun, 2011; Petzold & Aguilera, 2009; Sun & Li, 2003). This resistance contribution inside the cells increases with time as the ice crystals sublime and shrink thus leaving behind porous structures which further increase the tortuosity and thus the resistance (MacKenzie, 2006).

This difference in the structure of leaf or leaf-like products when compared to other plant-based solid products can help in explaining why the AFD of leaf-like products are found to be faster as they have a higher exposed surface area and less resistance to mass and heat transfer due to their thin cross section, and so dry more uniformly throughout the product. It is on this premise that AFD can be an alternative or a good complement for freeze drying of leaf or leaf-like products. This aspect is incorporated in the model development in this thesis.

2.4 Rate limiting mechanism and debottlenecking

Regarding the rate limiting mechanism, researchers generally assume that AFD is internally mass transfer limited while VFD is externally heat transfer limited (Claussen, Ustad, et al., 2007; Duan et al., 2016; Heldman & Hohner, 1974; Rahman & Mujumdar, 2012). This assumption is subscribed by all without much of a definite experimental analysis and is found early as with Dr Meryman who only considered the resistance to mass transfer as the rate limiting factor for AFD (Meryman, 1959).

The comprehensive research work by Di Matteo et al., (2003) studied in detail the role of heat and mass transfer in atmospheric freeze drying of foods in a fluidized bed. Their study reported that within the range of fluidization, air speed was important only for the initial atmospheric freeze-drying rate and so concluded that external mass transfer resistance plays a role only during initial drying. They also found that the AFD rate increased with the fluidized bed temperature, which they attribute to the increase in partial pressure gradient of water vapour rather than any increase in heat transfer because the temperature difference between the product and the bed was only ever of the order of 0.6 ^{o}C. They also studied the initial product freezing temperature, carried out before the start of AFD, and found that AFD rate increased with freezing temperature, which they hypothesise is due to higher freezing temperatures resulting in bigger ice crystals and so

producing bigger pores when they sublime, allowing for easier internal moisture diffusion. However, this is contradicted by their experimental result for product frozen with liquid nitrogen (-196 °C) which showed a rate faster than that product frozen at -50 °C, a result which could be due to the cryogenic freezing producing smaller crystals, and therefore a larger surface area of ice for sublimation as previously discussed. Their study also extended to the type and characteristics of the adsorbent, where they found that AFD rates increased both with smaller adsorbent particle size and with greater adsorbent to product weight ratio. The study concludes that the AFD rate is limited by internal mass transfer due to the relatively constant temperature difference between the product and the bed and the air velocity having an effect only during initial drying (Di Matteo et al., 2003).

Another study on the kinetics of AFD used apple as the product and used a heat pump to control the partial pressure of water vapour in the drying air and found that increasing drying air temperature increased the AFD rate. The authors attributed this to the increase in mass transfer which was assumed to be limiting the AFD (Stawczyk, Li, Witrowa-Rajchert, et al., 2007). One of the early research works done on AFD of solid biological products was with beef cubes and reported that the rate of drying increased with the drying air temperature and that the mode of heat transfer through the product was primarily through conduction. The effective diffusion coefficient for internal mass transfer was a product of the diffusion coefficient of water vapour through air and a structural constant for the product beef and this constant can be considered as an attenuation factor used to compensate for the constrictions of the porous media for the free flow of moisture through the drying product (Heldman & Hohner, 1974). They also reported that drying rate increases with decrease in thickness of the product.

On the other hand (Stawczyk, Li, & Modrzejewska, 2007) reported that AFD of chitosan materials including chitosan membranes and granules, gave a long constant rate drying period followed by a short falling rate period unlike other AFD studies based on solid plant or animal origin products which showed a falling rate from the start; the authors inferred that this was due to rate control by surface water vapour diffusion rather than rate control by internal mass transfer diffusion. This difference in rate control mechanism for different products with different internal structures is one of the motivations to study the AFD of leaf-like structures and find the rate controlling mechanism for the process.

Most recent research on AFD has focussed on enhancing the AFD rate. Two methods are by microwaves or ultrasound (Carrión et al., 2018; Colucci et al., 2018; Mello et al., 2020; Merone et al., 2020; Santacatalina et al., 2012). These studies report that the rate of drying is significantly increased when AFD is assisted with high power ultrasound, and they attribute it to the effects of compressions and expansions (sponge effect) which occur in the product when sound waves pass through it and thus increasing the effective internal diffusion for water vapour (Awad et al., 2012; Garcia-Perez et al., 2012). Similarly, the drying rate is reported to increase with increasing applied power of the ultrasound (Carrión et al., 2018; Moreno et al., 2017). The experiments do not specifically address the effect of mechanical energy introduced into the system and the heat energy thus generated and its effect in increasing the drying rate. Consequently, it is not evident whether the increased drying rate is due to the increased internal mass transfer rate alone or whether there is an effect of heat transfer rate (Santacatalina et al., 2015).

Eikevik et al., (2012) studied AFD of green peas assisted by microwave and showed that the drying time can be reduced by 30% by subjecting the material to microwaves inside the atmospheric freeze dryer. It is to be noted that the microwave energy efficiency based on the efficiency of the magnetrons used is generally low and for a microwave assisted convective system it is less than 50%. Microwave-assisted freeze drying was originally used for VFD, to increase the heat transfer into the product as the water molecules can directly absorb the energy without the interference of the dry layer leading to the heating of the material volumetrically. This energy can be used for sublimation or increase in the ice core temperature and thus a higher water vapour pressure and higher mass transfer gradient for faster drying (Duan et al., 2010, 2016; Xu et al., 2015).

Researchers have studied similar mechanisms of ice sublimation in atmospheric conditions in another field of study, glaciology, where it is an important phenomenon. For example, the loss of snow in the Himalayan glaciers by sublimation is almost 21% higher in the regions affected by wind when compared to non-wind affected regions (Stigter et al., 2018). Researchers in this field use the eddy covariance method to relate wind turbulence fluctuations to sublimation rates, using data obtained from weather stations at different heights and locations. This method focusses on the surface sublimation of water vapour, and so is not of principal interest here where the internal resistances dominate. At the level of single ice crystal sublimation, glaciologists report

that the sublimation rate is limited by water vapour diffusion rather than heat transfer into the ice (Jambon-Puillet et al., 2018). Later, chapter 6 tries to validate this for ice in AFD with an adsorbent system and finds it true.

Another area where the atmospheric sublimation of ice is being studied is weight loss during freezing and storage of unpacked food products (Campañone et al., 2005). Here the weight loss by ice sublimation is assumed to be determined by mass transfer parameters and differs from the AFD settings in that the air RH can be above 75% while in AFD it is generally 5-10%; also, the development of a frozen layer on the product surface can affect both the heat and mass transfer parameters. Similarly in a case of packed food product in storage, (Phimolsiripol et al., 2011) have reported that the extent of moisture weight loss of a frozen bread dough under conditions of fluctuating temperature storage depended on the magnitude of the fluctuation. The authors have used both a physical model and an artificial neural network model to predict the weight loss.

The common theme with most of the research cited above is that researchers develop a model and validate it against the experimental results for their material of interest. The section below discusses the types of models and the approaches used on products that are atmospheric freeze dried.

2.5 Current models for AFD

Researchers have developed mathematical models for the atmospheric freeze drying of biological materials, but these are fewer in number compared to vacuum freeze drying. As noted earlier, experiment studies with AFD and model development have been mostly on biological materials like apple cubes, carrot slices, potato, green peas, and few other materials like red pepper, poultry meat, sea cucumber, orange peels, eggplant, etc (Claussen et al., 2007; Duan et al., 2016; Rahman & Mujumdar, 2012). No model development studies have been found for AFD of leaf-like products.

The most common model used by AFD researcher is that of a uniformly retreating ice front (URIF) or a two-zone model, where the ice interface is assumed to retreat as a uniform plane when heat is supplied to it in one direction and the sublimation takes place at the interface with water vapour moving through the dried layer (Claussen et al., 2007; Ingrid Camilla Claussen, Andresen, et al., 2007; Heldman & Hohner, 1974; Wolff &

Gibert, 1990). The model simulations give good predictions for the removal of the first 75-90% of the moisture but then start to deviate (Claussen et al., 2007). The URIF was developed for studying VFD and analysing the rate kinetics of the process (Sandall et al., 1967). One main concern with URIF based models is that the assumption of the ice front being a single plane is not accurate and can only be useful when the heat and mass flow is limited to one dimension like that of freeze drying of pharmaceutical active ingredients in vials and heat is supplied from the bottom in the axial direction alone.

A second approach is the Diffuse Interface Model (DIM), which assumes that the ice front could take a form of a gradient instead of a plane as used in the URIF model (Bobba et al., 2020; Warning et al., 2015). Here a third phase is assumed between the dry and frozen regions, a partially frozen region where only a part of initial ice is present. This takes care of the fact that the sublimation rate is affected by the material properties and occurs from multiple heat influx directions. Thus, this model could be used for developing a 3D model for freeze drying where URIF is inappropriate.

A third approach for modelling freeze drying is to use the Dusty Gas Model within CFD codes, which have been used for freeze drying of solutes in vials. Dusty gas model assumes the mass transfer of water vapour as taking place through a continuum of gas and a structure which is modelled using a structural parameter estimated by the simulations (Capozzi et al., 2019; Liapis & Bruttini, 1995). Some studies have combined CFD modelling approach along with DIM and URIF models (Li et al., 2007; A. Warning et al., 2014).

A fourth approach used by researchers is to use a Weibull distribution to fit their experimental data, and so obtain the Weibull best fit parameters. It is based on defining the temporal moisture ratio curve of the specimen as a function of effective diffusivity, characteristic length and the shape factor of the specimen (Bantle et al., 2011; Eikevik et al., 2012). This approach modifies a Weibull distribution model to a physical model and was able to model the AFD kinetics quite accurately. However, most of the physics involved in the process were compressed into a shape factor parameter of the model which must be calculated from experiments through non-linear regression analysis. So, while the model predictions are in good agreement with the experiment results this approach will not be pursued here.

The common approach to solving mass and heat transfer problems in spray dryers and fluidised bed dryers is to use a CFD model with an appropriate sub-model for the suspended droplets undergoing evaporation. There are a few studies using this method for AFD. A study based on CFD modelling of AFD apple cubes by (Li et al., 2007) considered the URIF model as the basis for model development and the simulation results matched the experiment results to a large extent with R^2 values ranging from 0.803 to 0.996, but visually the model and the experiment results showed more deviation in the high moisture region. CFD solves the Navier-Stokes equations in the vapour phase which, allow determination of the exchanges at the air-product interface of the mass, momentum, and energy. While CFD is a strong tool for modelling heat and mass transfer in the mainstream of drying air and at interfaces, it needs a sub-model that accurately describes the sublimation inside the food matrix, the structure of which can vary widely across product types. For the above reasons, the present study is about the sub-model, and does not include this within a CFD model for air flow. Furthermore, the experimental set-up, which is described later, accommodates the scenarios of forced and natural convection.

Researchers have developed numerical simulations of AFD for carrot slices in a fluidized bed based on sublimation-condensation model (Sheehan & Liapis, 1998) which considers a food product as an unsaturated porous medium which has porous regions partially covered with ice and a solid matrix (Bubnovich et al., 2009, 2012). They have used finite difference methods to solve the partial differential equations for unidirectional and bidirectional models for heat and mass transfer in the carrot slices during AFD, assuming a base model of URIF with a dry region and a frozen region separated by a mobile sublimation front (Bubnovich et al., 2009). The effective diffusivity of the water vapour was defined as a product of diffusivity of water vapour in air and a constant to include the difficulty for the water vapour to diffuse through the porous medium. They compared these to experiments where they changed the carrot slice dimensions. It was found that the unidirectional and bidirectional heat and mass transfer models predicted more and more similarly when the ratio of thickness to length of the product was decreasing (Bubnovich et al., 2012). Where the thickness of the product is very low, like a leaf-like product, the unidirectional model was found to be sufficient. These simulations by the unidirectional model were found to underpredict the moisture content in the early-stage

high moisture period and then cross over and start to overpredict the moisture content in the late-stage low moisture content region (Bubnovich et al., 2009).

More recently a research group has modelled AFD considering the drying product as a single zone of uniformly mixed ice and liquid/rubber phases which has an apparent vapour pressure lower than the vapour pressure exhibited by pure ice at the same temperature (Nakagawa et al., 2020). The concept of temperature and moisture content-dependent apparent vapour pressure is used to include the effect of glass transition temperature on the structure of the product. AFD operating temperatures are always assumed well above the glass transition temperature for agricultural products which means that the frozen product would actually be like a rubbery/liquid phase with ice crystals spread in between (Nakagawa, 2018; Nakagawa et al., 2020). The model predictions show good agreement with the experimental results in most places, but deviated at some regions, this may be due to the experiment having been done in changing temperature scheme.

2.6 Experimental Set-up

To study the rate controlling mechanism and to model the process a good experiment set-up is required to provide the researcher with quality data. In many reported experiments, the sample or the drying chamber was taken out of the sub-zero conditions to measure the weight loss at regular intervals (Alves-Filho et al., 2007; Bantle et al., 2011; Claussen, Andresen, et al., 2007; Di Matteo et al., 2003; Eikevik et al., 2012; Xu et al., 2015). This introduces inaccuracies as the sample and system is exposed to higher temperatures and absolute humidity. The sample needs to be taken out for weighing, because commercially available analytical balances can only operate between 5 to 40 °C (from email correspondence with analytical balance manufacturers, National Metrology Institutes in New Zealand and Japan).

Ideally, experimental set-ups need to obtain continuous *in-situ* weight loss measurements during AFD. Obtaining continuous, high-accuracy weight data in freezing conditions is not easy. Two studies that do that to an accuracy of 0.001g both used a proprietary weighing mechanism from Martin Christ (Lyobalance), which is supplied as a part of their pilot freeze dryer and works only on their proprietary software (Pikal et al., 1983; Roth et al., 2001). The alternative is to use an external load cell or mass balance with a

hanging member that penetrates the freeze-drying chamber. All weighing methods require that the sample mass is sufficiently within the accuracy range of the weighing device; this is more important for load cells which typically work best in the middle of their range and are not as finely calibrated as mass balances. Furthermore, the amount of sample for a closed experimental system must be matched with an appropriate amount of desiccant, if this is the method of water vapour removal (Carrión et al., 2018; Garcia-Perez et al., 2012; Moreno et al., 2017; Stawczyk, Li, & Modrzejewska, 2007; Stawczyk, Li, Witrowa-Rajchert, et al., 2007). To get data of high accuracy (0.0001g), with continuous *in-situ* measurement of weight loss of product during AFD, it was necessary to develop a new experiment set-up which was small in scale and was also cost effective per trial.

2.7 Research gaps

The literature review above highlights that the physical models have a simple construct, that is, the substrate is divided into two sections: the ice-free zone and the frozen zone with a planar receding interface (URIF), although some propose a gradient of ice concentration across an interface thickness (DIM). These approaches work to a large extent, because the model is amenable to experimental studies of cubes or spheres. While no studies have been reported on leaf or leaf-like products, they are approximated by the work of Bubnovich et al., (2012)who investigated carrot slices and showed that unidirectional models are appropriate when the slices were thin enough. This work is the first that specifically focusses on leaves and leaf-like plant materials.

The above two-section approach seems to be an adequate simplification of freeze drying. However, it does not reflect the structural differences between plant materials. For leaf and leaf-like plant material, there are factors that can be quantified, such as the intercellular air spaces for gas exchange within the leaf, and size and number of portals (stomata) for gas exchange between the leaf and external environment. Transport of water and exchange of gases in plants have been studied by researchers to provide a detailed understanding of the structure of the specimens in terms of cell structure, arrangement, porosity, the different layers in the product with varying transport properties and pathways for moisture movement. The most advanced technique used for this was X-ray micro-tomography (Halder et al., 2011; Nugraha et al., 2019; Verboven et al., 2008; A. Warning et al., 2014). There are also many postharvest water loss studies that show that

the resistance to moisture removal is very much affected by the cuticle, which is a hydrophobic layer, and the gas exchange structures of the stomata (in the leaf), and lenticels (in the stem) and cracks (Veraverbeke et al., 2003). Similar studies using X-ray micro-tomography have also been reported on mass transport properties and gas exchange pathways in horticultural products (Janssen et al., 2020; Nugraha et al., 2019). This prior knowledge in related fields will be useful in the AFD model development of leaf or leaf-like structures to be carried out in this thesis.

Introducing plant structure dependent factors will offer a more physically realistic model to the existing URIF and DIM models. Here, it can be argued that a leaf or leaf-like structure is thin in section, with a vascular network with many external gas exchange structures that remain open when frozen. Therefore, it can be hypothesized that a leaf-like product will have ice crystals spread throughout the cells of the plant, all of which are nearby or exposed to a common intercellular pathway filled with air, so will favour faster mass transfer compared to larger cube or sphere-like shapes. This hypothesis is checked in this project.

The experiments conducted in this thesis use a desiccant to remove moisture. The equilibrium and dynamics of adsorption by the desiccant must be considered in the model development to both determine the practical adsorbent-to-sample mass ratio, and to ensure that the kinetics of adsorption are fast relative to the kinetics of sublimation. The study of the rate of adsorption into the desiccant has not been the focus of any model in the literature and so its inclusion here is a new addition to the model development.

Due to the complexity of biological substrates, drying models need many input parameters for the properties of the components to define the heat and mass transfer resistances. To be predictive and useful industrially, models should have as few adjustable parameters as possible. Nevertheless, some will be required because models are simplifications of the three-dimensional plant structure. Further simplifications are also possible for the particular geometry of leaf and leaf-like structures where edge effects can be assumed negligible. The model will be detailed later but, as an introduction here, it offers a different approach to the URIF, and DIM models used by previous researchers detailed above. It does this by assuming the leaf structure to consist of an intracellular ice crystal, and a vascular network open to the external gas portals (i.e., stomata and

lenticels). As ice crystals sublime, they recede into the intracellular matrix and the internal resistance to water vapour movement increases. This is the first time the leaf structure has been described in this way for sublimation. The external resistance is the series sum of the resistances from the leaf surface-to-bulk air boundary layer and the bulk air-to-desiccant boundary layer, if the bulk air is assumed to be a well-mixed region. Out of this reasoning, with the assumptions to be discussed later, a two-parameter model arises one for the internal resistance specific to intracellular matrix regions, and the other for the resistance in the extra cellular region including the cell membranes and the vascular pathways. Defining the model and determining and validating these parameters is the focus of this thesis. These parameters then can be used for all further simulations for permutations of the drying conditions, such as system temperature, initial product moisture content, and environmental humidity.

AFD is generally assumed to be an internal mass transfer-limited process, although there is no comprehensive experimentation to prove it. Here, both heat and mass transfer will be rigorously studied to provide a definitive conclusion for leaf and leaf-like biomaterials.

AFD can exhibit both constant rate and falling rate drying, and so any model developed must also describe these phenomena. As noted earlier, (Stawczyk, Li, & Modrzejewska, 2007) found that for AFD of highly porous chitosan membrane a long constant drying rate was followed by a short falling rate period, which was unlike the results of others who found only a falling rate period for AFD of low porosity products like apple and carrot. While the latter is explained by a URIF model, this project on leaf-like products offers a different model as explained above, and so the experimental data and model will be compared to determine whether or not there is a transition from constant rate to falling rate drying.

Accurate experimental data is needed to advance the model development in the field, and this requires designing an experimental apparatus that enables continuous *in situ* measurement and at the same time uses a commercially available analytical balance and has a low sample and adsorbent requirement per trial. This experimental system is detailed in chapter 4 on the development of experimental set-up.

Chapter 3 Materials and Methods

The materials used in the study and the analysis methods used are described in this chapter.

3.1 Materials

3.1.1 Hops

The hops used for the experiment were collected from the single plant growing on Riddet Road, on the Massey University campus and maintained by the Massey University micro-brewery. Green hops (1.5 kg) were harvested on 25th March 2021 and transferred to labelled airtight plastic bags and stored in a chest freezer maintained at -18 ^{o}C. A photo of the harvested fresh hops is shown below in Figure 3-1.

Figure 3-1 Hops sample used during the AFD experiment

3.1.2 Ice

The ice was prepared using distilled water (CAS-7732-18-5) from Thermo Fisher Scientific, Auckland, New Zealand. The water was poured into a 3D-printed ice cube holder of dimensions 28 mm × 28 mm × 20 mm (W × L × H) and kept inside the experimental set-up (see Section 4.5) to freeze. The ice cube holder with ice is shown in the Figure 3-2 .

Figure 3-2 Ice cube holder with ice

3.1.3 Silica gel

Self-indicating (active-orange, exhausted-green) silica gel (CAS-7631-86-9) of size 2-6 mm from Thermo Fisher Scientific, Auckland, New Zealand was used in the experiments. Fresh silica gel from the company packaging was only used for all the experiments to avoid any variations in initial moisture content.

3.2 Methods

3.2.1 Measurement of weight loss during AFD

An analytical weighing balance (Entris II Balance 120gx0.1mg SARBCE124I-1S) from Sartorius, Gottingen, Germany with maximum capacity of 120 g, resolution of 0.1 mg, repeatability of ± 0.08 mg, and with accuracy class I is used. The calibration is verified and maintained by Wedderburn Scales Ltd, Palmerston North, New Zealand. The data were logged by a data logger application made with LabVIEW. Weight of the sample was captured every second.

3.2.2 Measurement of temperature and RH of air

Measurement of temperature and RH of air was done using wireless sensors from Seeed Technology Co. Ltd, California, USA - (SenseCAP Wireless Air Temperature and Humidity Sensor – LoRaWAN - LoRa-S-915-TH-01). The air temperature sensor has a range of -40 ^{o}C to +85 ^{o}C, a resolution of 0.1 ^{o}C and an accuracy of ±0.2 ^{o}C. The air humidity sensor has a range of 0 to 100 % RH, a resolution of 1 % RH and an accuracy

of ±1.5 % RH. The current consumption of the sensors during the data transmission is 120 mA, and 5 µA while in sleep mode. It has a battery voltage of 3.6V and a battery capacity of 19 Ah. The calibrations of the RH sensors were verified by keeping the sensors in an airtight box in equilibrium with standard salt solutions (LiCl, MgCl, NaCl) with known equilibrium RH values. The measurements from the sensors were compared with the known equilibrium values of the salt solutions. The calibration of the temperature readings of the sensors were verified by comparing the measurement of temperature by the sensors with that of the calibrated precision RTD thermometer (Center 376 from Center Technology Corp, Taipei, Taiwan) available in the lab for calibrating similar sensors. The measurement readings from the sensors were continuously transmitted across the internet and logged on the online portal from SenseCAP. The readings can be viewed in real-time and can be downloaded after each experiment.

3.2.3 Measurement of temperature of ice

The ice temperature during the experiment is measured using a button-like temperature sensor (Thermochron iButton - DS1922L) from Maxim Integrated, California, USA, which has inbuilt storage for measurement readings. The sensor has a range of -20 °C to +85 °C, a resolution of 0.0625 °C and an accuracy of ±0.035 °C. It has a storage capacity of 512 bytes and can store 8192 8-bit or 4096 16-bit readings.

3.2.4 Measurement of air velocity

Air velocity in the drying chamber near the hops was measured using a hotwire thermo-anemometer, (Digi-Sense 20250-16, Hot Wire Thermo-Anemometer from Cole-Parmer, Illinois, USA). The air velocity measurement has a range of 0.1 to 25.0 m/s, a resolution of 0.01 m/s and an accuracy of ± (5% + 1 digit) reading.

3.2.5 Measurement of RH and temperature of air near hops

The air temperature and RH near hops during the experiment is measured using a button-like temperature sensor (Hygrochron iButton - DS1923) from Maxim Integrated, Illinois, USA, which has an inbuilt storage for measurement readings. The temperature sensor has a range of -20 °C to +85 °C, a resolution of 0.0625 °C and an accuracy of ±0.035 °C. The air humidity sensor has a range of 0 to 100 % RH, a resolution of 0.6 % RH and an accuracy of ±0.5 % RH. It has a storage capacity of 512 bytes and can store 8192 8-bit or

4096 16-bit readings. The calibration is done same as for the RH sensors as described above for SenseCAP sensors.

3.2.6 Area of Hops

The area for hops was measured on dry a basis. Three sets of raw hop samples were dried in an oven and then weighed. It is assumed that there is only a negligible shrinkage for the petals during drying. The petals and all the parts were separated and kept flat on a white paper and scanned. The scanned image was analysed using ImageJ software (developed by National Institute of Health, Maryland, USA) to calculate the total area. The total surface area including both sides of the petals was found to be 78.1 m^2/kg of dry hops with a standard deviation of 1.4 m^2/kg.

3.2.7 The thickness of hops petals

The petal thickness was measured using an optical microscope OLYMPUS BX53 from OLYMPUS, Tokyo, Japan with inbuilt image analysis and measuring tool. A thin cross section of the fresh hops' petal was cut and put carefully on the glass slide for the measurement. Five sets of measurement were taken on each of the five cross sections of the hops' petals. The thickness of the hops' petals was found to be 81 microns with a standard deviation of 36 microns.

3.2.8 The density of hops – pycnometer

The density of hops was measured on a dry basis using a gas displacement pycnometry system, AccuPyc II 1340 from Micrometrics Ltd, Georgia, USA. The sample was dried in an oven first and then analysed for density. Three repetitions were done for the measurement. The dried hops density was found to be 1487.2 kg/m^3 with a standard deviation of 2.0 kg/m^3.

3.2.9 Moisture content hops

The moisture content was measured according to the standard procedure by the Association of Official Analytical Chemists standard method no. 934.06, by placing the hops sample in vacuum oven (EV 018 from NUVE, Ankara, Turkey) at 70 ^oC for 6 hours (Horwitz, 2010). Three sets of hops samples were used and the moisture content in the fresh hops was found to be 80.4 % on dry basis with a standard deviation of 1.1%.

3.2.10 Water activity of hops

The water activity of the hops is measured using the water activity meter, AQUALAB 4TE from Decagon Devices Inc, Pullman, USA. It has an accuracy of ±0.003 a_w. The equipment setting was kept for 3 repetitions of the measurement and display the average value. The water activity of the fresh hops found to be 0.987 a_w.

Chapter 4 Development of Experiment Apparatus

4.1 Introduction

High-quality temporal weight loss data is essential to study the kinetics of the atmospheric freeze-drying process and identify the rate limiting mechanism involved. However, the AFD drying is both a cold and slow process, which introduces two problems. First, while a high-resolution balance is needed to pick up small changes in sample weight, available laboratory balances are not designed for such cold temperatures, and they are also susceptible to background vibration and noise. Second, the drying period is long, possibly up to several weeks, and so electrical drift may occur.

To date, there are no AFD experimental systems that record high-accuracy experimental data without disturbing the drying process. In the literature, most data were collected by intermittent weight measurement by removing the sample from the drying chamber. This disturbance usually brings variations in sample temperature, drying air temperature and humidity.

In the current study of AFD of ice and hops with silica gel as adsorbent, the system has been designed to run undisturbed throughout each experiment with continuous logging of the system conditions. The following sections show how the experiment set up was developed.

4.2 Maintaining freezing conditions

AFD occurs in sub-zero temperatures. As the purpose of the current study is to identify the control mechanisms in the AFD process, the drying temperature is both a control parameter and an experimental variable. One easy and cost-effective method is to use a chest freezer to maintain constant sub-zero temperature, contain the AFD chamber, and establish controllable air environment. A 376 litres chest freezer from Fisher & Paykel Ltd was selected for the experiment set-up (376L Chest Freezer, RC376W1, Fisher & Paykel Ltd, Auckland, New Zealand) with a temperature range of -26 to -12 ^{o}C. The size of the chest freezer was selected based on the internal size relative to the two-box experiment unit (as discussed in the section 4.5) to be housed inside the freezer. The experiment set-up general arrangement can be seen in Figure 4-1.

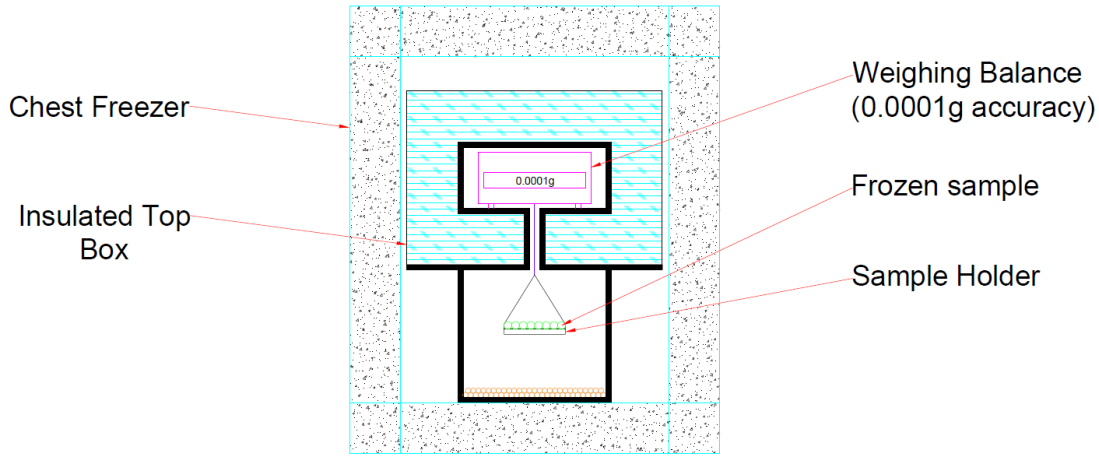

Figure 4-1 Side view of the experiment set-up with the polycarbonate set-up inside the chest freezer (376L, Fisher & Paykel)

4.3 Weight loss measurement

To continuously measure small weight changes from a few grams of sample over several weeks, requires both a high-precision weighing balance and an experimental set-up in a static air environment. Running the experiments in static conditions would help avoid possible disturbances of moving air.

The selected analytical weighing balance described in section 3.2.1 has maximum capacity of 120 g and resolution of 0.1 mg, which is an improvement on the best resolution of 1 mg for an AFD experiment by (Roth et al., 2001). This balance has top pan and also a hook at the bottom. In these experiments, a sample holder was hung from the bottom hook.

AFD requires the drying process to be conducted in sub-zero conditions, but the analytical weighing balance manufacturer specifies the operating temperature range to be 5 °C to 40 °C. To meet this specification, the design was developed as shown in Figure 4-2 where the balance is housed in an insulated top box with temperature controlled to 8°C using resistors (ARCOL HS50, Arcol UK Ltd, UK) and a PID temperature controller (UR3274Sx, Wachendorff Prozesstechnik GmbH & Co. KG, Germany). The heating system is shown in Figure 4-4.

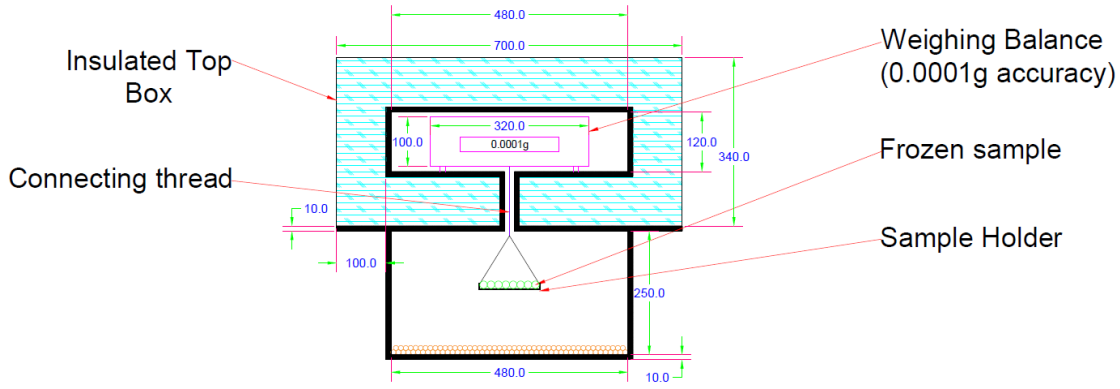

Figure 4-2 Front view of the experiment set-up

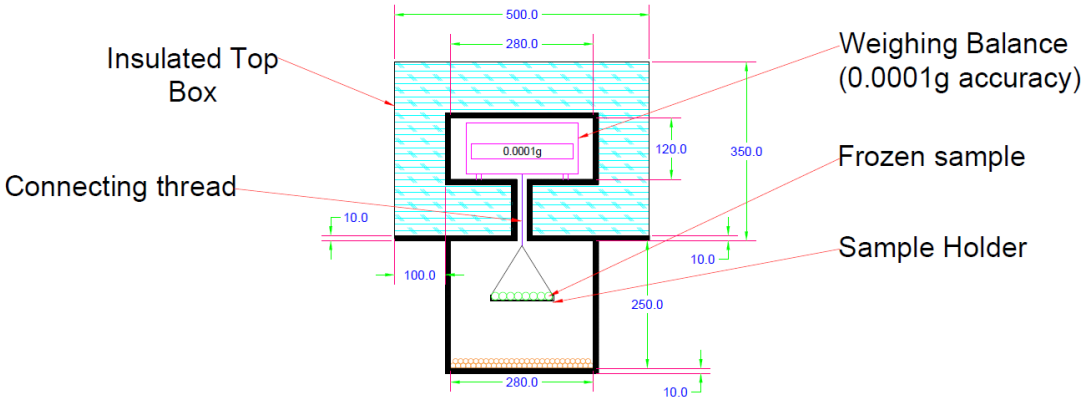

Figure 4-3 Side view of the experiment set-up

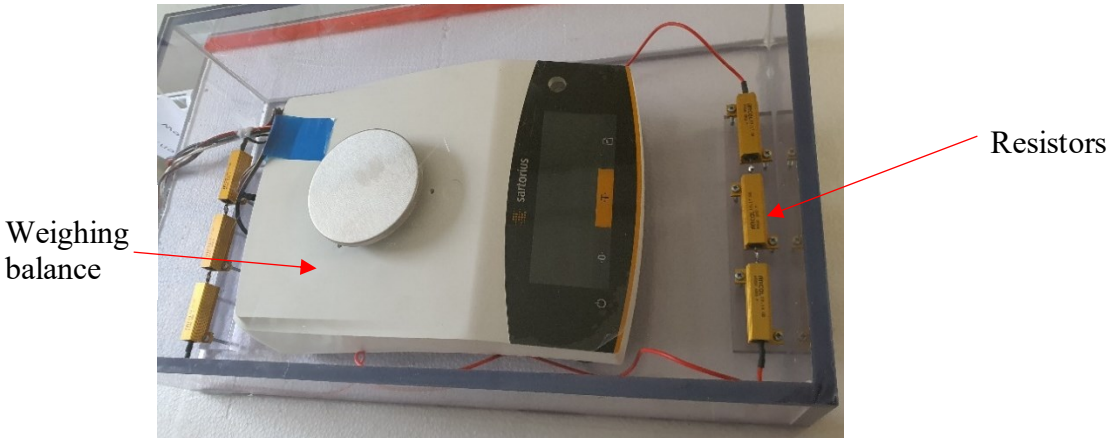

Figure 4-4 Top view of the experiment set-up top box

The bottom box is uninsulated as its temperature is controlled by the chest freezer. It contains the sample holder hanging by a connecting thread directly underneath the balance. The connecting thread and the narrow tube (a polycarbonate connecting tube of

inner diameter of 12.7 mm and a length of 100 mm) minimise the conduction of heat between the cold bottom box and the warm top box. A consequence of having the warmer top box above the colder bottom box is that the more buoyant warmer air is above the colder air and prevents natural convection of air through the connecting tube. For any moisture ingress up from the bottom box to the top box, some adsorbent is kept in the top box.

4.4 Air RH and temperature measurement

For continuous measurement of air temperature and RH, the wireless sensors described in section 3.2.2 were used. Their advantage is that holes were not needed in the walls of the experiment set-up and so decreased the chance of moisture seepage into the drying chamber. Their disadvantage is that they are bigger in size compared to non-wireless sensors. This is due to the additional electronics for the wireless transmission of data and the battery to power it. There is about half a watt of power consumption by the sensor for a couple of seconds every 5 minutes for data transmission and a portion of this would be heat energy. This is very low to be considered as a source of heat in the system. The wireless sensors communicate with a data logger which is connected to the internet thus making it easy to collect the data and monitor the process remotely in real time. The data can be seen in the SenseCAP online portal and can be downloaded from the portal as a spreadsheet. The minimum interval between the readings can be adjusted where the least value is 5 mins, even though it sometimes takes some random readings in an interval below 5 mins too.

4.5 Design and sizing of the two-box unit

The sizing of the two boxes for the weighing balance and AFD drying of the sample was done using SolidWorks software so that the experiment set-up can be visualized for the placement of the balance and the sensors, and to check whether there was enough space before the set-up was fabricated. The weighing balance and air RH and temperature sensor dimensions were taken from the respective product specification sheets, and models were developed in the SolidWorks. The box and connecting unit were designed to accommodate equipment as shown in Figure 4-5 and Figure 4-6.

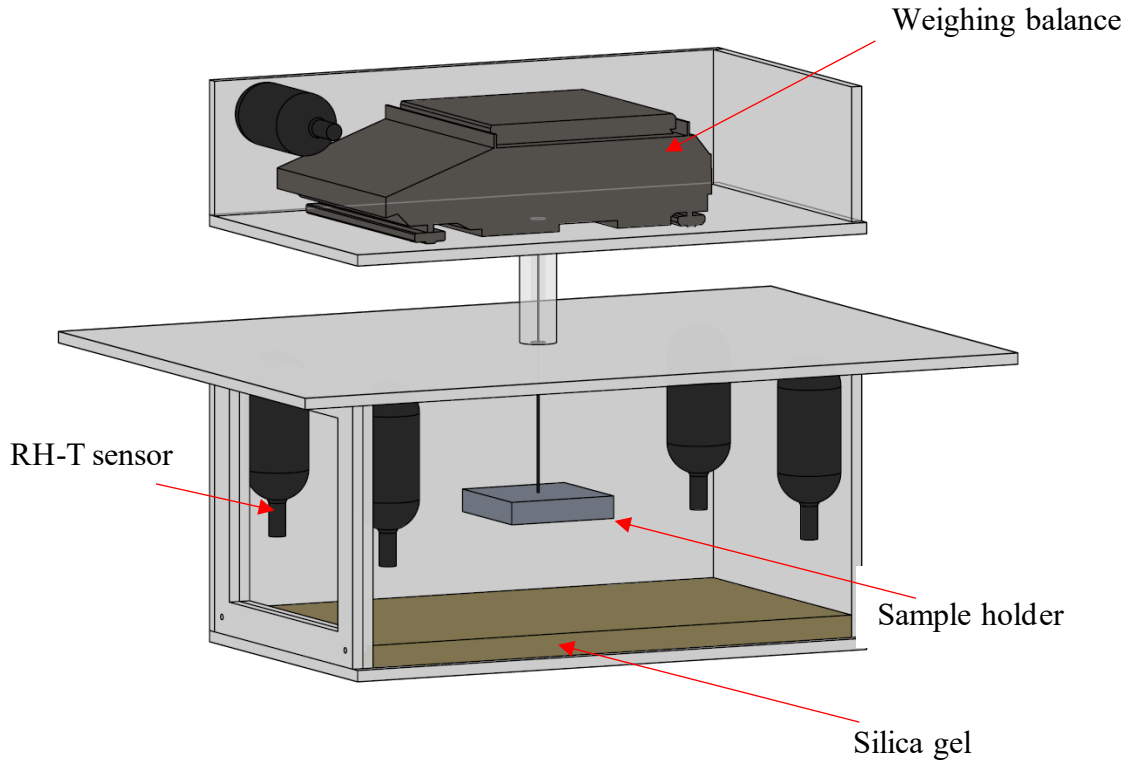

Figure 4-5 Supressed view of the experiment set-up

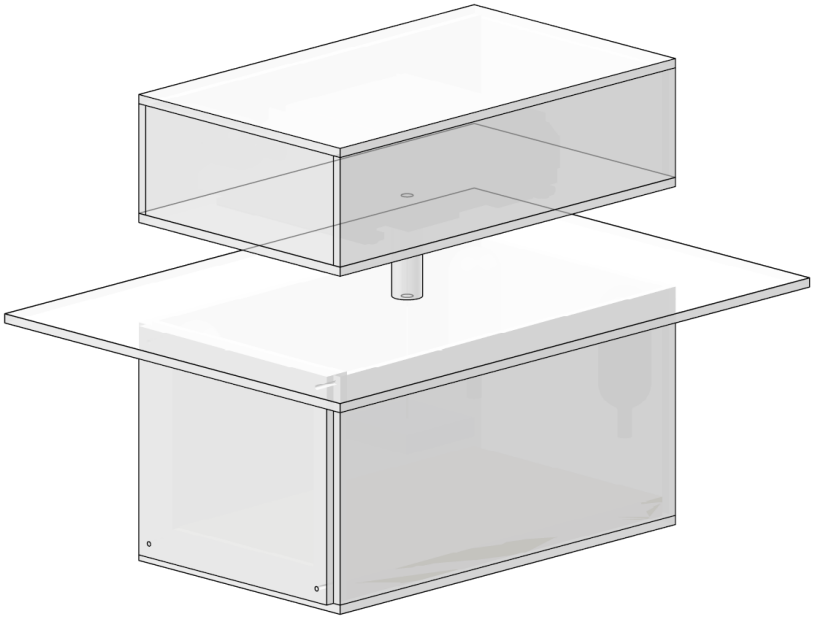

Figure 4-6 Dimetric view of the experiment set-up

Polycarbonate clear sheets were considered as the material of choice for the fabrication of the apparatus for availability and ease of fabrication. The polycarbonate sheets had a thickness of 10 mm, a thermal conductivity of 0.20 W/mK and a thermal capacity of 1200 J/kgK. The fabricated two box unit is shown in the Figure 4-7.

The silica gel was placed at the floor of the bottom box as a single layer. The quantity of silica gel (200g) was calculated such that when all the moisture in the product has sublimed and adsorbed onto the adsorbent, the equilibrium air moisture content in the chamber should be at 5% of the saturated air moisture content for the air temperature.

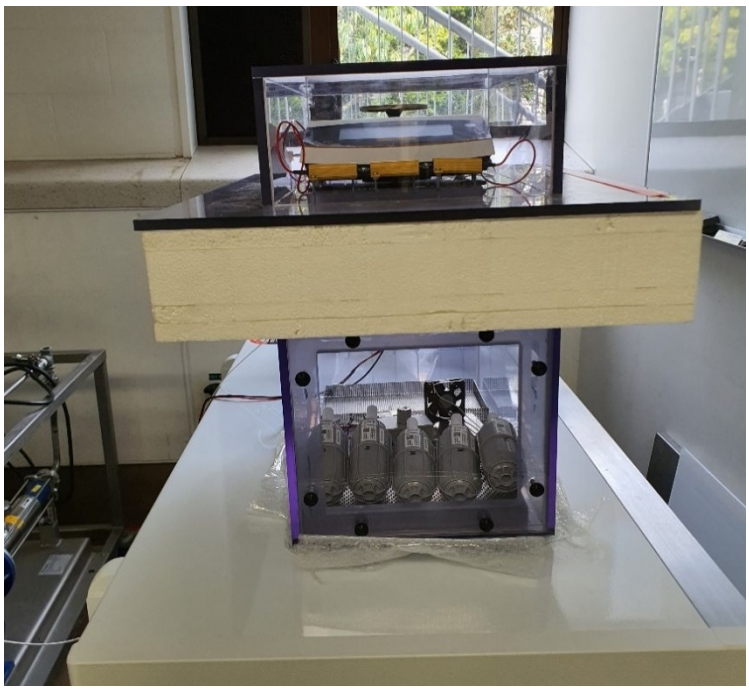

Figure 4-7 Fabricated two box unit for the experiment

The final specifications for each side of the boxes were collated and pieces of polycarbonate sheet were cut and joined in the workshop; the exploded view is shown in Figure 4-8 and sizing of the material is given in the Table 4-1.

The two-box unit with the top box insulated on all sides with 100 mm (foamed polystyrene) sheets was housed inside the chest freezer. The weight of the sample was continuously logged along with the air temperature and humidity. A small brushless DC fan of 12V, 0.19A (Model– 06015VA-12P-AT, NMB Technologies, Michigan, USA) with a dial control was installed in the upper wall of drying chamber to perform experiments for the cases when air circulation is required. The fan is located 200 mm away from the centre and the air blows parallel to the upper wall towards the centre. A trial run was performed, and the system was found to be working as expected. Changes in atmospheric pressure with weather are assumed to have no effect on the experimental system, as no effect was observed. Since the set-up was kept inside the freezer, it was

only dependent on the freezer temperature. The main experiments and the results are discussed in the following chapters for ice and hops systems.

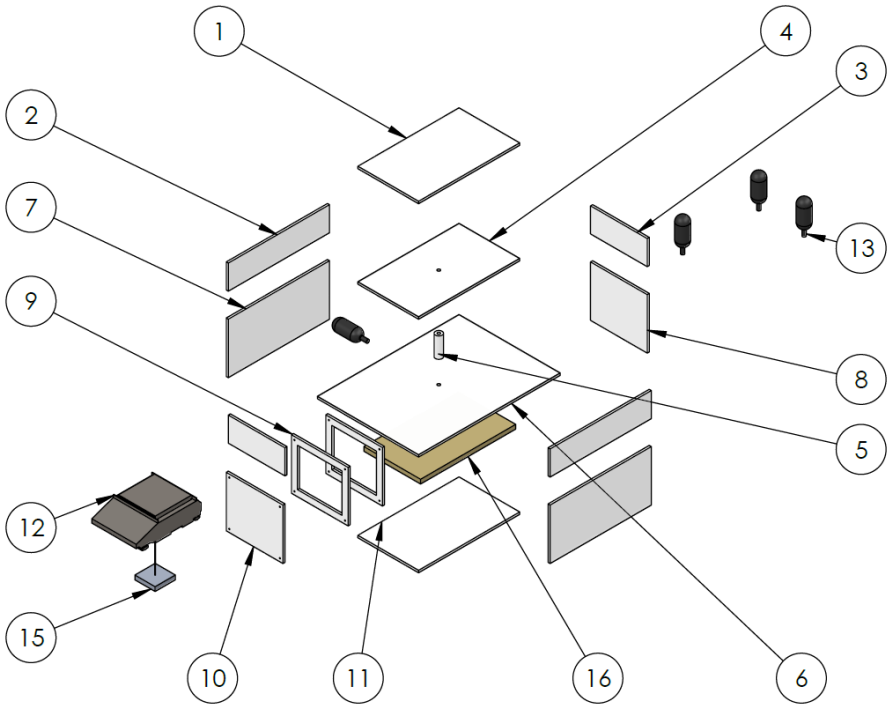

Figure 4-8 Exploded view of the experiment set-up

Table 4-1 Bill of materials of the experiment set-up

ITEM NO.	*PART NUMBER*	*QTY.*	*Length (mm)*	*Width (mm)*	*Thickness (mm)*
1	AFD Top box_top part	1	500	300	10
2	AFD Top box_side part_large	2	500	120	10
3	AFD Top box_side part_small	2	280	120	10
4	AFD Top box_bottom part	1	500	300	10
5	AFD Middle tube	1	100	12.7	2.5
6	AFD Bottom box_top part	1	700	500	10
7	AFD Bottom box_side part_large	2	500	250	10
8	AFD Bottom box_side part_small	1	280	250	10
9	AFD Bottom box_side part_small frame	2	280	250	10
10	AFD Bottom box_side part_door	1	280	250	10
11	AFD Bottom box_bottom part	1	500	300	10
12	Weighing Balance	1			
13	Temp and Humidity Sensor	5			
14	Thread	1			
15	Sample plate	1			
16	Silica gel box	1			

Chapter 5 Model Development

During atmospheric freeze-drying of plant material ice sublimes to water vapour at the ice surface, then diffuses through the plant matrix and out into the bulk air. Opposing this outflowing mass transport is the inflowing heat transport which is needed to supply the latent heat of sublimination. Each flow is driven by a gradient, a vapour pressure gradient between the ice surface and the bulk air, and a temperature gradient in the opposite direction. Here, each of the resistances to mass and heat transfer are assumed to be additive; that is, there exists an internal resistance within the leafy material from the ice surface to the leaf surface, and an external boundary layer resistance from the leaf surface to the bulk air.

Together, alongside the material and state properties, the gradients and the resistances of mass and heat transport define the kinetics. To help understand which are more or less rate controlling in AFD, this chapter develops a heat and mass transfer model to validate against experimental data. The model has been developed in two stages; first, a model of pure ice sublimation in the AFD system in order to identify the external boundary layer resistances; and second, to model the atmospheric freeze drying of hops, which is the leafy model material used in this thesis. By doing this in two stages, the additional internal resistances to heat and mass transfer within the leafy material can be added. The important assumption here is that the boundary layer resistance from the leaf surface to bulk air is equal to the boundary layer resistance for pure ice sublimation from its surface to the bulk air. The model is carefully constructed, because assumptions must be included about the geometry of the apparatus, which affects the external boundary layer thickness. In the second stage, assumptions are also required about the way internal resistance changes with the extent of sublimation within the leaf. The model also includes silica gel adsorption of water vapour which, as will be shown, maintains the mass transfer gradient for sublimation. The resistance terms are then able to be extracted by comparing the models to the experimental data.

The model is expressed as a set of ordinary differential equations (ODEs). With the model tuned to the best fit resistances, it can then predict the mass of ice remaining and the change in air relative humidity in the AFD chamber during the whole drying process.

5.1 Ice sublimation in the AFD apparatus

For the ice experiments, the experimental system is visualized in Figure 5-1. The ice sample is held in a 3D printed container with dimensions 28 × 28 × 20 mm (W × L × H), which sits on the sample holder with internal dimensions of 74 × 93 × 15 mm (W × L × H), which in turn is 100 mm above the silica gel adsorbent. The whole system sits inside a freezer at -12 °C. The dimensions of the drying chamber are 280 × 480 × 250 mm (W × L × H).

This experimental system is three-dimensional; however, it is simplest for a model to assume that the system is one-dimensional, and this approach is taken here. In order to do this, a series of assumptions is required, which reduce model complexity without losing accuracy. Here, the principles behind the assumptions concerning heat transfer are discussed first, followed by those concerning mass transfer. Afterwards, a detail list of assumptions is provided.

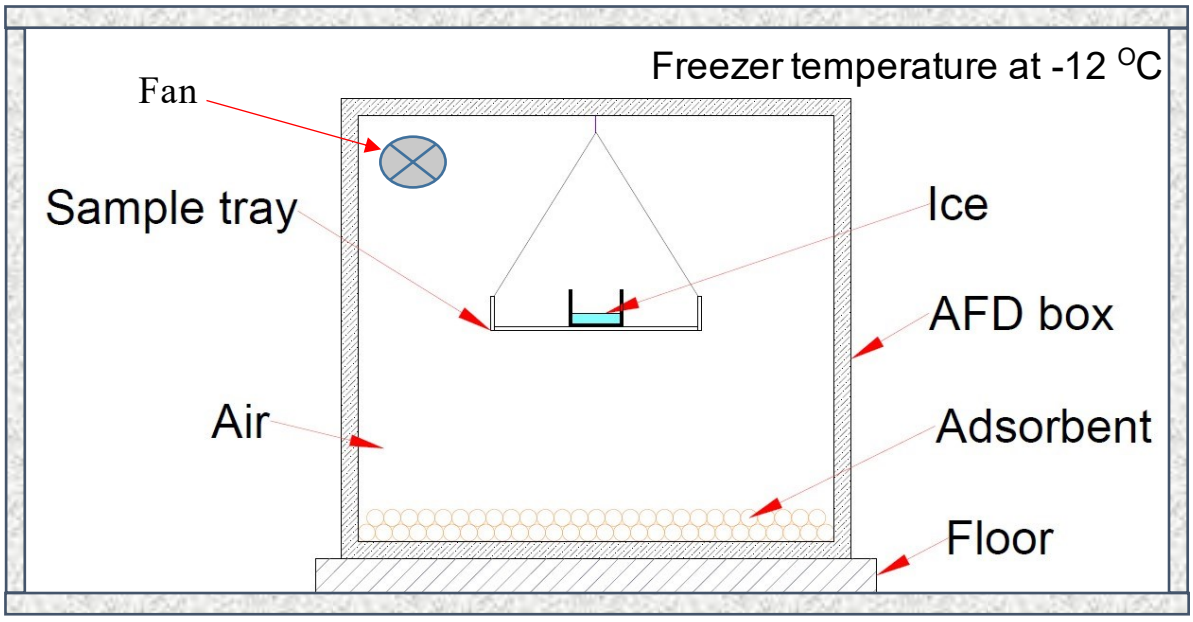

Figure 5-1 Diagram of the ice sublimation in the AFD drying chamber

The one-dimensional assumption is straightforward for mass transfer, where the ice in the sample holder shown in Figure 5-1 sublimes to water vapour only from its exposed surface. Vapour ends up adsorbed by the silica. Here, two quiescent boundary layers are relevant, BL_1 between the ice surface and the bulk air, and BL_2 between the bulk air and the surface of the silica gel bed. The bulk air is assumed well mixed, as explained below.

For heat transfer, two ameliorating assumptions are required. First, the surrounding freezer is assumed to keep the silica gel and the air at the freezer set point temperature, because both have high contact surface areas with the AFD box walls. The silica gel is a thin layer of particles sitting directly on the chamber wall. For the air, in addition to the high wall area, it is also assumed to be naturally convecting and thus well mixed, and so it can be assumed that heat transfer into the chamber is fast compared to the heat transfer needed to drive sublimation. This constant temperature assumption removes the necessity to describe a heat transfer boundary layer resistance between the silica gel and the air. The second ameliorating assumption concerns heat transfer at the ice where, to convert it from a three dimensional to a one-dimensional problem, the ice is assumed to be a thin sheet. This assumption means edge effects can be neglected. The ice therefore can be assumed to accept heat from the bottom and the top, but not through the sides (see Figure 5-1). Heat flows through the bottom from the bulk air as conduction across a quiescent boundary layer, followed by conduction through the tray and the wall of the sample holder. Heat flows from the top from the bulk air as conduction across a quiescent boundary layer. For model simplicity, these top and bottom quiescent boundary layer thicknesses are assumed the same, and also equal to the mass transfer boundary layer BL_1 described above. A further simplifying assumption is that, as ice accepts heat, the conduction through the ice is fast compared to the surface heat transfer. This is consistent with a low Biot number, i.e., the ratio of convective to conductive heat transfer. This allows the assumption that the ice has a uniform temperature, although during sublimation, it will be lower than the bulk air temperature.

The above assumption that the air and silica gel temperatures are constant at the freezer temperature, while the ice temperature can vary, is also supported by the much larger thermal mass of the silica. The thermal properties for ice, air, and silica gel are given in Table 5-1. At ten times the thermal mass, despite the similar values of the latent heat and heat of adsorption, a change in ice temperature of 1°C corresponds to only a 0.1°C change in the silica gel.

Table 5-1 Material thermal properties

Material	Mass (g)	Specific heat capacity (J/kg K)	Thermal mass (J/K)
Ice	12.7	2108	26.8
Air	45.7	1005	45.9
Silica gel	200	1130	226

In the same way a 1°C change in ice temperature corresponds to a 0.5 °C change in the air temperature; however, the air has a high contact surface with the walls of the chamber, and is undergoing natural convection, and so therefore it is reasonable to assume it remains constant at the freezer temperature for the purpose of the model.

The assumption that the heat transfer resistance can be neglected across the silica to air boundary layer is possible because the thermal argument above shows that the temperature gradient would in reality be low, and that the conductive heat transfer from the silica gel to the drying chamber wall will dominate heat transfer from the silica gel. Thus, only a fraction of heat would move from the silica gel to the air through the boundary layer, therefore negating the need for a silica gel to air boundary layer.

The assumption that the air temperature is equal to the freezer temperature is further supported by considering the surface areas. The air is directly in contact with the drying chamber walls on four sides, whereas it is in contact with the silica gel on only one wall. This was also observed in the experiments reported in Chapters 6 and 7.

Taken in concert the supplying assumptions made allow the complex three-dimensional system to be reduced to a one-dimensional model shown in Figure 5-2 schematically. Thus, four variables change during drying, T_{ice}, M_{ice}, X_{air} and $X_{silica\ gel}$.

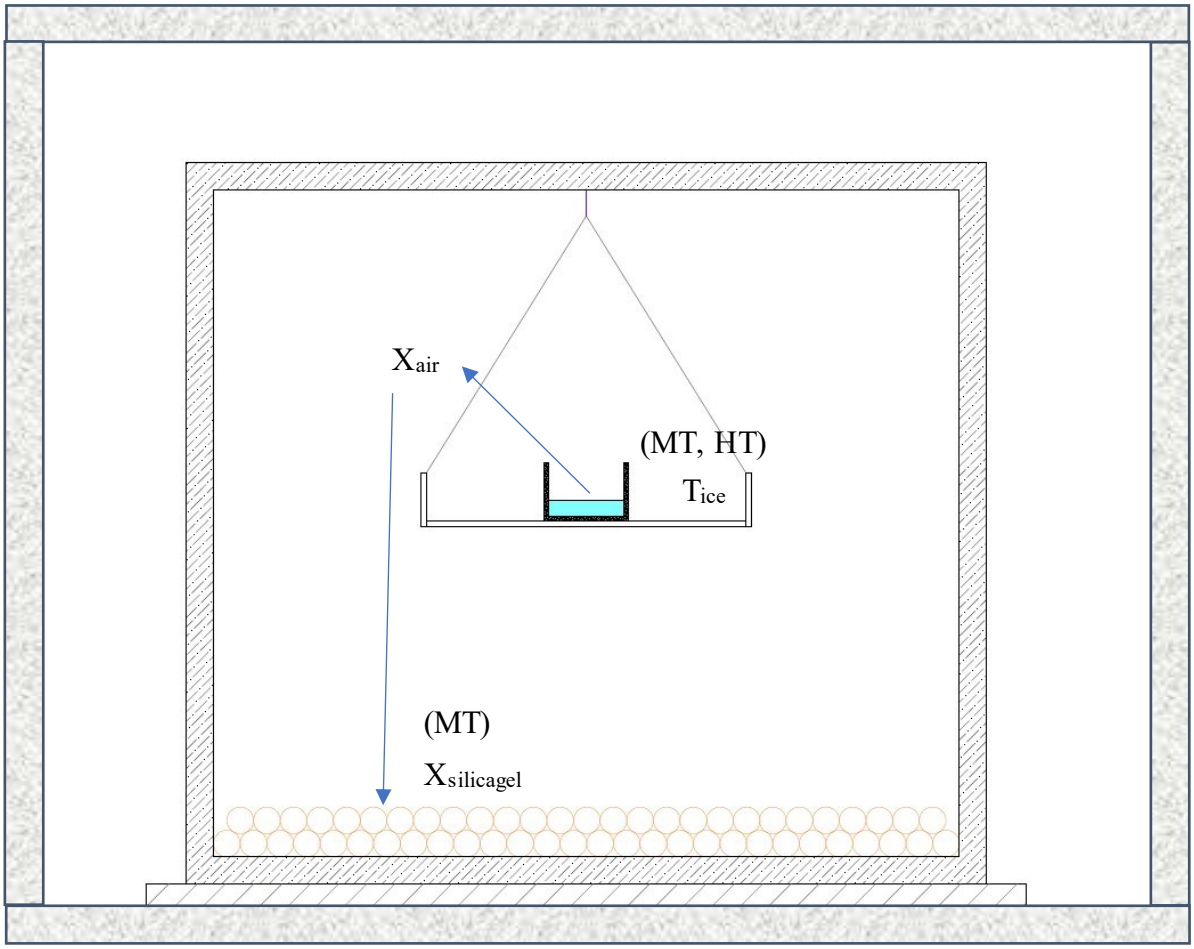

Figure 5-2 Diagram of the ice sublimation in the AFD drying chamber with resistances

5.1.1 Assumptions and Parameters

The following assumptions define the model. Refer also Figure 5-2.

1. The system has constant mass, i.e., there is no exchange of mass with surroundings.
2. All moisture is initially in the ice, i.e., the silica gel and air are initially dry.
3. Moisture only exists in the ice, air, or silica gel, i.e., no condensation occurs on the side walls.
4. Ice sublimes or condenses only at the ice-air interfacial surface.
5. The moisture content of the bulk air is spatially uniform.
6. The moisture content of the silica gel is spatially uniform.
7. The moisture content only varies in the mass transfer boundary layers between the ice surface and the bulk air, and between the bulk air and the silica gel. This means the resistance to mass transfer is limited to these boundary layers.

8. The initial temperature of the system is constant and equal to the external freezer temperature.
9. The temperature of the air and the silica gel are always constant and equal to the external freezer temperature. This means a heat transfer boundary layer is not required between the bulk air and the silica gel.
10. The temperature of the ice is spatially uniform. This is consistent with a low Biot number, i.e., the ratio of convective to conductive heat transfer, at the ice-air interface, and at the tray-air interface.
11. The temperature only varies in the heat transfer boundary layer between the ice surface and the bulk air, and between the tray surface and the bulk air. The boundary layer thickness of these boundary layers is assumed to be the same. This means the resistance to heat transfer is limited to these boundary layers.
12. Following from assumption 10, the temperature gradient is assumed the same for both the ice surface to bulk air boundary layer and the tray surface to bulk air boundary layer.
13. The specific heat capacities of the ice, silica gel and air are independent of temperature for the operating range.
14. The heat of sublimation is independent of temperature for the operating range.

The system can be defined by the parameters in Table 5-2.

Table 5-2 System nomenclature with units and parameter classes

Symbol	Description	Units	Type
A_{ice}	Area of Ice	m^2	SI
b_{box}	width of box	m	SI
$C_{p,ice}$	Specific heat capacity of ice	J/kg/K	SI
$D_{H2O\text{-}air}$	Diffusivity of water vapour in air	m^2/s	CV
$D_{H2O\text{-}eff\text{-}silicagel}$	Effective diffusivity of water vapour in silica gel	m^2/s	CV
$D_{H2O\text{-}silicagel}$	Diffusivity of water vapour in silica gel	m^2/s	CV
h_{air}	Heat transfer coefficient for air	$W/m^2/K$	SI
$K_{MT\text{-}silicagel}$	Mass transfer coefficient of H_2O for silica gel	m/s	CV
l_{box}	Length of box	m	SI
$l_{ice\text{-}air}$	Effective path length for diffusion in ice sublimation	m	CV
$l_{ice\text{-}air,o}$	Initial effective path length for diffusion in ice sublimation	m	SI
M_{ice}	Mass of ice	kg	D

$M_{ice,i}$	Initial mass of ice	kg	IV
$M_{silicagel}$	Mass of Silica gel (dry basis)	kg	SI
P_{air}	Vapour pressure of H_2O in air	Pa	CV
$P_{air-sat}$	Saturated vapour pressure of H_2O in air	Pa	CV
P_{ice}	Saturated vapour pressure of water over ice	Pa	CV
P_{total}	Total system pressure	Pa	SI
RH_{air}	RH of air		CV
$r_{silicagel}$	Average radius of silica gel	m	SI
t	Time	s	I
T_{air}	Temperature of air	K	SI
T_{ice}	Temperature of ice	K	D
$T_{ice,o}$	Initial temperature of ice	K	IV
$T_{silicagel}$	Temperature of silica gel	K	SI
u_{air}	Air velocity	m/s	SI
V_{box}	Volume of air in box	m^3	SI
V_{ice}	Volume of ice	m^3	CV
$V_{ice,o}$	Initial volume of ice	m^3	SI
X_{air}	Moisture content in bulk air (dry air basis)	kg/kg	D
$X_{air,o}$	Initial moisture content in bulk air (dry air basis)	kg/kg	IV
$X_{ice\ surf}$	Moisture content at ice surface in equilibrium with the air (dry air basis)	kg/kg	CV
$X_{silicagel}$	Moisture content in silica gel (dry silica basis)	kg/kg	D
$X_{silicagel,o}$	Initial moisture content Silica gel (dry silica basis)	kg/kg	IV
$X_{silicagel,equil}$	Moisture content of silica gel in equilibrium with air (dry silica basis)	kg/kg	CV
z_{box}	Height of box	m	SI
λ_{sub}	Heat of sublimation of Ice	J/kg	SI
ρ_{air}	Density of air	kg/m^3	CV
ρ_{ice}	Density of ice	kg/m^3	SI

Parameter classes

Type	Name	Definition
I	Independent	Value stands irrespective of any other variable
D	Dependent	Value changes as a function of independent variable, history not important
CV	Consequential value	Value changes as a function of independent variable, history important
SI	System input	Value defined by external operator
IV	Initial value	Initial value

The above system, as constrained by its assumptions, means that four ordinary differential equations are needed to model the time dependence of atmospheric freeze drying (Table 5-3 and Table 5-4). A series of consequential equations (also known as constitutive equations) are also needed to relate parameters to system inputs, which are either measured variables, fundamental constants, or empirical constants (Table 5-5).

Table 5-3 Defining the number of equations

1	Independent variable	
4	Dependent variables	4 ODEs required
4	ODEs	4 Initial conditions
13	CV's	at least 13 algebraic equations required
17	SI's	need estimates for these parameters

Here $l_{ice\text{-}air,o}$ (initial effective path length) which is an SI type parameter in the model, will be used as a fitting parameter with the experiment data.

Table 5-4 shows the ODE equations.

Table 5-4 List of ODEs

Mass balance of ice				
rate of accumulation of mass in ice sample	=	*rate of moisture added to ice from air by condensation*	-	*rate of moisture lost to air through sublimation*
$$\frac{dM_{ice}}{dt} = 0 - D_{H2O-air}\ A_{ice}\ \frac{[X_{ice\,surf} - X_{air}]}{l_{ice-air}}\ \rho_{air}$$				*5.1*
Note: In a very dilute system, the unidirectional diffusion of a component through stagnant inert gas can be considered as equivalent to a system undergoing equimolar counter current diffusion (Green & Southard, 2019). Ice sublimation in the context of AFD of hops is considered a dilute system and thus, to simplify the maths, moisture diffusion is appropriately modelled as an equimolar counter current process.				
Mass balance of moisture in air				
rate of accumulation of moisture in air	=	*rate of moisture added to air due to sublimation*	-	*rate of moisture removed by adsorption by silica gel*

$$V_{box}\ \rho_{air}\ \frac{dX_{air}}{dt} = D_{H2O-air}\ A_{ice}\ \frac{[X_{ice\ surf} - X_{air}]}{l_{ice-air}}\ \rho_{air} - M_{silicagel}\ \frac{15}{r_{silicagel}^2}\ D_{H2O-eff-silicagel}\ [X_{silicagel,equil} - X_{silicagel}] \quad 5.2$$

In equations 5.2 & 5.3, the rate of adsorption by the adsorbent is based on the linear driving force model (Ouchi et al., 2019), and the term $\frac{15}{r_{silicagel}^2}$, represents the parabolic concentration profile of moisture inside a spherical bead of silica gel.

Mass balance of moisture in silica gel

rate of accumulation of moisture in silica gel = *rate of moisture added adsorption by silica gel from air* - *moisture lost desorption by silica gel*

$$M_{silicagel}\ \frac{dX_{silicagel}}{dt} = M_{silicagel}\ \frac{15}{r_{silicagel}^2}\ D_{H2O-eff-silicagel}\ [X_{silicagel,equil} - X_{silicagel}] - 0 \quad 5.3$$

Heat balance in ice

rate of accumulation of heat in ice = *rate of heat entering ice from air* - *rate of heat leaving ice by sublimation*

$$\frac{d(M_{ice}\ \times\ Cp_{ice}\ \times\ T_{ice})}{dt} = 2A_{ice}\ h_{air}\ [T_{air} - T_{ice}] - \lambda_{sub}\ D_{H2O-air}\ A_{ice}\ \frac{[X_{ice} - X_{air}]}{l_{ice-air}}\ \rho_{air}$$

$$M_{ice}\ C_{p,ice}\frac{dT_{ice}}{dt} = 2A_{ice}\ h_{air}\ [T_{air} - T_{ice}] - [\lambda_{sub} - T_{ice} \times C_{p,ice}]\ D_{H2O-air}\ A_{ice}\frac{[X_{ice\ surf} - X_{air}]}{l_{ice-air}}\ \rho_{air} \quad 5.4$$

Table 5-5 shows a list of constitutive equations for ice.

Table 5-5 List of constitutive equations for ice

Vapour pressure of H_2O near ice surface– P_{ice}

$$P_{ice} = \frac{exp(43.494 - \frac{6545.8}{T_{ice} + 4.85})}{(T_{ice} + 594.85)^2}\ ;\ T <= 0\ ^oC \quad 5.5$$

Pressure temperature relationship for saturated vapour pressure of water over ice at any given temperature (Huang, 2018)

Saturated vapour pressure of H_2O in air – $P_{air\ sat}$

$$P_{air\_sat} = \frac{exp(43.494 - \frac{6545.8}{T_{air} + 4.85})}{(T_{air} + 594.85)^2} \; ; \; T <= 0 \;\; ^oC$$	5.6
Pressure temperature relationship for saturated vapour pressure of water over ice at any given temperature (Huang, 2018)	
Diffusion coefficient of H_2O in air - $D_{H2O\text{-}air}$	
$$D_{H2O-air} = 1.735 \times 10^{-9} \times (T_{air})^{1.685}$$	5.7
This relationship is obtained from the literature (Pesaran & Mills, 1987)	
Effective diffusion coefficient of H_2O in silica gel - $D_{H2O\text{-}eff\text{-}silicagel}$	
$$D_{H2O-eff-silicagel} = \frac{r_{silicagel}}{15[\frac{r_{silicagel}}{15\ D_{H2O-silicagel}} + \frac{1}{K_{MT-silicagel}}]}$$	5.8
This relationship is obtained from the literature (Ouchi et al., 2019). The effective diffusion coefficient is the overall diffusion coefficient for mass transfer from the air to the silica gel. It is assumed that the mass transfer resistance for moisture transfer from the bulk air to the silica gel can be defined as a sum of the resistance encountered in the boundary layer near the silica gel where it can be represented by the mass transfer coefficient and the resistance in the silica gel bead denoted by the diffusion coefficient for moisture in silica gel.	
Diffusion coefficient of H_2O in silica gel - $D_{H2O\text{-}silicagel}$	
$$D_{H2O-silicagel} = 5.58 \times 10^{-8} \; exp\,(-0.45 \frac{42000}{8.314\ T_{air}})$$	5.9
This relationship is obtained from the literature (Ouchi et al., 2019)	
Mass transfer coefficient of H_2O in silica gel boundary - $K_{MT\text{-}silica\ gel}$	
$$K_{MT-silicagel} = 1.09 \; exp\left(\frac{-42000}{8.314\ T_{air}}\right) + 1.80 \times 10^{-8} \, (u_{air})^{0.5}$$	5.10
This relationship is obtained from the literature (Ouchi et al., 2019). The velocity range is from 0 to 0.4 m/s.	
Density of air – ρ_{air}	
$$\rho_{air} = \frac{0.0034848}{T_{air}} \, [101325 - 6.65 \times 10^8 \, RH_{air} \, exp\left(-\frac{5315.76}{T_{air}}\right)]$$	5.11
This relationship is obtained from the literature (Jones, 1978)	
Moisture content of air at ice surface – $X_{ice\ surf}$	

$$X_{ice\ surf} = \frac{0.018\ P_{ice}}{0.029\ [P_{total} - P_{ice}]} \quad 5.12$$

This is the expression for vapour phase moisture content based on vapour pressure from ideal gas law using molecular weights of water and air respectively.

Moisture content of silica gel in equilibrium with air - $X_{silicagel,\ equil}$

$$X_{silicagel.equil} = 0.445\ RH_{air};\ RH_{air} \leq 10\ \% \quad 5.13$$

This relationship is obtained from the literature (Tétreault & Bégin, 2018)

Relative humidity of air – RH_{air}

$$RH_{air} = \frac{P_{air}}{P_{air\_sat}} \quad 5.14$$

Vapour pressure of moisture in air – P_{air}

$$P_{air} = \frac{X_{air} \times P_{total}}{X_{air} + 0.622} \quad 5.15$$

This is the expression for vapour pressure based on ideal gas law using vapour phase moisture content and molecular weights of water and air respectively.

Effective path length for diffusion in Ice sublimation – $l_{ice\text{-}air}$

$$l_{ice-air} = l_{ice-air,o} + \frac{V_{ice,o} - V_{ice}}{A_{ice}} \quad 5.16$$

The "effective path length" layer is the notional path length representative of the summed resistances for the water vapour to travel from the ice surface to the bulk air, and. In the case of pure ice in air the effective path length can be calculated as the sum of the initial boundary layer, which is set as the height difference between the lip of the sample holder and the surface of the ice, and the increment in the boundary layer due to the ice subliming and the ice surface receding into the sample holder. This increment can be calculated by dividing the volume of ice lost by sublimation by the area of ice which is equal to the cross-sectional area of the ice sample holder.

Volume of Ice – V_{ice}

$$V_{ice} = \frac{M_{ice}}{\rho_{ice}} \quad 5.17$$

Table 5-6 shows the initial conditions.

Table 5-6 Initial conditions

$M_{ice,i}$	=	M_{ice}	@ t=0
$X_{silicagel,i}$	=	$X_{silicagel}$	@ t=0
$T_{ice,i}$	=	T_{ice}	@ t=0
$X_{air,i}$	=	X_{air}	@ t=0

Table 5-7shows the list of system inputs.

Table 5-7 List of system inputs

Symbol	Description	Type		Value	Units
A_{ice}	Area of Ice	SI	=	0.000784	m^2
b_{box}	width of box	SI	=	0.28	m
$C_{p,ice}$	Specific heat capacity of ice	SI	=	2108	J/kg/K
h_{air}	Heat transfer coefficient for air	SI	=	25	$W/m^2/K$
l_{box}	Length of box	SI	=	0.48	m
$l_{ice\text{-}air,o}$	Initial effective path length for diffusion in ice sublimation	SI	=	0.0197	m
λ_{sub}	Heat of sublimation of ice	SI	=	2836000	J/kg
$M_{silicagel}$	Mass of Silica gel (dry)	SI	=	0.2	kg
P_{total}	Total system pressure	SI	=	101325	Pa
$r_{silicagel}$	Average radius of silica gel	SI	=	0.002	m
ρ_{ice}	density of ice	SI	=	920	kg/m^3
T_{air}	Temperature of air	SI	=	261.15	K
$T_{silicagel}$	Temperature of silica gel	SI	=	T_{air}	K
u_{air}	Air velocity	SI	=	0	m/s
V_{box}	Volume of air in box	SI	=	l_{box} b_{box} z_{box}	m^3
$V_{ice,o}$	Volume of ice	SI	=	$M_{ice,o}$ /ρ_{ice}	m^3
z_{box}	height of box	SI	=	0.25	m

5.2 AFD of Hops in the AFD apparatus

The second tranche of experiments used hops which allows determination of the internal resistances to mass and heat transfer, assuming that the external resistances are the same as determined for pure ice.

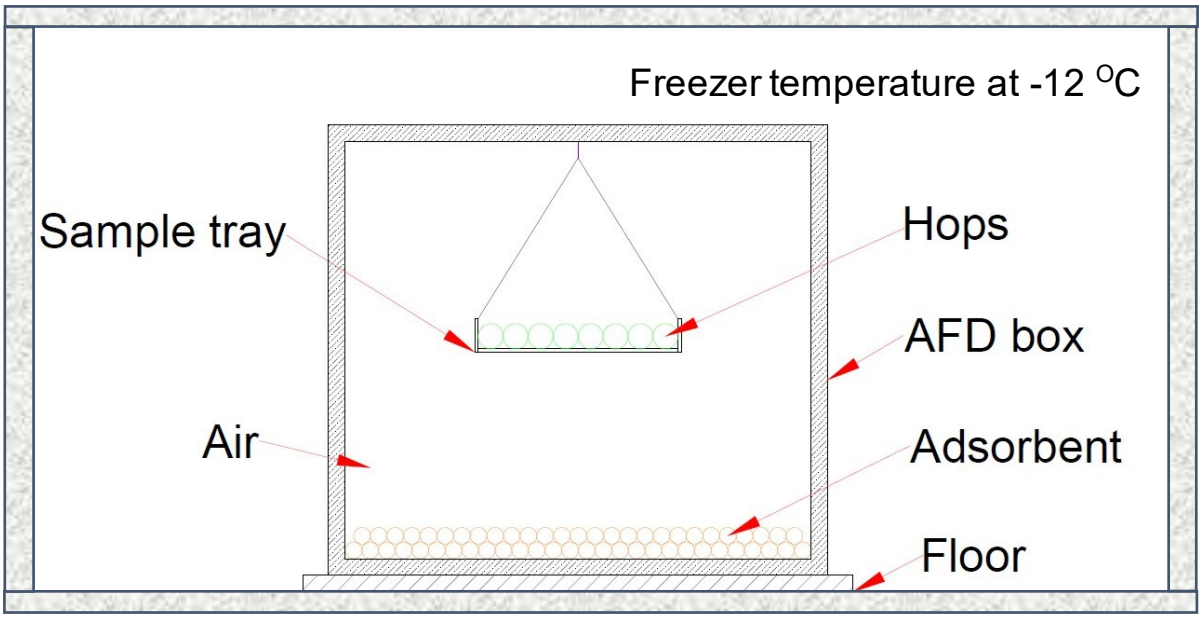

Figure 5-3 Diagram of the AFD of hops in the AFD drying chamber.

The system used is the same as that described in Section 5.1, except that the sample holder now holds the hops, as shown in Figure 5-3.

Assumptions 1-14 for the pure ice system also apply here, with some modifications to account for the presence of the hops plant matrix, as follows:

3. Modified. The plant material consists of ice crystals and non-ice plant matrix. Moisture only exists in the ice, air, or silica gel, i.e., no condensation occurs on the side walls or within the plant matrix.
7. Modified. The moisture content only varies in the mass transfer boundary layers between the ice surface and the surface of the hops, and between the surface of the hops and the bulk air, and between the bulk air and the silica gel. This means the resistance to mass transfer is limited to these boundary layers. It also means the overall resistance is the additive sum of the resistances to each of these boundary layers.
10. Modified. The temperature of the ice and the plant matrix of the hops is spatially uniform and equal to the bulk air and silica gel temperature. This assumption is a consequence of the pure ice results (see Section 6.3.2) where the heat transfer was found to be fast compared to mass transfer, and so can be neglected. In the hops, this effect will be accentuated because the ice is dispersed within the heat

conducting plant matrix, and so localised cooling of ice crystals due to the latent heat of sublimation can be neglected.

11. Deleted.
13. Modified. The specific heat capacities of the plant matrix, ice, silica gel and air are independent of temperature for the operating range.

Of these, the most notable is the assumption 10, which arises from the experimental results of the pure ice experiments which showed that the heat transfer is not limiting. The consequence is that a heat balance equation is not needed, and so has been removed, making the system of equations simpler.

However, the presence of the plant matrix does impede the mass transfer as the water vapour has to travel from the ice surface to the surface of the hops, then through a quiescent boundary layer into the bulk air, then from the bulk air across another quiescent boundary layer to the surface of the silica gel. As noted in the modified assumption 7, these are resistances in series, the overall mass transfer resistance in the hops is the additive sum. Of these, the hops internal mass transfer resistance requires some discussion.

Upon freezing of the hops before atmospheric freeze drying begins, the hops can be assumed to have a vascular pathway network corresponding to that used by the leaves and petals for photosynthesis when alive. The ice can be assumed to be crystals that have formed within the cellular structure of the plant material. The issue of crystal size and number of crystals will be discussed in the next paragraph, but here, the discussion is focussed on the resistance to mass transfer and how this may be interpreted from experimental observations. At the beginning of AFD, an initial resistance can be defined, which is an average mass transfer coefficient for sublimation from the ice surface area within the cells, through the cellular matrix (i.e., through the cytoplasmic residue and across any intact cell walls), and diffusion along the tortuous path of the vascular network to arrive at the surface of the hops leaves. As the cells are distributed through the plant matrix, there is expected to be significant natural variation, but which for a first approximation can be considered as an averaged quantity. This resistance is called the *initial resistance*, denoted R_2. However, as AFD proceeds, the ice front recedes within each cell meaning that an *extent dependent resistance* arises because; (i), the diffusion

path length increases; and (ii), the water vapour must now diffuse through extra left-behind cellular matrix. As the increase in diffusion path length within the cells is small compared to the tortuous path length in the vascular network, it can be assumed that the increase in resistance is dominated by the left-behind cellular matrix which increases the diffusion resistance and will be a function of the extent of sublimation. This *extent dependent resistance* is denoted R_1(extent). The overall resistance is the sum of these two terms, R_1(extent) + R_2. The simplification of this system is shown in Figure 5-4.

The above use of an *initial* and *extent-dependent resistance* is a compromise to the experimental method. For thorough investigation of the sources of resistance, it is arguably better to divide resistance into *intra-* and *extracellular* and *trans-cell wall resistance*; however, it is not possible to separate the parts of the plant matrix. The value in the approach used here is that it is able to be adopted for other materials without requiring detailed knowledge of the plant structure.

Surface area is an important parameter in sublimation, where (rate) = (total surface area) × (overall mass transfer coefficient) × (water vapour gradient). In the ice experiments the surface area is well defined as the ice is a continuous surface, but here the hops surface area is not at all well-defined. The ice is mostly frozen water distributed among the cells of the hops. (Some will remain unfrozen due to freezing point depression although this is neglected here.) Therefore, it is assumed that each cell contains one ice crystal, which therefore defines its initial size and, assuming it is also spherical (for simplicity), its surface area. This assumption is justified if accumulated resistances to vapour diffusion dominate those at the ice crystal surface itself. In this way, total initial surface area becomes a consequential value (Table 5-11).

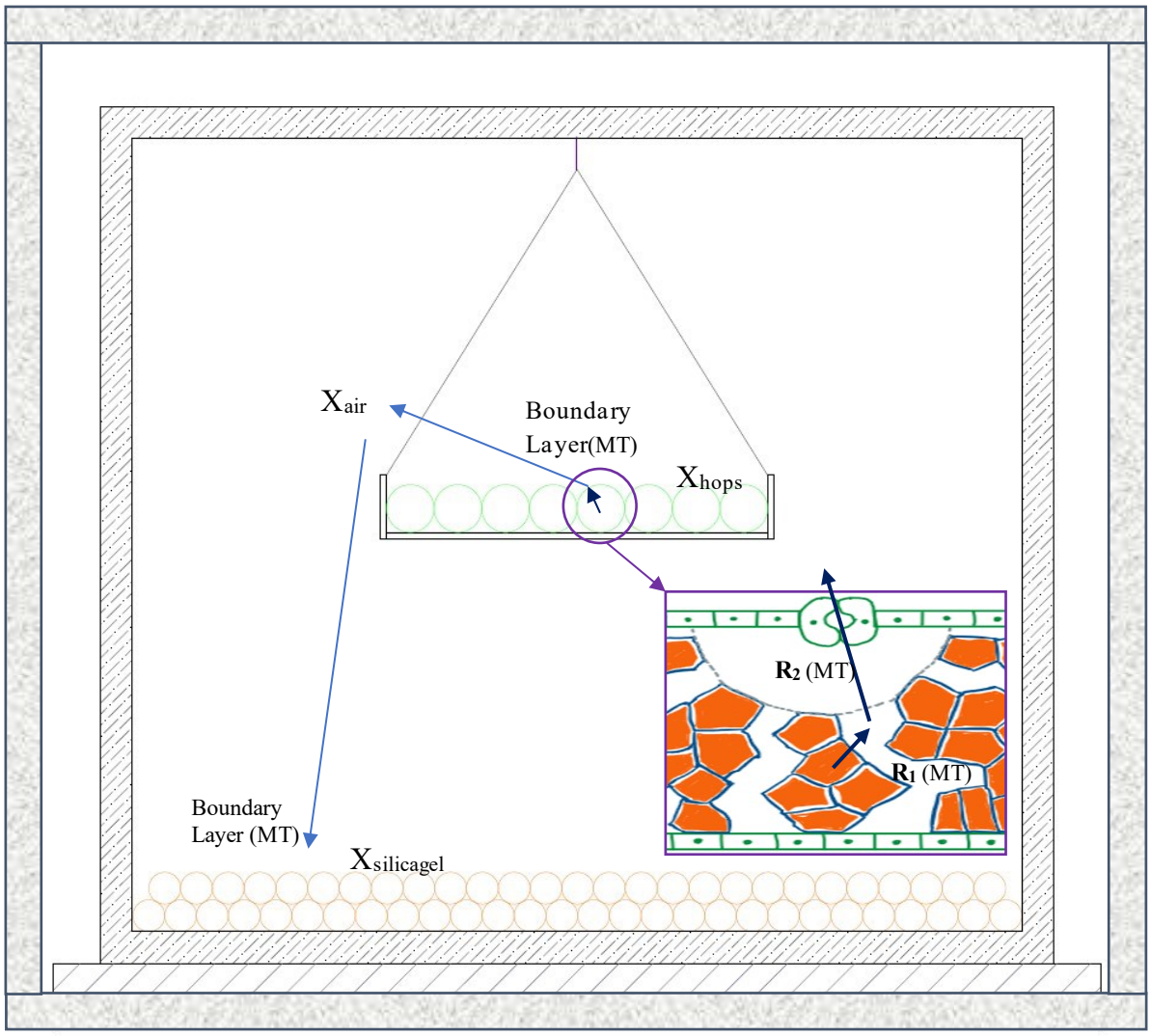

Figure 5-4 Diagram of the AFD of hops in the AFD drying chamber with resistances.

5.2.1 Assumptions:

In addition, the assumptions 1-14 and their modifications above, the following also apply for the hops system.

15. The mass transfer resistance inside the hops consists of two resistances in series, the *initial resistance* (R_2), and the *extent dependent resistance* (R_1(extent)).
16. The *initial resistance* R_2 is the product of the tortuous diffusion path length through the plant matrix and a resistance factor that accounts for diffusion through the plant matrix, RF_2. RF_2 is a fitted parameter, determined from the experimental results.
17. The *extent dependent resistance* R_1 is the product of the change in diffusion distance as the ice crystal sublimes and a resistance factor that accounts for diffusion through that left behind plant matrix, RF_1. RF_1 is a fitted parameter, determined from the experimental results.

18. For simplicity A single spherical ice crystal is assumed to occupy each cell within the hops plant matrix.

The hops system can be defined by the parameters in Table 5-8.

Table 5-8 System nomenclature with units and parameter classes - AFD of hops

Symbol	Description	Units	Type
A_{ice}	Area of ice in hops for sublimation	m^2	CV
b_{box}	width of box	m	SI
d_{cell}	Average diameter of a cell	m	SI
$D_{H2O\text{-}air}$	Diffusivity of water vapour in air	m^2/s	CV
$D_{H2O\text{-}eff\text{-}silicagel}$	Effective diffusivity of water vapour in silica gel	m^2/s	CV
$D_{H2O\text{-}silicagel}$	Diffusivity of water vapour in silica gel	m^2/s	CV
d_{ice}	Diameter of ice crystal	m	CV
$d_{ice,o}$	Initial diameter of ice crystal	m	SI
$K_{MT\text{-}silicagel}$	Mass transfer coefficient of H2O for silica gel	m/s	CV
l_{box}	Length of box	m	SI
$l_{hops\text{-}air}$	Boundary layer thickness for hops	m	SI
$l_{hops\text{-}cell}$	Path length for diffusion in cell	m	CV
$l_{hops\text{-}inter}$	Average intercellular path length	m	SI
$M_{hops\text{-}dry}$	Mass of hops dry (dry)	kg	SI
M_{ice}	Mass of ice in hops	kg	CV
$M_{ice,o}$	Initial mass of ice in hops	kg	SI
$M_{silicagel}$	Mass of silica gel (dry)	kg	SI
N_{ice}	Number of ice crystals		SI
P_{air}	Vapour pressure of H2O in air	Pa	CV
$P_{air\text{-}sat}$	Saturated vapour pressure of water over ice	Pa	CV
P_{ice}	Vapour pressure of ice near the ice surface in hops	Pa	CV
P_{total}	Total system pressure	Pa	SI
$r_{silicagel}$	Average radius of silica gel	m	SI
RF_1	Resistance factor for resistance in cell	*	SI
RF_2	Resistance factor for resistance in intercellular region	*	SI
RH_{air}	RH of air	Pa	CV
ρ_{air}	Density of air	kg/m^3	CV
$\rho_{hops\text{-}dry}$	Density of dry hops	kg/m^3	SI
ρ_{ice}	density of ice	kg/m^3	SI
t	Time	sec	I
T_{air}	Temperature of air	K	SI
T_{hops}	Temperature of hops	K	SI

$T_{silicagel}$	Temperature of silica gel	K	SI
u_{air}	Air velocity	m/s	SI
V_{box}	Volume of air in box	m^3	SI
V_{cell}	Volume of a cell	m^3	SI
V_{hops}	Volume of hops	m^3	SI
V_{ice}	Total volume of ice in hops	m^3	CV
$V_{ice,o}$	Volume of ice	m^3	SI
X_{air}	Moisture content in air (dry basis)	kg/kg	D
$X_{air,o}$	Initial moisture content in air (dry basis)	kg/kg	IV
X_{hops}	Moisture content in hops (dry basis)	kg/kg	D
$X_{hops,o}$	Initial moisture content in hops (dry basis)	kg/kg	IV
X_{ice}	Moisture content at ice surface (dry basis)	kg/kg	CV
$X_{silicagel}$	Moisture content in silica gel (dry basis)	kg/kg	D
$X_{silicagel,equil}$	Moisture content of silica gel in equilibrium with air (dry basis)	kg/kg	CV
$X_{silicagel,o}$	Initial moisture content silica gel (dry basis)	kg/kg	IV
z_{box}	height of box	m	SI

* Dimensionless

The above system with its constraints requires three ordinary differential equations to model the time dependence of atmospheric freeze drying (Table 5-9 and Table 5-10). In addition to this, a series of consequential equations (also known as constitutive equations) are also needed to relate parameters to system inputs, which are either measured variables, fundamental constants, or empirical constants as done for the model for ice sublimation in AFD apparatus (Table 5-11).

Table 5-9 Defining the number of equations.

1	Independent variable	
3	Dependent variables	3 ODEs required
3	ODEs	3 Initial conditions
16	CVs	at least 16 algebraic equations required
25	SIs	need estimates for these parameters

Table 5-10 shows the ODE equations to model the AFD of hops.

Table 5-10 List of ODEs – AFD of Hops

Mass balance of moisture in hops				
rate of accumulation of moisture in hops sample	=	*rate of moisture added to hops from air by deposition*	-	*rate of moisture lost to air through sublimation*
$M_{hops-dry}\frac{dX_{hops}}{dt} = 0 - A_{ice}\frac{[X_{ice} - X_{air}]}{[\frac{l_{hops-air}}{D_{H2O-air}} + RF_2\frac{l_{hops-inter}}{D_{H2O-air}} + RF_1\frac{l_{hops-cell}}{D_{H2O-air}}]} \times \rho_{air}$				5.18
Mass balance of moisture in air				
rate of accumulation of moisture in air	=	*rate of moisture added to air due to sublimation*	-	*moisture removed by adsorption by silica gel*
$V_{box}\ \rho_{air}\ \frac{dX_{air}}{dt} = A_{ice}\frac{[X_{ice} - X_{air}]}{[\frac{l_{hops-air}}{D_{H2O-air}} + RF_2\frac{l_{hops-inter}}{D_{H2O-air}} + RF_1\frac{l_{hops-cell}}{D_{H2O-air}}]} \times \rho_{air} - M_{silicagel}\ \frac{15}{r_{silicagel}^2}\ D_{H2O-eff-silicagel}\ [X_{silicagel,equil} - X_{silicagel}]$				5.19
Mass balance of moisture in silica gel				
rate of accumulation of moisture in silica gel	=	*rate of moisture added adsorption by silica gel from air*	-	*rate of moisture lost desorption by silica gel*
$M_{silicagel}\ \frac{dX_{silicagel}}{dt} = M_{silicagel}\ \frac{15}{r_{silicagel}^2}\ D_{H2O-eff-silicagel}\ [X_{silicagel,equil} - X_{silicagel}] - 0$				5.20

Table 5-11 shows a list of constitutive equations for hops.

Table 5-11 List of constitutive equations for hops (cf Table 5-5 for ice)

Vapour pressure of H_2O near ice surface– P_{ice}	
$P_{ice} = \frac{exp(43.494 - \frac{6545.8}{T_{ice} + 4.85})}{(T_{ice} + 594.85)^2}\ ;\ T <= 0\ ^oC$	5.21

Pressure temperature relationship for saturated vapour pressure of water over ice at any given temperature (Huang, 2018)	
Saturated vapour pressure of H_2O in air – $P_{air\ sat}$	
$$P_{air\_sat} = \frac{exp(43.494 - \frac{6545.8}{T_{air} + 4.85})}{(T_{air} + 594.85)^2} \; ; \; T <= 0 \;\; ^oC$$	5.22
Pressure temperature relationship for saturated vapour pressure of water over ice at any given temperature (Huang, 2018)	
Diffusion coefficient of H_2O in air - $D_{H2O\text{-}air}$	
$$D_{H2O-air} = 1.735 \times 10^{-9} \; (T_{air})^{1.685}$$	5.23
This relationship is obtained from the literature (Pesaran & Mills, 1987)	
Effective diffusion coefficient of H_2O in silica gel - $D_{H2O\text{-}eff\text{-}silicagel}$	
$$D_{H2O-eff-silicagel} = \frac{r_{silicagel}}{15[\frac{r_{silicagel}}{15\ D_{H2O-silicagel}} + \frac{1}{K_{MT-silicagel}}]}$$	5.24
This relationship is obtained from the literature (Ouchi et al., 2019)	
Diffusion coefficient of H_2O in silica gel - $D_{H2O\text{-}silicagel}$	
$$D_{H2O-silicagel} = 5.58 \times 10^{-8} \; exp\,(-0.45 \frac{42000}{8.314\ T_{air}})$$	5.25
This relationship is obtained from the literature (Ouchi et al., 2019)	
Mass transfer coefficient of H_2O in silica gel boundary - $K_{MT\text{-}silica\ gel}$	
$$K_{MT-silicagel} = 1.09 \; exp\left(\frac{-42000}{8.314\ T_{air}}\right) + 1.8010^{-8} \; (u_{air})^{0.5}$$	5.26
Pressure temperature relationship for saturated vapour pressure of ice at any given temperature (Huang, 2018)	
Density of air – ρ_{air}	
$$\rho_{air} = \frac{0.0034848}{T_{air}} \; [101325 - 6.65 \times 10^8 \; RH_{air} \, exp\left(-\frac{5315.76}{T_{air}}\right)]$$	5.27
This relationship is obtained from the literature (Jones, 1978)	
Moisture content of air at ice surface inside hops – $X_{ice\ surf}$	
$$X_{ice\ surf} = \frac{0.018\ P_{ice}}{0.029\ [P_{total} - P_{ice}]}$$	5.28
This is the expression for vapour phase moisture content based on vapour pressure from ideal gas law using molecular weights of water and air respectively.	

Moisture content of silica gel in equilibrium with air - $X_{silicagel,\ equil}$

$$X_{silicage,equil} = 0.445\ RH_{air};\ \ RH_{air} <= 10\ \%$$ 5.29

This relationship is obtained from the literature (Tétreault & Bégin, 2018)

Relative humidity of air – RH_{air}

$$RH_{air} = \frac{P_{air}}{P_{air\_sat}}$$ 5.30

Vapour pressure of moisture in air – P_{air}

$$P_{air} = \frac{X_{air}\ P_{total}}{X_{air} + 0.622}$$ 5.31

This is the expression for vapour pressure based on ideal gas law using vapour phase moisture content and molecular weights of water and air respectively.

Path length for diffusion in cell – $l_{hops\text{-}cell}$

$$l_{hops-cell} = \frac{d_{ice,o} - \ d_{ice}}{2}$$ 5.32

The mass transfer resistance for water vapour inside the cell depends on the thickness of this layer and it increases as the crystal shrinks.

Volume of Ice – V_{ice}

$$V_{ice} = \frac{M_{ice}}{\rho_{ice}}$$ 5.33

Average crystal size of Ice in hops – d_{ice}

$$d_{ice} = \left(\frac{6\ V_{ice}}{3.14\ N_{ice}}\right)^{1/3}$$ 5.34

Mass of ice in hops – M_{ice}

$$M_{ice} = X_{hops} \times M_{hops,dry}$$ 5.35

Area of ice in hops – A_{ice}

$$A_{ice} = 3.14\ \ {d_{ice}}^2\ \ N_{ice}$$ 5.36

Table 5-12 shows the initial conditions.

Table 5-12 Initial conditions

$X_{hops,o}$	=	X_{hops}	@ t=0
$X_{silicagel,o}$	=	$X_{silicagel}$	@ t=0
$X_{air,o}$	=	X_{air}	@ t=0

Table 5-13 shows the list of system inputs for AFD of hops.

Table 5-13 List of system inputs for AFD of hops

Symbol	Description	Type		Value	Units
b_{box}	width of box	SI	=	0.28	m
d_{cell}	Average diameter of a cell	SI	=	0.0000107 (Canny & Huang, 2006)	m
$d_{ice,o}$	Initial diameter of ice crystal	SI	=	$(6\times V_{icei}/N_{ice}/3.14)^{(1/3)}$	m
l_{box}	Length of box	SI	=	0.48	m
l_{hops_air}	Boundary layer thickness for hops	SI	=	0.0058	m
$l_{hops\text{-}inter}$	Average intercellular path length	SI	=	0.00005 (Slaton & Smith, 2002)	m
$M_{hops,dry}$	Mass of hops dry (dry)	SI	=	0.001174	kg
$M_{ice,o}$	Initial mass of ice in hops	SI	=	$X_{hops,i} \times M_{hops,dry}$	kg
$M_{silicagel}$	Mass of Silica gel (dry)	SI	=	0.2	kg
N_{ice}	Number of Ice crystals	SI	=	V_{hops}/V_{cell}	
P_{total}	Total system pressure	SI	=	101325	Pa
$r_{silicagel}$	Average radius of silica gel	SI	=	0.002	m
RF_1	Resistance factor for resistance in cell	SI	=	1.19×10^6	
RF_2	Resistance factor for resistance in intercellular region	SI	=	1.70×10^5	
$\rho_{hops,dry}$	Substance density of dry hops	SI	=	1486	kg/m^3
ρ_{ice}	density of ice	SI	=	920	kg/m^3
T_{air}	Temperature of air	SI	=	261.15	K
T_{hops}	Temperature of hops	SI	=	T_{air}	K

$T_{silicagel}$	Temperature of silica gel	SI	=	T_{air}	K
u_{air}	Air velocity	SI	=	0	m/s
V_{box}	Volume of air in box	SI	=	$l_{box} \times b_{box} \times z_{box}$	m^3
V_{cell}	Volume of a cell	SI	=	$3.14\times (d_{cell}^3)/6$	m^3
V_{hops}	Volume of hops	SI	=	$M_{ice,o}/\rho_{ice} + M_{hops,dry}/\rho_{hops,dry}$	m^3
$V_{ice,o}$	Volume of ice	SI	=	$M_{ice,o}/\rho_{ice}$	m^3
z_{box}	height of box	SI	=	0.25	m

5.3 Conclusions

AFD can be modelled as a simple one-dimensional model when taken in concert with the simplifying assumptions made here. AFD of hops can be modelled as sublimation of pure ice with an additional layer of resistance for mass transfer. The ODE models for pure ice sublimation and ice sublimation within hops in the AFD apparatus with silica gel adsorbent are developed. The model predictions are compared with the experiment results in the following chapters to determine the fitting mass transfer coefficients. This comparison is used to validate the model assumptions and to understand the rate limiting mechanisms for the AFD process.

Chapter 6 Ice Experiment System and Discussion

6.1 Introduction

In chapter 2, previous literature describes moisture removal in the AFD process as a retreating interface of ice sublimation in spheres and cubes of plant material followed by movement of the water vapour to the object surface, into the bulk air and to the moisture sink. In chapter 5, a model was developed with similar assumptions, but specific to leaves and leaf-like plant materials by considering their structure: the plant cells are assumed to each contain an ice crystal, and the sublimed water vapour makes its way through the near-ice cellular matrix, then out into the vascular network to the surface of the leaf or petal and then into the well-mixed bulk air, after which it is adsorbed into the silica gel.

Thus, the model contains mass and heat transfer resistances that need to be determined from experimental data. For the plant material and the adsorbent, these resistances are assumed to be in series as internal and external resistances. The experimental programme has been designed to investigate these separately. First ice is sublimed to establish the external resistances, then hops are freeze-dried to determine the internal resistances with the assumption that the external resistances for hops are the same as determined for ice.

This chapter details the first experiments done with ice using the experimental apparatus described in Chapter 4. These experiments were conducted under the same conditions used for AFD of hops which are presented in Chapter 7. These ice results are then used to determine the external resistances for the AFD model and are discussed relative to the efficacy of the model in predicting the full span of freeze drying.

6.2 Experimental procedure

Ice was made by freezing distilled water poured into a 3D-printed ice cube holder of inner dimensions 28 mm × 28 mm × 20 mm (W × L × H). This resulted in ice with one flat side with constant surface area exposed to the air and available for sublimation (Figure 6-1).

The freezer was operated at -12 ^{o}C and the same temperature was maintained for all experiments in this chapter. The AFD apparatus was first equilibrated in the freezer for 24 hours. It was then opened, and 200 g of silica gel was placed on the floor of the drying

chamber. The silica gel beads spread out on the floor to form a single layer. The RH and temperature sensors were then placed inside. The drying chamber was then closed for a further of 24 hours to reach an equilibrium with the silica gel at an RH value around 2% RH. After this, the chamber was re-opened to place the ice sample on the sample tray.

Before the start of the experiment, the weighing balance and sensors were turned on and checked for their proper working and data logging. The weight was logged each second and the fluctuations in the data were smoothed by taking a moving average of 30 mins using an algorithm in R during the data analysis stage. The air RH and temperature were logged every 5 minutes. To measure the ice temperature during the experiment, an iBbutton sensor (Thermochron) was kept inside the ice in the 3D printed ice cube holder before it was frozen (Figure 6-1). The iButton was vacuum sealed in a small plastic cover to prevent entry of water during the freezing of ice.

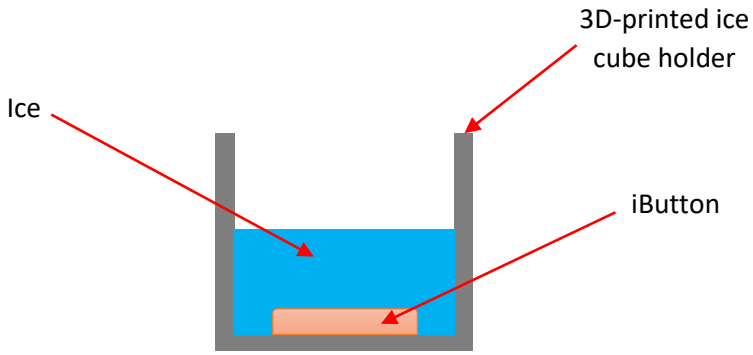

Figure 6-1 Ice in the 3D-printed ice cube holder with iButton

The ice weight data was used to find the differential weight loss curve by calculating the change in the weight of ice for each second based on the moving average data. The flux was then calculated by dividing the above value by the ice surface area. Algorithms for this were written on R (version 4.1.0 (2021-05-18)) for calculating and plotting these values.

The moving average was calculated as below,

$$M_{MA-ice,i} = \frac{\sum_{i-\frac{n}{2}}^{i-\frac{n}{2}} M_{ice,i}}{n+1} \qquad 6.1$$

The differential weight loss was calculated as below,

$$rate_{sub,i} = \frac{M_{MA-ice,i-1} - M_{MA-ice,i}}{t_i - t_{i-1}} \quad 6.2$$

The sublimation flux was calculated as below,

$$flux_{sub,i} = \frac{rate_{sub,i}}{A_{ice}} \quad 6.3$$

where,

$M_{MA\text{-}ice,i}$	=	Moving average value of mass of ice at time instant, i
$M_{ice,i}$	=	Mass of ice raw data at time instant, i
n	=	Time interval window of moving average in seconds
$rate_{sub,i}$	=	Differential weight loss
t_i	=	Time value at i
$flux_{sub,i}$	=	Ice sublimation flux
A_{ice}	=	Surface area of ice

The experiments are listed in Table 6-1.

Table 6-1 Ice sublimation experiments

		Temp (°C)	Silica gel (g)	Starting ice qty. (g)	Fan Status
Constant surface area					
1	Case I	-12	200	4.4176	OFF
2	Case II	-12	200	12.6669	OFF for 120 hrs and ON thereafter
Ice temperature					
3	Case III	-12	200	5.9667	OFF
Changing surface area					
4	Case IV	-12	200	4.3327	OFF

6.2.1 Constant ice surface area experiments

To quantify the resistances to mass transfer across the boundary layer near the subliming ice surface, cases I and II were done with constant area for ice sublimation to avoid the effects of area of ice available for sublimation. These two experiments have the subliming ice surface at different distances from the open top of the ice sample holder (Figure 6-2). This would help in quantifying the boundary layer thickness for the mass transfer more accurately during the model development of the process.

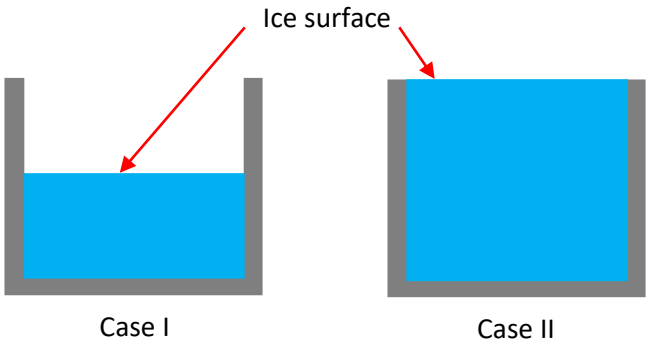

Figure 6-2 Constant ice surface experiments- case I & case II

6.2.1.1 Case I

The 4.4176 g of ice occupied a volume of 4.8064 cm^3 with a thickness of 6.1 mm. This meant the distance from the ice surface to the lip of the ice sample holder was initially 13.9 mm growing to 20 mm as the ice sublimed. The experiment was done in the absence of any forced convection in the drying chamber. In this experiment, a molecule of sublimed water vapour has to diffuse up through the inside of the sample holder then through a quiescent boundary layer before entering the bulk air which, despite the fan being OFF, can be assumed well-mixed noting that the long time frames of the experiment mean even the slightest of temperature differences around the chamber will induce natural convection (The well-mixed bulk air assumption is also supported by the following observations- 1) same air RH values measured by the RH sensors at different locations; 2) the air velocities measured by the thermo-anemometer; 3) the high Rayleigh number; 4) the model's robust prediction based on this assumption). The molecule of water vapour must then diffuse from the bulk air through another quiescent boundary layer to the silica gel whereupon it is adsorbed, in what is assumed a fast process relative to the diffusion.

6.2.1.2 Case II

Case II was conducted with ice filled to the brim of the ice sample holder. This removed the diffusion path from the ice surface to the lip of the sample holder. In this way, the effect of the travel path could be examined by comparing Cases I and II. After 120 hrs with the fan OFF, it was switched ON so that the ice sublimation experiment could be continued with forced convection. This change meant that the effect of the quiescent boundary layer close to the sample holder and close to the silica gel could be collectively examined.

6.2.2 Ice temperature

Ice sublimation is an endothermic process, requiring heat. These experiments test whether ice sublimation was limited by heat transfer, with the hypothesis that, if it were so limited, then a temperature depression would be noticeable between the ice and air. It also tests the modelling assumption that the temperature of the ice remains uniform, on the basis of the low Biot number of 0.07 calculated for the ice cube (calculations shown in appendix), which means that the heat transfer rate in the ice by conduction is much faster than the heat transfer from air to the ice. This means that any change in the temperature measured by the iButton is the change in temperature throughout the ice.

6.2.2.1 Case III

The experiment was done like case I as described above. Here, 5.9667 g of ice was used, and the temperature of the ice was measured using an iButton placed inside the ice, as shown in Figure 6-1. An iButton is also placed in case II for ice temperature measurement.

6.2.3 Changing ice surface area

An ice sublimation experiment was done to study the effect on ice sublimation rate when the area of the ice available for sublimation was changing and to see whether the area influenced the ice sublimation rate.

6.2.3.1 Case IV

Ice was made by freezing a large droplet of distilled water (4.3327 g) on a cuboidal shaped container made of aluminium foil with dimensions 45 mm × 60 mm × 15 mm (W × L × H) as shown in Figure 6-3. The initial water droplet did not extend to the walls of the

container and thus the ice formed had both its top and side edges exposed to the air. Only the bottom surface was not exposed to the air. The initial total surface area of the ice was 19.02 cm^2 and with a top surface area of 14.67 cm^2 at a thickness of 0.32 cm. The AFD experiment for the ice with decreasing surface area was done in the same conditions as described in the section 6.2.1.1.

Figure 6-3 Changing ice surface area experiment- case IV

6.3 Results & discussion

6.3.1 Ice sublimation experiment for constant surface area

6.3.1.1 Weight loss by sublimation

Figure 6-4 compares the weight loss and Figure 6-5 compares sublimation flux for Cases I and II up to 120 hours. The difference in rate can be explained by the lower mass transfer resistance in case II, where the ice is filled to the brim of the ice sample holder and so the water vapour has a smaller diffusion path length from the ice surface to the bulk air. In quiescent air, the mass transfer resistance is directly proportional to the path length of vapour diffusion. The slow decrease in sublimation flux for case I can be attributed to both its longer path length due to the ice surface being well inside the sample holder, and the small relative change in overall path length as sublimation proceeds. For the case II, the ice surface starts at the top edge of the ice sample holder, and so two features are apparent; first, the higher sublimation flux is due to the initially shorter diffusion path length; and second, the faster decrease in sublimation flux is due to the greater relative change in diffusion path length as sublimation proceeds.

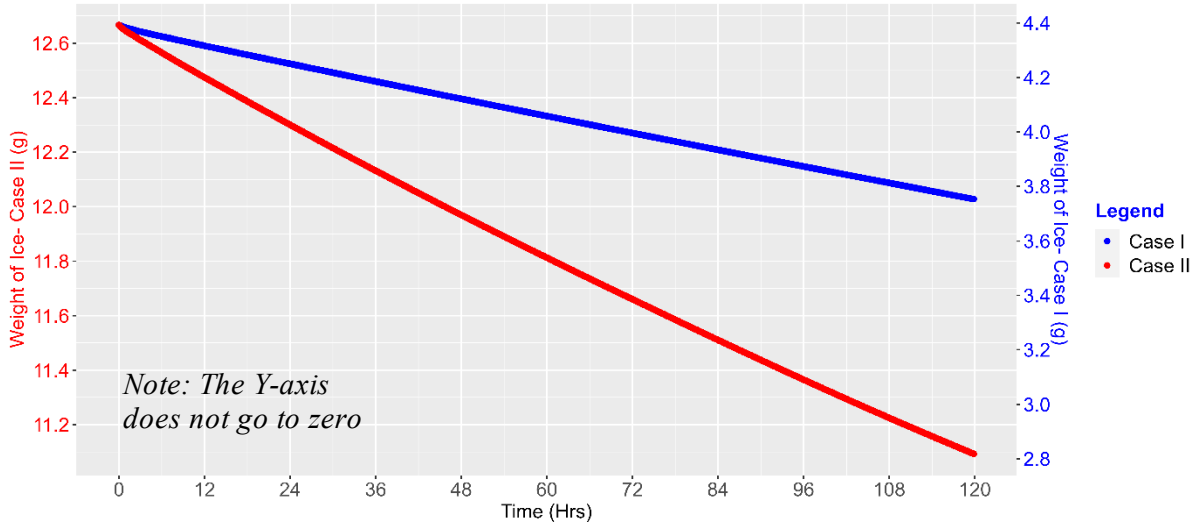

Figure 6-4 Weight loss comparison during the ice sublimation – no air circulation region -case I (ice surface deeper inside the 3D printed ice holder) & case II (ice surface near the outer edge of the 3D printed ice holder)

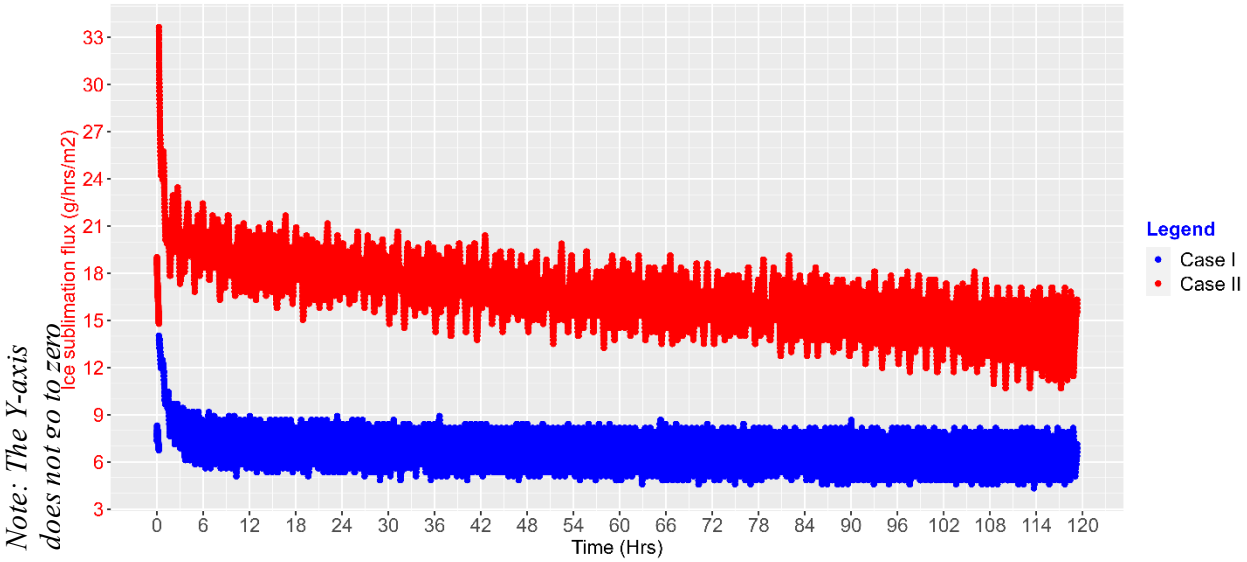

Figure 6-5 Sublimation flux comparison during the ice sublimation – no air circulation region -case I (ice surface deeper inside the 3D printed ice holder) & case II (ice surface near the outer edge of the 3D printed ice holder)

Figure 6-6 adds the weight loss and sublimation flux of ice beyond 120 hours where, for case II, the fan was switched ON. The effect of the forced convection is clearly seen. The increase in the sublimation flux can be attributed to the reduction in the diffusion path length between the ice and the bulk air which defines the resistance to mass and heat transfer. After 120 hours, the dramatic change in rate suggests that bulk air may also be circulating into the head space of the sample holder.

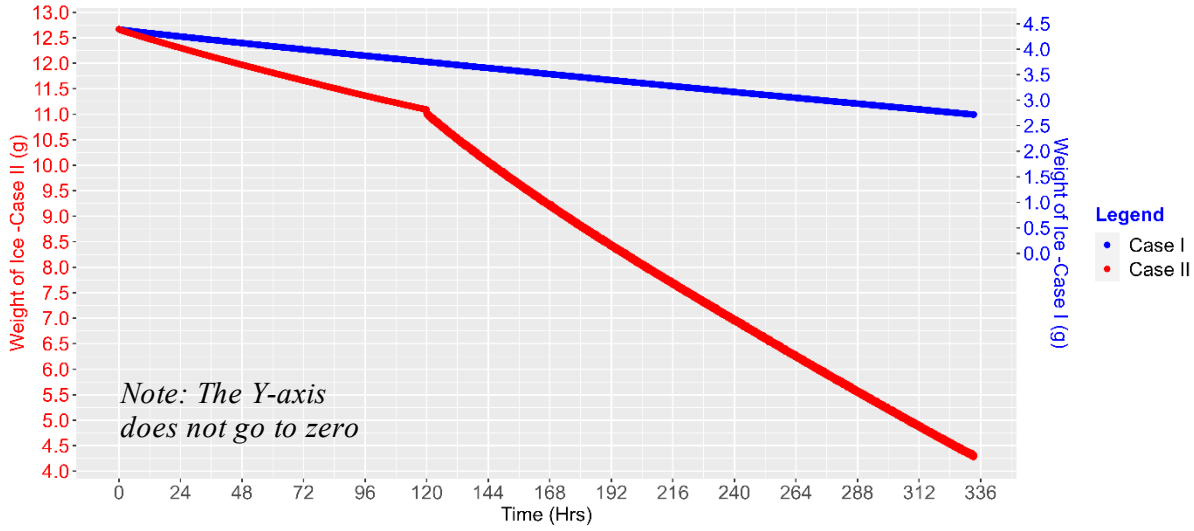

Figure 6-6 Weight loss comparison during the ice sublimation experiments–case I (no air circulation) & case II (no air circulation for 120 hrs and then with air circulation)

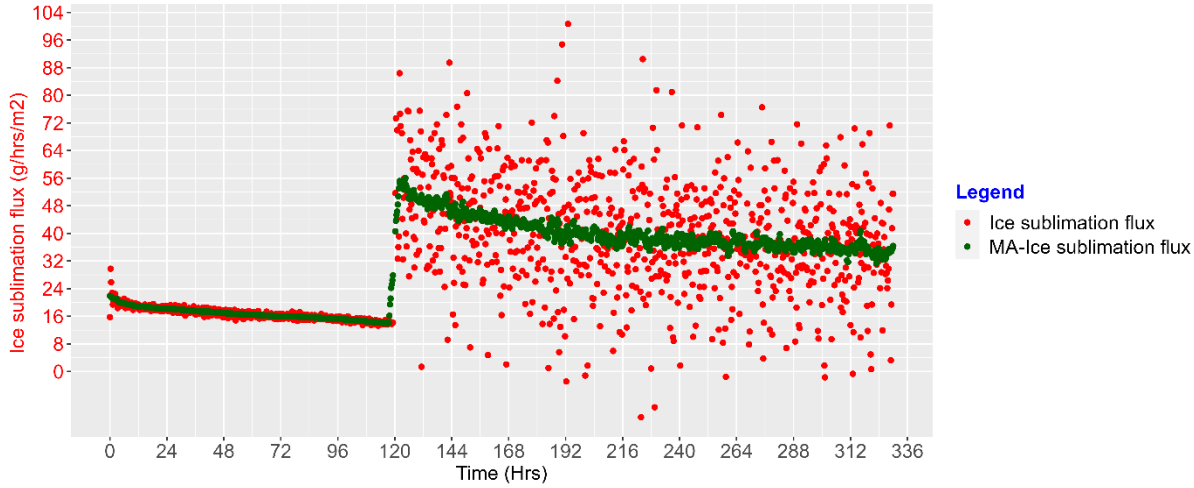

Figure 6-7 Sublimation flux & Moving average of ice sublimation flux for experiment-case II (no air circulation for 120 hrs and then with air circulation)

The fluctuations shown in Figure 6-7 in the ice sublimation flux values (red) after 120 hours (start of air circulation) are due to the oscillations in the weight measurement due to the small movement of the sample holder as air moves in the drying chamber.

Without assuming any boundary layer between the top of the sample holder and the bulk air, a proxy for path length is given by the equation below. The initial path length for case I is the distance from the edge of the sample holder to the ice surface, 13.9 mm, and for case II it is 0 mm.

$$l_{path,i} = l_{path,0} + \frac{M_{MA-ice,0} - M_{MA-ice,i}}{\rho_{ice}\, A_{ice}}$$

where,

$M_{MA\text{-}ice,0}$	=	Initial mass of ice at time zero
$M_{MA\text{-}ice,i}$	=	Mass of ice at time, i
$l_{path,0}$	=	Initial path length at time zero
$l_{path,i}$	=	Path length at time, i
ρ_{ice}	=	Density of ice
A_{ice}	=	Surface area of ice

The sublimation flux plotted against the path length for mass transfer in the 3D-printed ice cube holder is shown in Figure 6-8 and Figure 6-9. For the two cases, the ice sublimation flux is plotted as a function of the path length of diffusion from the ice surface to the bulk air. During the first 120 hours, both cases I and II had the fan off, i.e., the diffusion environments were the same. It can be seen that the sublimation flux decreased with increasing path length. The sensitivity of flux to path length decreases with increasing pathlength.

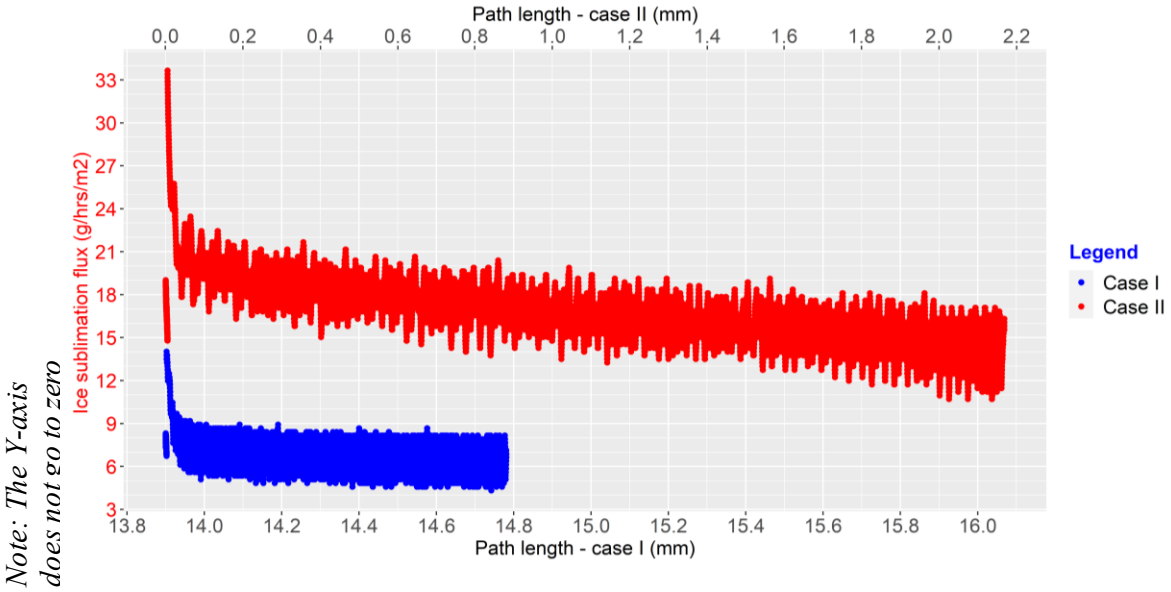

Figure 6-8 Ice sublimation flux comparison for same 120 hours duration– plot of mass transfer path length in the 3D printed holder for -case I (ice surface deeper inside the 3D

printed ice holder) & no air circulation region -case II (ice surface near the outer edge of the 3D printed ice holder)

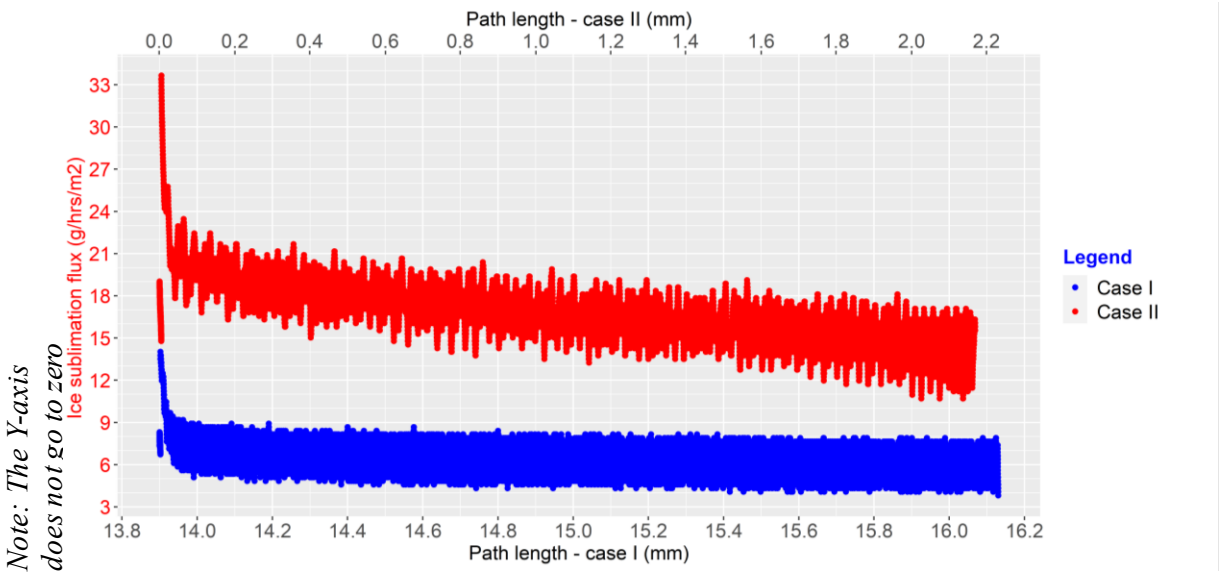

Figure 6-9 Ice sublimation flux comparison for same pathlength change– plot of mass transfer path length in the 3D printed holder for -case I (ice surface deeper inside the 3D printed ice holder) & no air circulation region -case II (ice surface near the outer edge of the 3D printed ice holder)

6.3.1.2 Air humidity in the AFD apparatus drying chamber

Mass transfer is also affected by the potential which is the water vapour pressure difference between the ice surface and the silica gel. In this system, the overall potential is the sum of two, the potential between the ice surface and the bulk air, and that between the bulk air and the silica gel assuming, as discussed earlier (in 6.2.1.1), that the bulk air is well-mixed, and that adsorption is fast relative to the time frame of mass transfer. Figure 6-10 shows the comparison between the air relative humidity measured at a distance of 30 mm from the sample holder in both the experiments. At this position, it represents the bulk air humidity. The high initial humidity is due to ambient air ingress into the drying chamber when it was opened to place the ice inside.

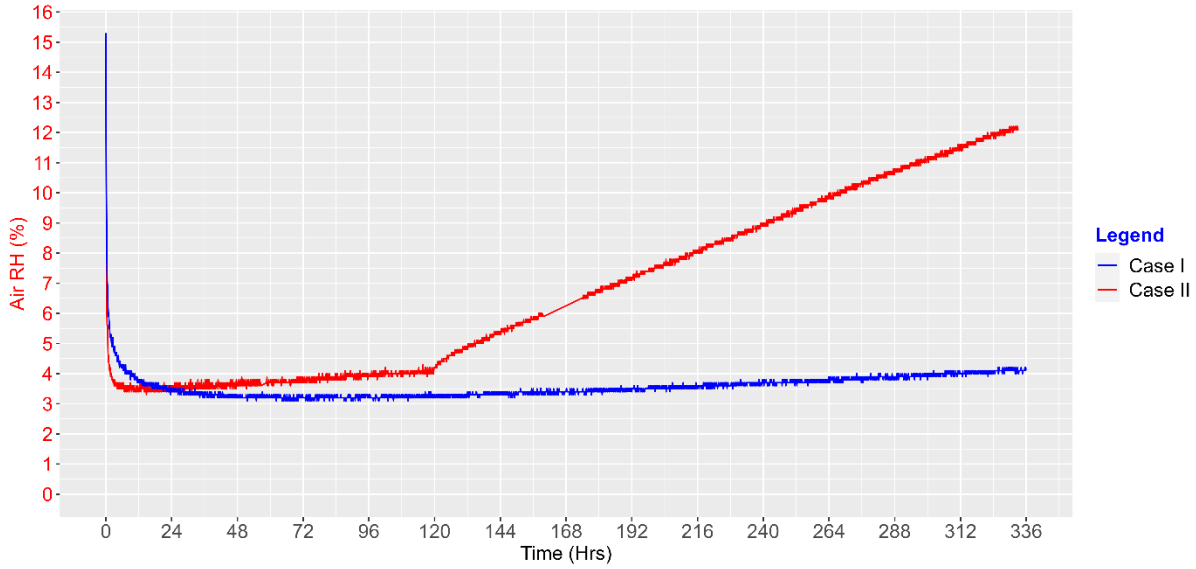

Figure 6-10 Air RH in the drying chamber of the AFD apparatus - case I (no air circulation) & case II (no air circulation for 120 hrs and then with air circulation)

Without air circulation (until 120 hours), and after the initial effect has receded, the air humidity increases slowly as the experiment progresses, but more quickly for case II. This can be interpreted two ways; (i), that the resistance to mass transfer from the bulk air to the silica gel is higher than between the ice and the bulk air and so water vapour accumulates in the bulk air; and/or (ii), because case II has a faster sublimation rate than case I, moisture accumulates more quickly in the silica gel and so is reflected in an increased equilibrium moisture content in air. Interpretation (ii) is more likely.

After air circulation begins at 120 hours, Figure 6-6 shows the rate of air humidity increase undergoes a step change increase. As argued above, forced circulation will reduce the quiescent boundary layer thicknesses between the bulk air and the sample holder, and between the bulk air and the silica gel. While it results in faster sublimation, the effect of this will be to reduce the influence of interpretation (i).

Whether or not interpretation (i) even exists is important, because the model assumption made in Chapter 5 says that resistance is overwhelmingly on the ice sublimation side and not on the silica gel adsorption side. If the assumption does not hold the mathematics, by necessity, becomes more complicated. Therefore, it is desirable to demonstrate that the mass transfer resistance is low between the bulk air and the silica gel compared to between the subliming ice and the bulk air. One way to do is to create a pseudo equilibrium adsorption isotherm between the moisture content in the air versus the moisture content

in the silica gel which is shown in Figure 6-11. The pseudo equilibrium adsorption isotherm is plotted by assuming that the moisture increase in the silica gel would be the difference between the moisture lost from the sample and the moisture in the air. This is based on initial assumption that the moisture lost from the sample would be either in the air or the silica gel.

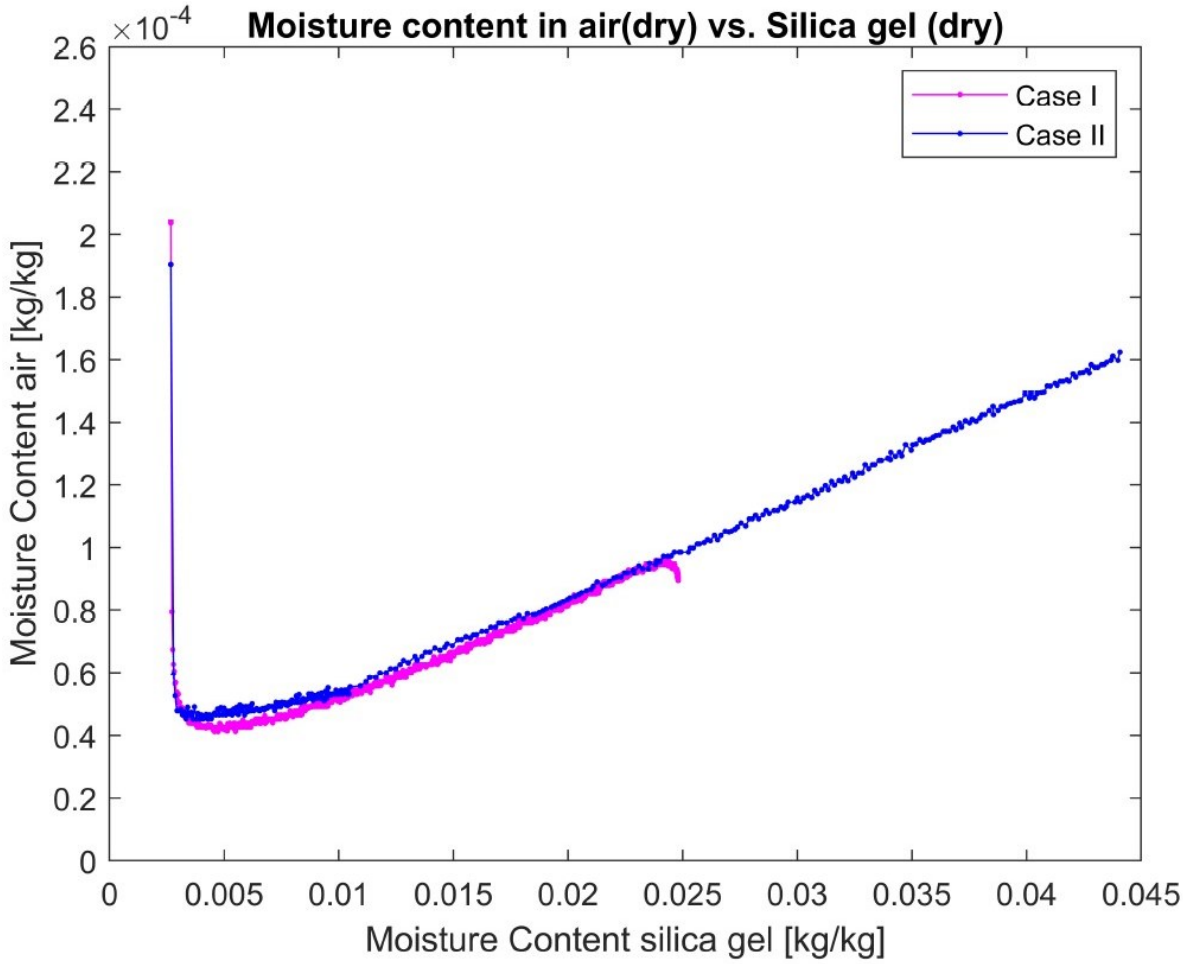

Figure 6-11 Pseudo equilibrium adsorption curve for case I and case II (Moisture content in air versus moisture content in silica gel)

We would expect the adsorption isotherm to follow Henry's Law at low levels of adsorption (i.e., a straight line as seen in the pseudo equilibrium curve above for both cases). If the bulk air is acting as a buffer and accumulating water vapour because of interpretation one, then when the fan is turned on, this effect will be much less, and so we will see a point of inflexion, i.e., a change in slope. However, this inflexion is very minor in Figure 6-11 with minimal accumulation of water in air for the early fan-off section of case II, implying that the silica gel area is so much larger than the ice area, and so the

overall mass transfer which is proportional to area/resistance will be overwhelmingly influenced by the larger area. This would mean that the resistance to mass transfer from air to silica gel is much lower than the resistance to mass transfer between the ice and the bulk air.

6.3.1.3 Air temperature in the AFD apparatus drying chamber

The aim for these ice experiments was to keep the system temperature constant. Figure 6-12 shows an initial high value is because slightly warmer air entered the drying chamber when it was opened to position the ice for the experiment. Thereafter, the temperature was maintained at a constant value of -12 °C throughout the no air circulation period (until 120 hours) for both case I and II, with a variation of ± 0.15 °C due to the freezer refrigeration cycle.

In case II from 120 hours, the air temperature remains constant during the air circulation but exhibits a step increase of 0.20 °C, which could be due to heat addition from the working of the fan. There is a small hiatus in the data from 159 hrs to 173 hrs as there was a failure in data capture by the data logger.

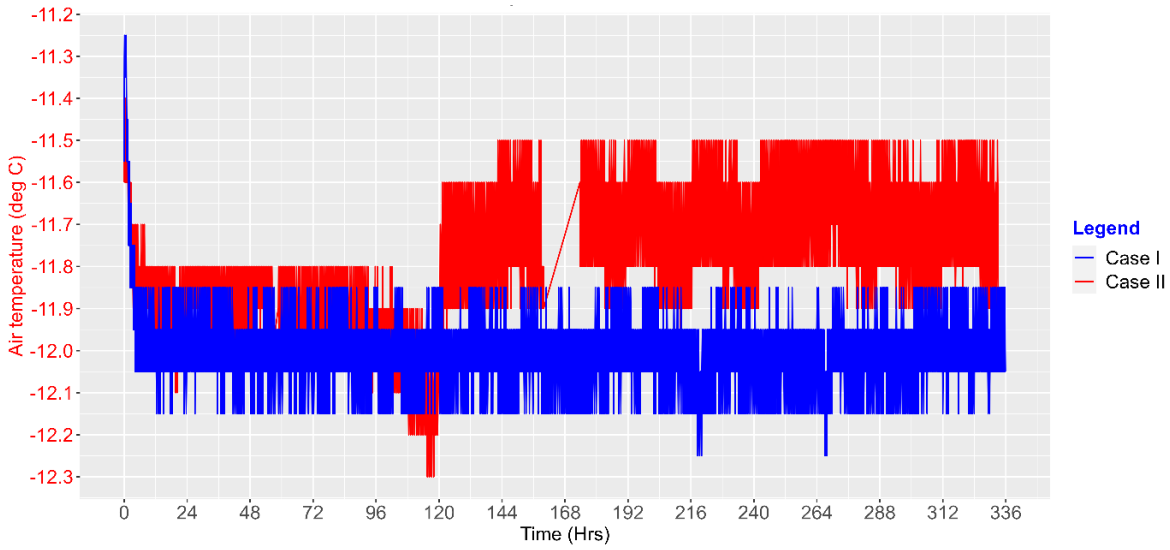

Figure 6-12 Air temperature in the drying chamber of the AFD apparatus- case I (no air circulation) & case II (no air circulation for 120 hrs and then with air circulation)

6.3.2 Comparing the ice and air temperatures during sublimation

Sublimation requires heat, which transfers from the bulk air into the ice. Air temperature is discussed above, and ice temperature was measured in case II and case III, which is a repeat of the case I experiment, using an iButton which was placed inside the ice. The results are shown in Figure 6-13, Figure 6-14 and Figure 6-15.

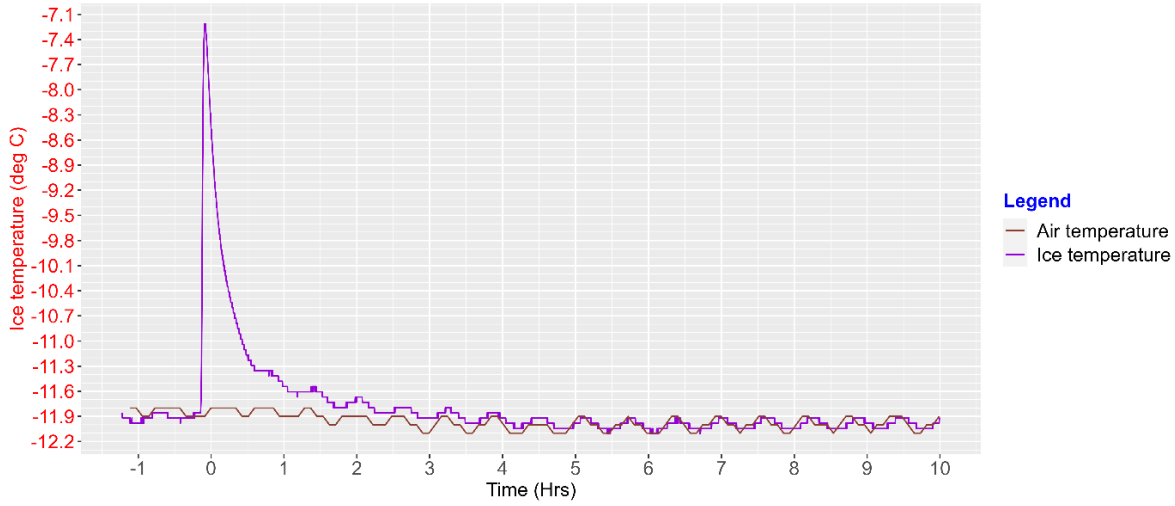

Figure 6-13 Temperature of ice and air during the experiment – case III

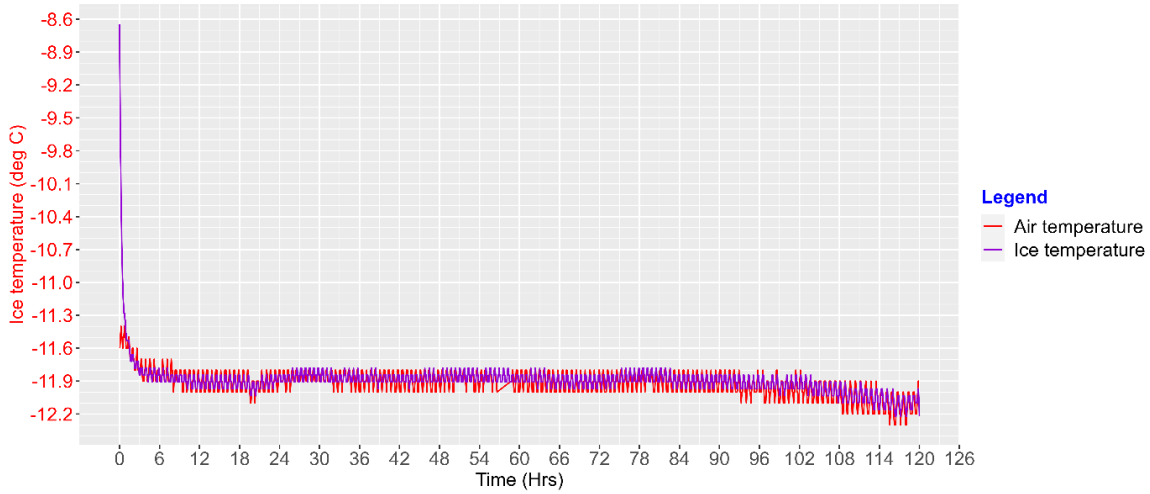

Figure 6-14 Temperature of ice and air - No air circulation period – case II

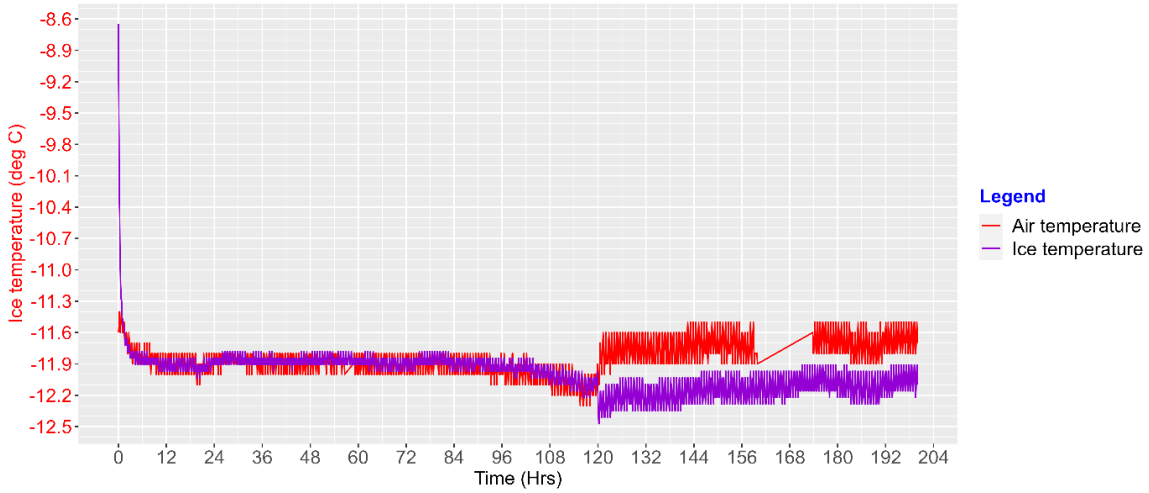

Figure 6-15 Temperature of ice and air - full experiment - case II

In both Cases III & II, the peak in ice temperature occurs when the ice sample holder cover is removed by hand to begin the experiment. The cover was a seal that prevented ice from subliming before the start of the experiment, prior to which distilled water was placed in the drying chamber to freeze. Four observations can be made in the period without air circulation; (i), the oscillations in the temperature of the ice and the air are identical in case III, but in case II the air temperature has a greater amplitude than the ice temperature; (ii), the oscillating air temperature slightly leads the ice temperature; (iii), after the door opening effect has subsided, the mean temperatures of the ice prior to and during sublimation are the same; and (iv), the mean ice and air temperatures are the same, i.e., in equilibrium. Observation (i) is due to the thermal cycle of the freezer and shows that the cycling is slow enough that the ice temperature closely tracks the air temperature. However, the two Cases have a different thermal masses of ice; in case II which has a much larger mass of ice, the amplitude of the ice temperature response is dampened compared to that of the air. The slight lag in observation (ii) is expected as heat transfers from the air to the ice to drive sublimation. Observations (iii) suggests that sublimation cooling (analogous to evaporative cooling of water) is not important, indicating that heat transfer is fast relative to mass transfer. Observation (iv) also support the hypothesis that heat transfer is fast relative to mass transfer.

This is further supported by Figure 6-16, where the ice and air temperatures are plotted directly against each other. That the data mostly falls on the diagonal confirms that both temperatures closely follow each other, i.e., are in equilibrium, and their responses are

fast with respect to the rate of change as driven by the thermal cycling of the freezer. This conclusion is in agreement with the findings reported by Jambon-Puillet et al., (2018), who reported that the sublimation of an ice drop in a closed chamber with air of low RH (around 5%) and temperature at -12 °C, is limited by the diffusive transport of the water vapour.

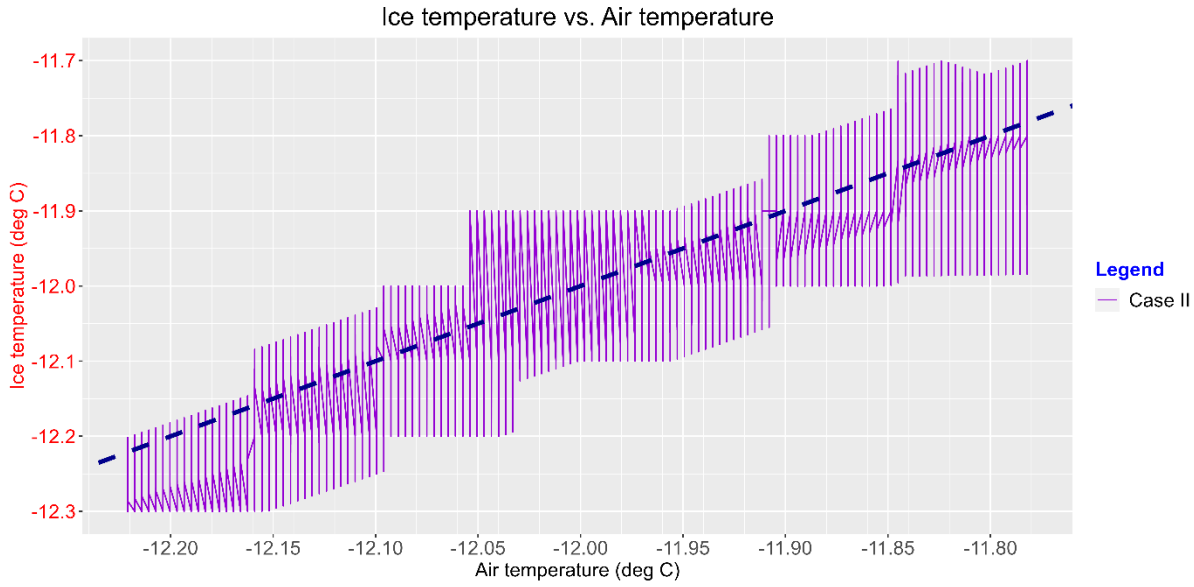

Figure 6-16 Temperature of ice versus air for case II for the first 200 hours without air circulation. The dashed line is the x=y line.

These results can also be considered alongside one of the model assumptions, which is that heat transfer, when considered on its own, is externally rather than internally limited. This assumption is based on the Biot number which, when calculated for the ice cube used in case I, is a very low a value of 0.07. Biot number is the ratio of the internal to external resistance to heat transfer. A low Biot number implies that the external resistance heat transfer is much greater than internal heat transfer resistance. By assuming this, the ice temperature can be regarded as constant throughout the sample. While the results presented in this section highlight that the heat transfer is fast relative to mass transfer, they do not directly allow deconvolution of the internal and external heat transfer; however, if internal heat transfer were limiting, then a greater lag between the air and ice temperatures would be expected, particularly for case III where the ice mass is relatively small. Instead, lag is minimal and so the model assumption is not challenged. Accepting this model assumption is an important conclusion as it is used in the further analysis of rate limiting mechanism for AFD of leaf-like products in the next chapter- chapter 7.

In case II, when air circulation occurs, Figure 6-15, in the period after 120 hrs with air circulation, the ice temperature is approximately ~0.4° lower than the air temperature, where the air has gained ~0.2°C and the ice is cooler by ~0.2°C. Both temperatures oscillate at the same frequency as before and are in synchrony with the trend of the air temperature. The air and ice temperature have the same amplitude too for this period while they were not same for the first part of the experiment with no air circulation. Here the ice sublimation can be assumed to be limited by external heat transfer as the temperature drop in the ice can be attributed to the slower rate of heat transfer into the ice to compensate the heat loss by sublimation, and the faster mass transfer resulting in evaporative cooling and temperature drop in ice.

6.3.3 Ice sublimation experiment for changing surface area

6.3.3.1 Weight loss by sublimation

Sublimation drying of ice involves a change in surface area. In the above experiments, Cases I – III, area was kept constant to reduce the number of change variables. Here, in case IV, area is specifically examined by starting with a pool of ice.

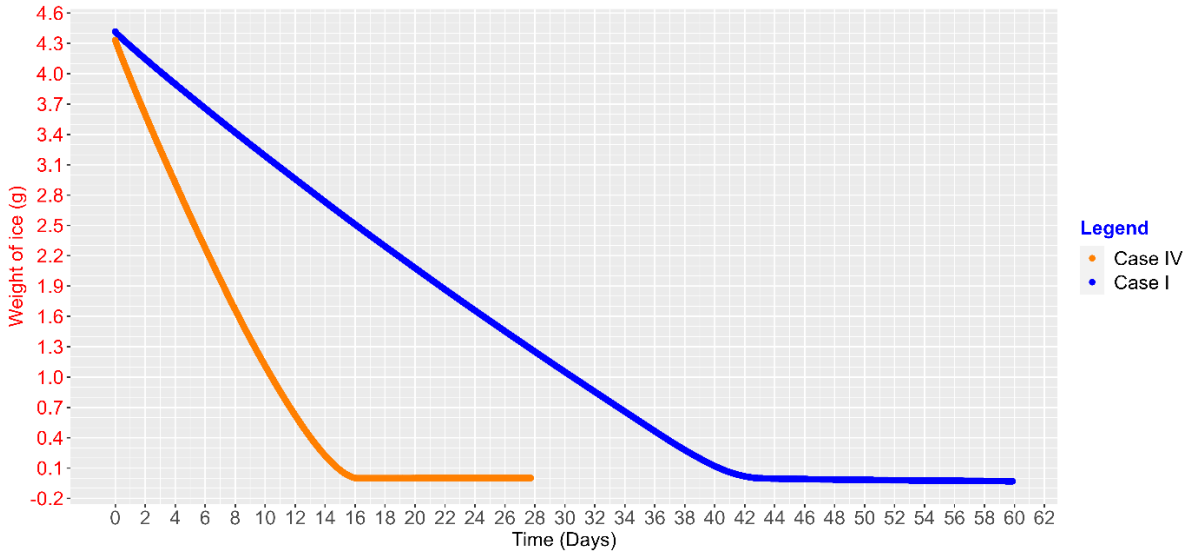

Figure 6-17 Comparison of weight loss by sublimation - case IV (changing area) & case I (constant area)

Figure 6-17 compares the weight loss during the experiment case IV (orange) with the ice with constant subliming area experiment case I (blue). The weight loss is faster in case IV even though both had similar initial mass of ice. It took almost 42 days for all the ice in

the sample holder to sublime in case I while only 16 days in case IV with larger initial ice surface area.

6.3.3.2 Sublimation flux and rate

Figure 6-18 shows the comparison between the rate of sublimation for ice with constant area of ice (case I) denoted by blue line and for decreasing area of ice (case IV) denoted by the orange curve.

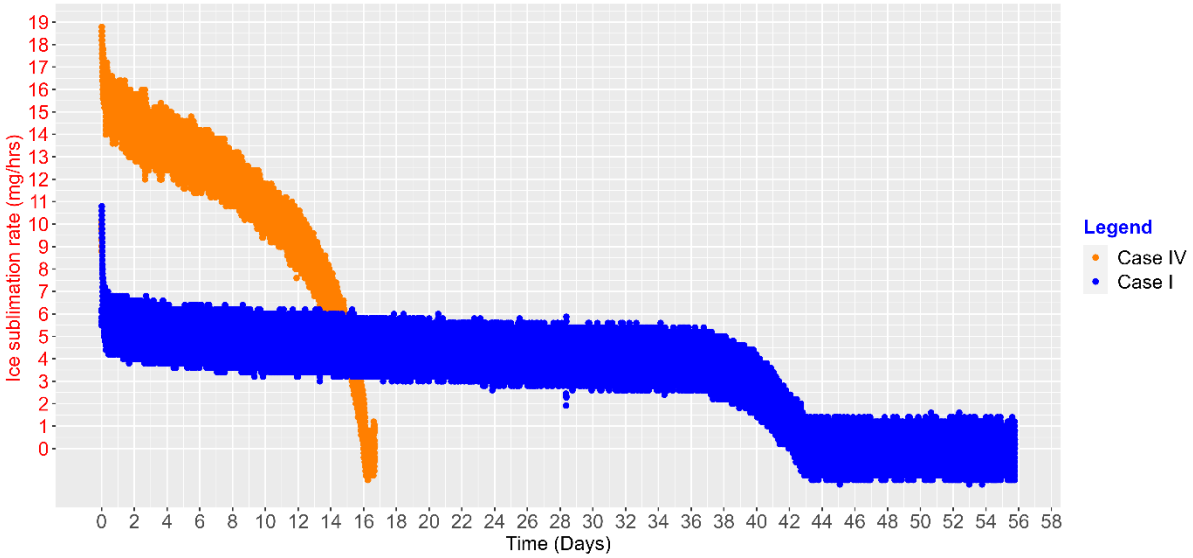

Figure 6-18 Rate of weight loss by sublimation – case IV (changing area) & case I (constant area)

The rate of ice sublimation for constant ice area remains almost constant until there is little ice remaining in the holder. The difference in the rate can be attributed to the constant area of ice available for sublimation in case I and the decreasing area of ice in case IV. The initial rates for ice sublimation are found to be proportional to the area of ice.

Figure 6-19 shows the comparison between the sublimation flux for ice with constant area of ice (case I) denoted by blue line and for decreasing area of ice (case IV) normalised denoted by orange line. The area used to find the sublimation flux for the case IV is calculated by assuming that the pool of ice to shrink uniformly with the ice loss. The initial sublimation flux of the two Cases is very similar and remains similar even though they have different sublimation rates. The difference in the pattern for ice sublimation rate is to be noted for future comparison in the ice sublimation rate for leaf-like products.

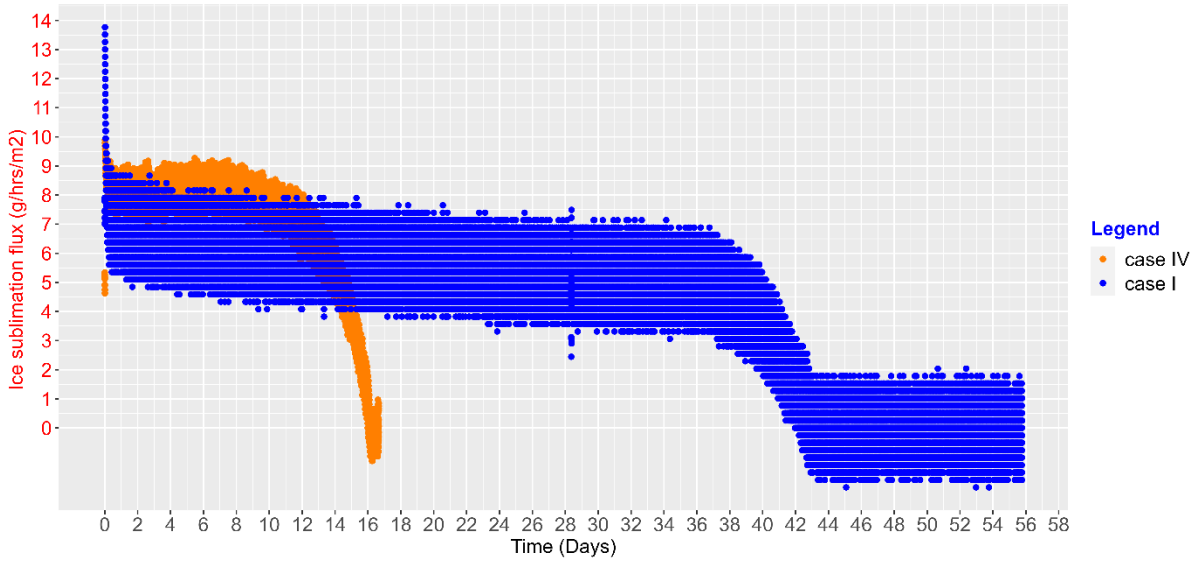

Figure 6-19 Ice sublimation flux comparison – case IV (changing area) & case I (constant area)

Figure 6-20 shows the sublimation flux when compared with the mass of ice remaining in the ice cube holder.

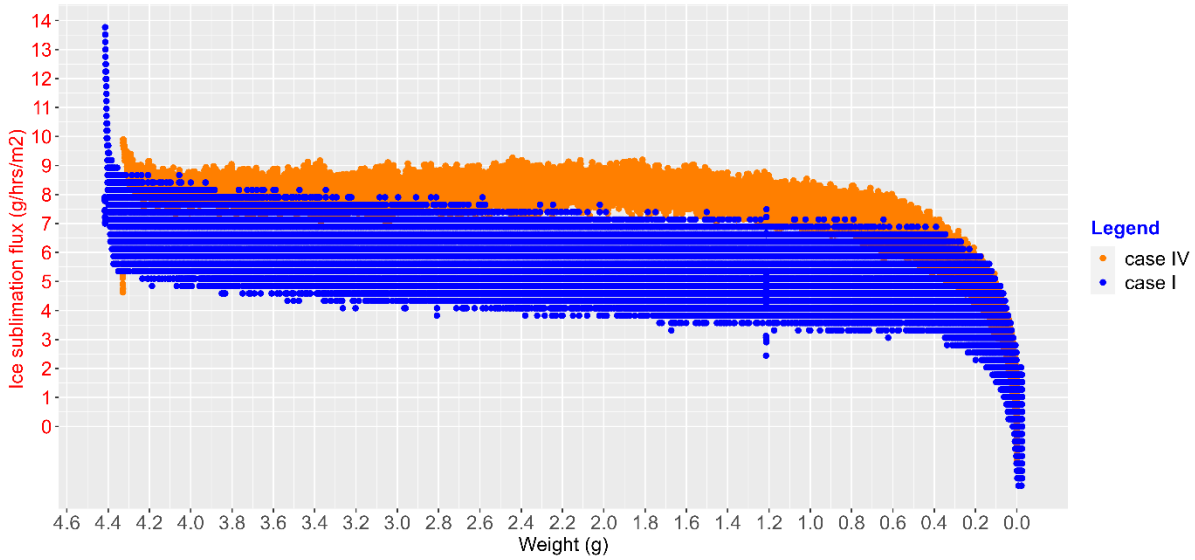

Figure 6-20 Ice sublimation flux comparison - mass of ice remaining in ice holder – case IV (changing area) & case I (constant area)

The ice sublimation for the changing area (case IV) denoted by orange remains mostly constant except at the end while the blue curve for the constant area experiment (case I) could be seen to decrease slowly. This slow change in the case I can be attributed to the increasing resistance for the mass transfer of water vapour as the ice surface recedes further into the ice cube holder. We can see a dependency of the sublimation rate on the

evolution of the area during the sublimation process and this is in agreement with the results of the ice drop sublimation experiment done by other researchers (Jambon-Puillet et al., 2018).

6.4 Comparison of experiment results - model fitting & predictions

In this section, the experiment results for case II are compared with the model predictions for the same experiment conditions. The model includes the assumptions listed in chapter 5.1.1, most of which have already been discussed with respect to the experimental results. However, relevant to matching the model in a simple way to the experimental results are two further model assumptions. These are that air temperature and ice temperature are constant over time. In reality, due to the freezer cycling, both temperatures oscillate, but this effect is minor as so is assumed negligible. Also, worth noting here is that, while the model for ice sublimation (as against the model for hops freeze-drying) assumes air and ice temperatures are constant, it does not assume they are the same temperature. Indeed, the experiments show that without air circulation they can be regarded as the same temperature, but with air circulation there was ~0.4°C difference, with the air increasing by ~0.2°C (probably an experimental anomaly because the fan is an additional heat source) and the ice decreasing by ~0.2°C. Later in the hops model, because the ice is within the leaf, the effect of air circulation is negligible, and so the model does assume the air and ice are at the same temperature.

The ice sublimation model developed in Chapter 5 is used to obtain a fitted value for the boundary layer thickness for mass transfer boundary layer thickness between the top of the sample holder and the bulk air for no air circulation using the weight loss data for case I (fitting procedure shown in appendix). It was found to be 0.0058 m and is used to predict the values for the case II with no air circulation. After 120 hours, when the fan was turned on, the total boundary layer thickness for mass transfer of water vapour from the surface of the ice to the bulk air was found to be a lower value of 0.003 m. This confirms that having the fan on did indeed circulate air into the head space of the sample holder thus reducing the boundary layer thickness and thus the mass transfer resistance.

6.4.1 Weight loss during sublimation

Figure 6-21 compares the model predicted weight loss with the experiment results. The experiment results are a good fit with the model predictions, using the above two best-fit parameters. Importantly, the model has the same form as the experimental results throughout freeze-drying. This fit implies that the model assumption that the ice is at constant temperature and sublimation is not limited by heat transfer in the present AFD setting is valid for the no air circulation period.

In the period with air circulation, the ice sublimation rate is limited by the heat transfer as there was a small difference of 0.25 °C in the temperature of ice and air, but the model was still able to predict the weight loss accurately with a constant temperature assumption as the temperature difference was very small implying that the mass transfer and heat transfer rates are in similar range in this case. The additional mass transfer resistance layer in the case of ice subliming inside the leaf-like product would mean that the assumption that ice sublimation is not limited by heat transfer would be very safe for our analysis of the leaf-like materials.

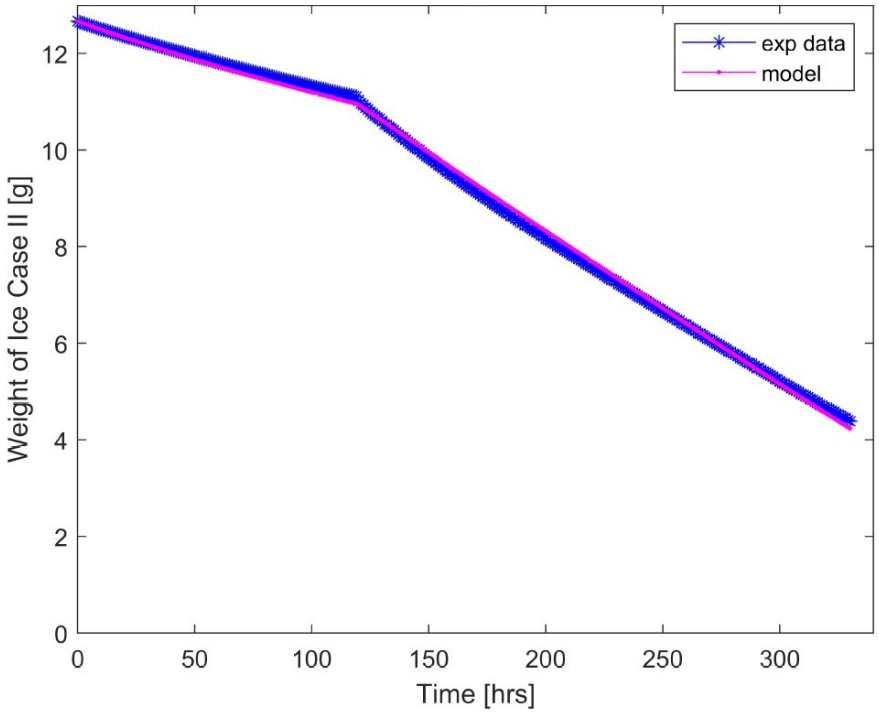

Figure 6-21 Comparison of weight loss during sublimation – Model prediction (no air circulation for 120 hrs and then with air circulation) vs case II (no air circulation for 120 hrs and then with air circulation)

6.4.2 Air RH during sublimation

Figure 6-22 shows the air RH measured during the experiment and the predicted values for same. The model calculates air RH is based on the moisture content in air accumulated during its transfer from the ice to the silica gel and changes with the increase in the moisture content in the silica gel. The model simulates the increase in the moisture content quite adequately. The model assumes an initial zero moisture content and that is reflected in the initial model predictions when compared to the experiment results.

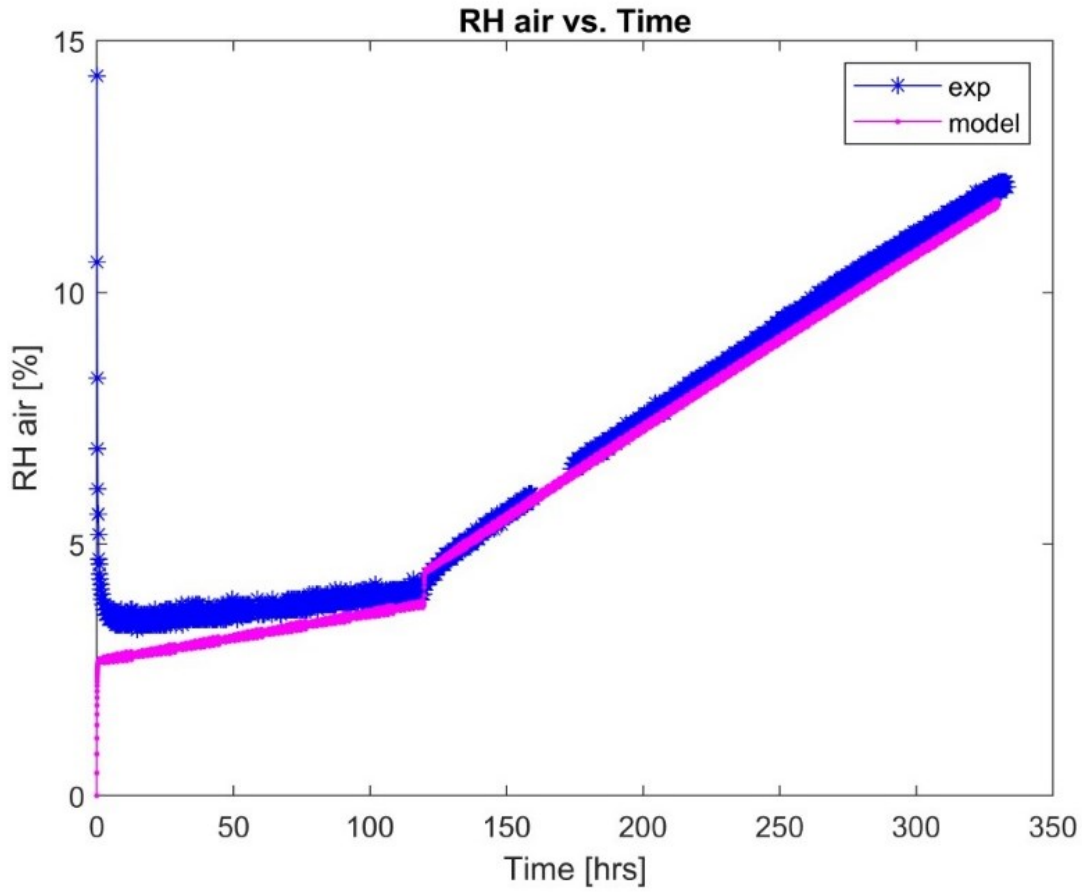

Figure 6-22 Comparison of Air RH (%) - Model with experiment

6.4.3 Silica gel moisture content during sublimation

Figure 6-23 shows the model prediction versus the experimental results for the moisture content increase in the silica gel during the experiment.

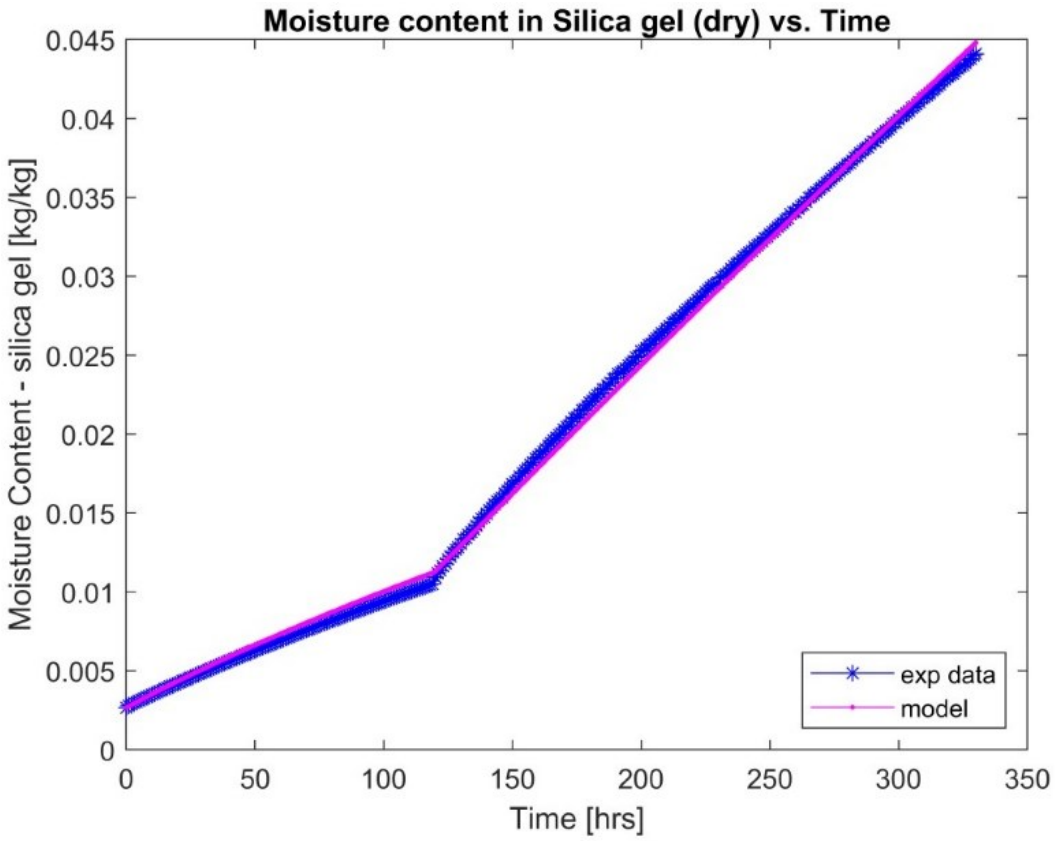

Figure 6-23 Moisture content increase in the silica gel

6.5 Conclusions

The measured temperature of ice during the experiment and the predictions by the model developed using the assumptions described in the section 5.1.1 suggest that for the current AFD settings, ice temperature can be considered a constant and that it is not limited by heat transfer and is limited by mass transfer in the case of no air circulation. In the case of ice sublimation with air movement, even though it is limited by heat transfer, it can be modelled quite accurately by the constant temperature assumption. The sublimation rate is found to be a strong function of the area of ice available for sublimation. These points will be used in the next chapters for developing a further understanding of the AFD of leaf-like materials.

Chapter 7 Hops Experiment System and Discussion

7.1 Introduction

This experimental study of the freeze-drying of hops follows that on pure ice, as detailed in Chapter 6. In that study, the ice sublimation results were compared to the model developed in Chapter 5, from which the best fit external mass and heat transfer coefficients were able to be calculated. Here the study is extended. Hops is a more complex system with ice crystals embedded deep within the leaf structure, through which the sublimed water vapour must pass to reach the bulk air environment. This has the net effect of increasing the heat and mass transfer resistances, which are assumed to be the sum of the internal and external resistances. With the external resistances already known from the pure ice study, this hops investigation aims to establish the internal resistances. Here, the experimental results are presented and interrogated. They are then compared to the model developed in Chapter 5, both for their goodness of fit, and to determine the parameters of best fit.

Hops is a leaf-like system for which, as noted in chapter 2, no AFD studies have been reported. Most research has been on cubes and spheres for which sublimation has generally been assumed to proceed with a uniformly retreating ice front. Because leaves are geometrically different to cubes and spheres, a different approach has been taken in this study, as detailed in Chapter 5. Here, the thin leaf-like system is assumed to contain intercellular gas exchange pathways and the ice crystals, which are distributed throughout the cells of the leaf-like structure, are assumed to all sublime from the beginning. This is quite unlike the uniform retreating ice front model.

These experiments with hops used the same apparatus detailed in chapter 4. The experiments were conducted under the same conditions as for the ice sublimation experiments described in chapter 6.

7.2 Experiment procedure

Similar to the experiment procedure followed in section 6.2, the experiment was conducted at a constant temperature. A frozen hop sample from storage was first kept in a plastic pouch inside the freezer used for AFD to equilibrate to the freezer temperature. From this sample, a sub sample of hops was transferred to the sample tray for the

experiments. Experiments were done with and without forced air circulation inside the drying chamber.

As for all the ice sublimation experiments described in Chapter 6, 200 g of silica gel was kept at the bottom of the drying chamber (the uninsulated chamber exposed to the freezer temperature), and the silica gel beads were spread out on the floor of the drying chamber to form a single layer. The AFD apparatus had been kept in the freezer 24 hours before the silica gel was introduced to the drying chamber, so that the apparatus would be at the process temperature when the silica gel is placed within. The drying chamber was then closed and kept closed for a further 24 hours to allow the drying chamber air moisture content/RH to reduce to its equilibrium with the silica gel which is at around 2% RH. The chamber is then opened to place the hops sample on the sample tray as quickly as possible.

The procedure outlined in section 6.2 regarding the weighing balance and the sensors was used for the experiment. Additionally, an iButton sensor (Hygrochron, see section 3.2.5) was used to measure the air RH and temperature near the hops above the sample tray. Differential weight loss and sublimation flux values were calculated and plotted based on the methods outlined in section 6.2. For calculating the sublimation flux the total area (upper and lower faces of the petals) of the hop petals was considered instead of the area of the ice. The experiments done are tabulated in Table 7-1.

Table 7-1 Hops AFD experiments

		Temp (°C)	Initial silica gel wt. (g)	Initial hops wt. (g)	Fan Status
0	Case 0	-12	200	5.6459	OFF
Effect of temperature					
1	Case I	-15	200	5.5183	OFF
2	Case II	-12	200	5.5751	OFF
Ratio of adsorbent to hops					
3	Case III	-15	200	1.4420	OFF
Air circulation					
4	Case IV	-12	200	5.8542	ON

7.2.1 Effect of temperature on AFD of hops kinetics

The ice sublimation studies in Chapter 6, concluded that ice sublimation in an environment with no air circulation is limited by mass transfer and for a leaf-like product

with an additional layer of product between the subliming ice crystal and moisture sink would also be a mass transfer limited process. Another extrapolation can be made for this, i.e., the drying rate can be increased by increasing the mass transfer rate by increasing the temperature which would increase the diffusion rate.

To study the effects of temperature on the AFD kinetics of hops, AFD of hops was performed under two temperature settings. The results are later compared with the model predictions for this temperature assuming no heat transfer limitations.

7.2.1.1 Case I

The AFD experiment was conducted at a constant temperature of -15 ^{o}C, with an initial sample quantity of 5.5183 g of hops, placed on the sample tray. There was no forced air circulation inside the drying chamber during the experiment. The quantity of fresh silica gel used was 200 g.

7.2.1.2 Case II

An experiment for AFD of hops at -12 ^{o}C was done to study the effect of higher temperature on AFD and a sample size of 5.5751 g of hops was used. The adsorbent quantity used was as in section 7.2.1.1 for case I.

7.2.2 Effect of ratio of mass of the adsorbent to hops on AFD kinetics

The mass transfer rate should increase if the concentration gradient between the subliming ice crystal and the moisture sink is increased for the same mass transfer resistance and temperature. This scenario can be simulated by increasing the quantity of adsorbent available for the same quantity for hops or decreasing the quantity for hops for the same quantity of adsorbent thereby effectively decreasing the air RH in during the experiment. To study this effect the following experiment was undertaken.

7.2.2.1 Case III

Hops were subjected to AFD at -15 ^{o}C to study the effect of the adsorbent quantity usage based on the procedures used for case I as described in 7.2.1.1. The quantity of hops sample for the experiment was reduced to 1.4420 g to increase the weight ratio of adsorbent to hops. The weight ratio of adsorbent to the hops is 139 for case III compared to 36 for case I.

7.2.3 Effect of air circulation on AFD kinetics

As described in the literature review in section 2.4, (Di Matteo et al., 2003) report that air movement increased the drying kinetics of AFD of biological products only in the initial period and thereafter there was no impact on the drying rate, and the authors further assumed that AFD was limited by internal mass transfer resistance alone. To verify this assumption for leaf-like products an experiment was done with hops with air circulation.

7.2.3.1 Case IV

Hops were subjected to AFD at -12 °C with air circulation. The procedures used in case II described in section 7.2.1.2, were followed in this experiment except for the addition of air movement induced by a fan. Air velocities measured by thermo-anemometer near the hops were found to be around 0.23 m/s. A hop sample of 5.8542 g was used for the experiment.

7.3 Results & discussion

Raw data for all the experiments were analysed, and the results are presented in the following sections.

7.3.1 Effect of temperature on AFD of hops kinetics

7.3.1.1 Air temperature in the AFD apparatus drying chamber

Figure 7-1 shows the air temperature for case I (blue) & II (red) and the air sensor temperature readings could be seen to be at a constant temperature of -12 °C and -15 °C respectively during the whole of the experiment with a variation within a range of ± 0.20 °C due to the freezer refrigeration cycle.

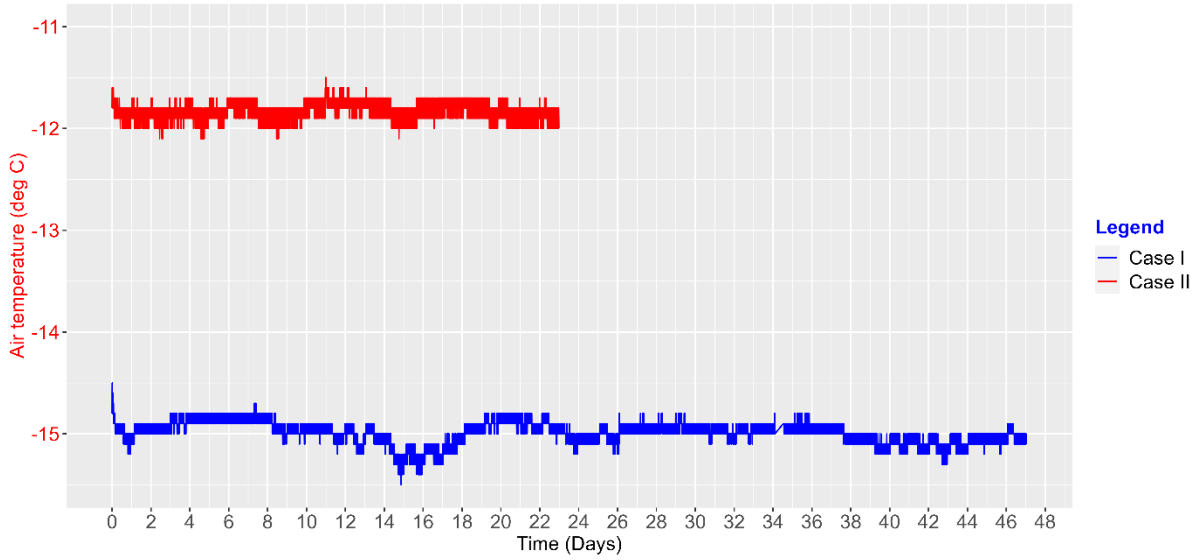

Figure 7-1 Air temperature in the drying chamber of the AFD apparatus - AFD of Hops - Exp VI – case I (-15 °C) & case II (-12 °C)

7.3.1.2 Weight loss by sublimation

Figure 7-2 shows the comparison between the weight loss of hops in case I (blue) & II (red) due to drying by ice sublimation. The drying in case II which is done at -12 °C takes almost 15 days to complete and is faster than the 26 days required for the case I at -15 °C. The decrease in drying time or the increase in drying rate can be explained by the expected increase in mass transfer by diffusion at higher temperature. The higher temperature has a greater saturation water vapour in air. Therefore, the potential for mass transfer is greater and air at the higher temperature is more energetic and so the diffusion coefficient will be greater. This effect of temperature can be seen in the model predictions for the AFD experiments for different temperatures in section7.4.2 & 7.4.3

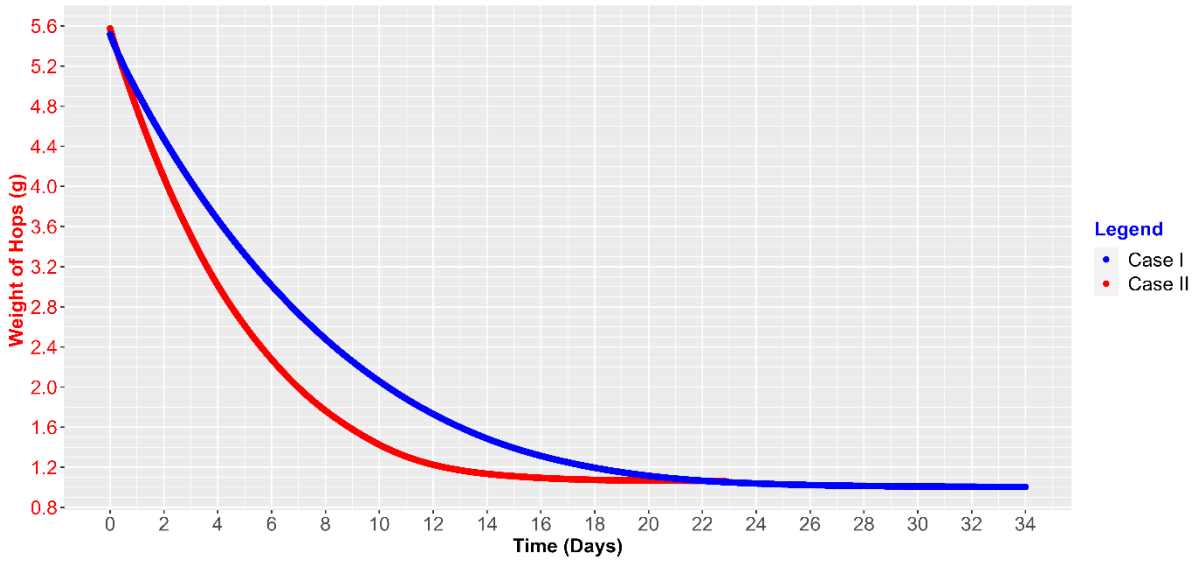

Figure 7-2 Weight loss comparison during AFD of Hops – case I (-15 °C) & case II (-12 °C)

7.3.1.3 Air humidity in the AFD apparatus drying chamber

Figure 7-3 shows the air RH during the AFD of hops experiments case I (blue) & II (red) measured at a distance of approximately 30 mm beside from the sample tray.

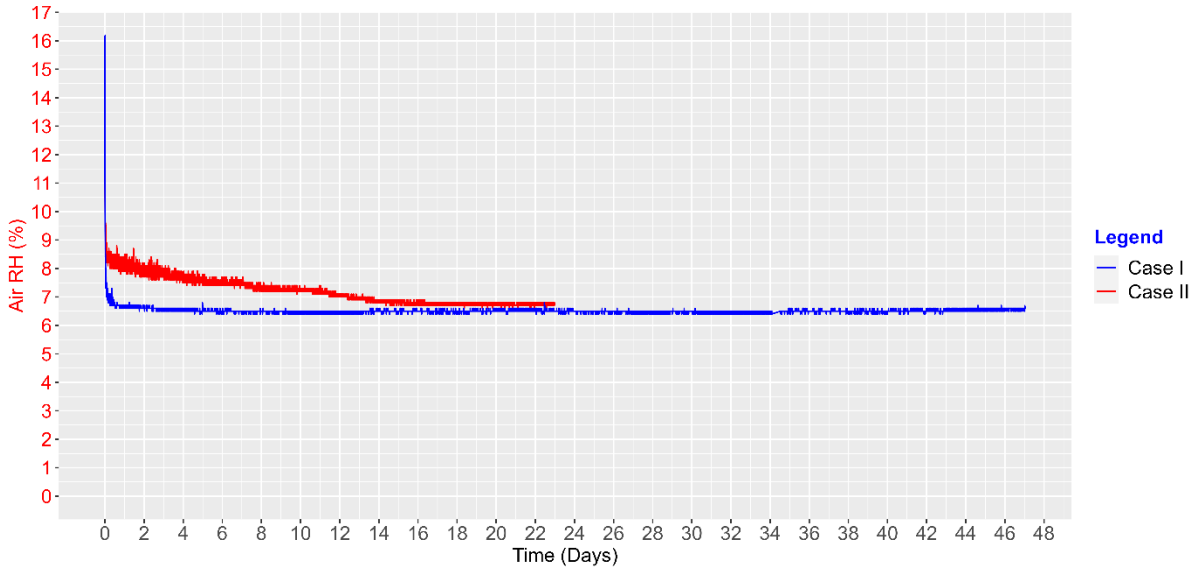

Figure 7-3 Comparison of air RH in the drying chamber of AFD apparatus– case I (-15 °C) & case II (-12 °C)

The air RH for case II can be seen as decreasing continuously till the end of drying and reaches an equilibrium value with silica gel moisture content while the air RH for case I can be seen to increase very slowly as the drying progresses reaching its final equilibrium value. This difference in air RH can be attributed to the higher rate of drying at higher temperature due to the higher mass transfer rate in case II which leads to a higher moisture content in the air compared to a similar adsorption rate by silica gel in both Cases. This is well captured in the model comparison in the section 7.4 of the current chapter.

7.3.1.4 AFD hops sublimation flux

Figure 7-4 shows the mass transfer flux for water vapour during the AFD of hops (calculation as described in section 6.2 & 7.2).

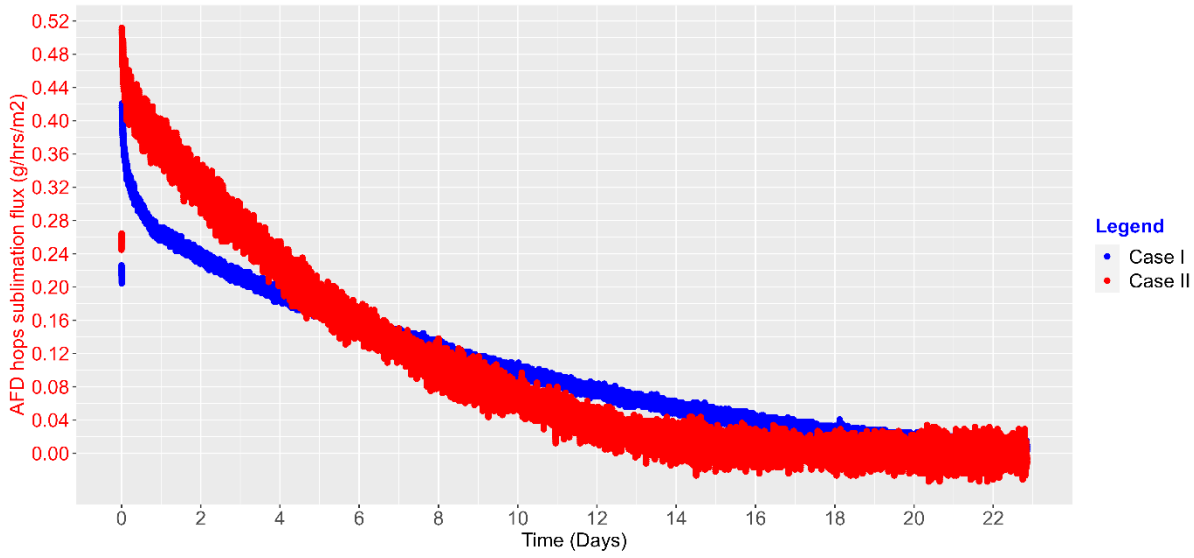

Figure 7-4 AFD hops sublimation flux comparison - AFD of Hops– case I (-15 °C) & case II (-12 °C)

The sublimation flux values for case II (red) at -12 °C are higher than the flux values for the AFD drying case I (blue) at -15 °C, indicating the influence of processing temperature on the drying rate. The decreasing flux as drying proceeds can be seen more easily in Figure 7-5 with the sublimation flux plotted against the ice content remaining in the hops. Sublimation flux for case I is shown in blue while case II is represented in red.

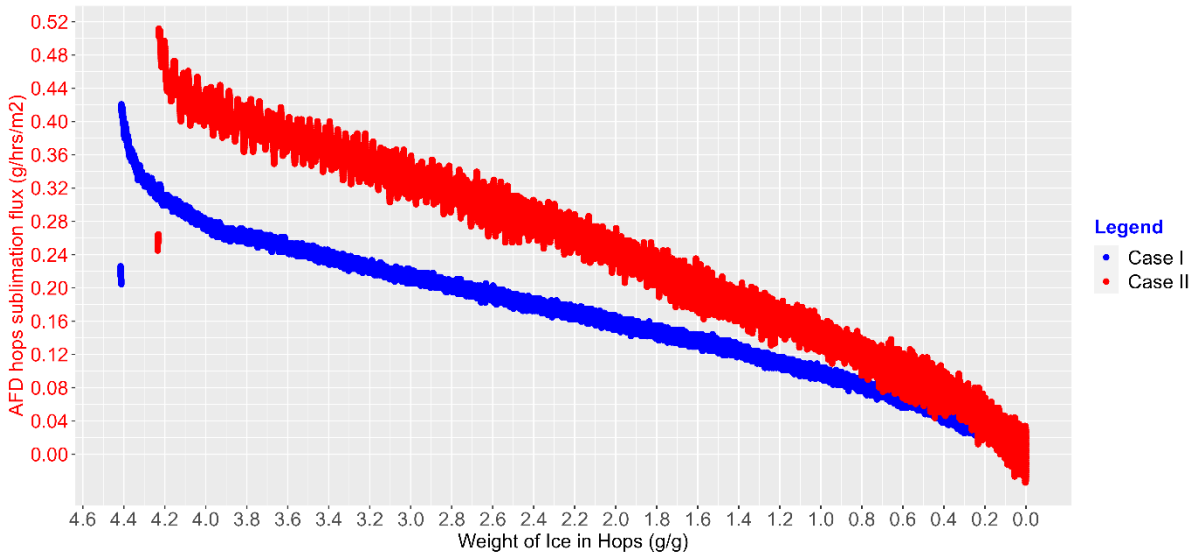

Figure 7-5 AFD hops sublimation flux comparison based on ice content remaining- AFD of Hops- case I (-15 °C) & case II (-12 °C)

The initial sublimation flux for case I (AFD at -15 °C) is around 0.30 g/hrs/m^2 while that of case II at -12 °C is around 0.45 g/hrs/m^2, which is almost 1.5 times higher. The different initial sublimation flux can be attributed to the lower mass transfer rate by diffusion affected by the lower temperature. The reason for decreasing sublimation flux can be hypothesized to be attributed to two factors; 1) the increase in resistance to mass transfer of water vapours formed by ice sublimation. The ice crystal surface moves further inside the cell as the ice sublimes and leaves behind porous regions of cellular material which in turn increases the path length for mass transfer and the resistance.; 2) the decreasing area available for ice sublimation as the size of the ice crystals decrease as the drying proceeds (the flux here is calculated based on the fixed surface area of the hops rather than the area of ice). These two factors are confounded and in combination, decrease the overall sublimation flux of the AFD as the drying progresses. It can be observed that there is greater variation within the curve for case II compared to case I, but the author could not attribute any particular reason for this.

7.3.2 Effect of ratio of mass of the adsorbent to hops on AFD kinetics

7.3.2.1 Weight loss by sublimation

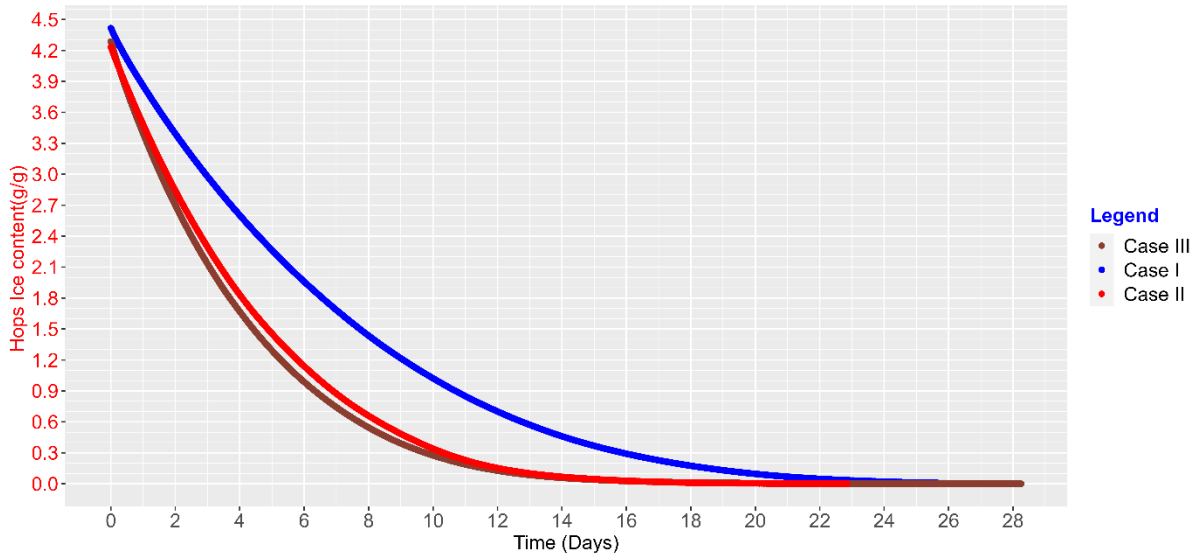

Figure 7-6 Specific weight loss during AFD of Hops - case III (-15 °C, High adsorbent ratio), I (-15 °C, Low adsorbent ratio) & II (-12 °C, Low adsorbent ratio). Vertical axis is plotted in grams of ice/gram of dry matter.

Figure 7-6 compares the specific weight loss for AFD of hops for Cases III, I, II. It can be seen that for experiments all conducted at -15 °C, the time to dry is faster for higher adsorbent to hops ratio case III (brown) when compared with the case I and is comparable to case II at a higher temperature of -12 °C with lower adsorbent to hops ratio. So, it can be seen from the comparison that the drying time was reduced when the adsorbent to hops ratio was increased and when the process temperature was increased.

7.3.2.2 Air humidity in the AFD apparatus drying chamber

Figure 7-7 shows the air RH during the AFD of hops experiments case I (blue) and case III (brown) at the same temperature (-15 °C).

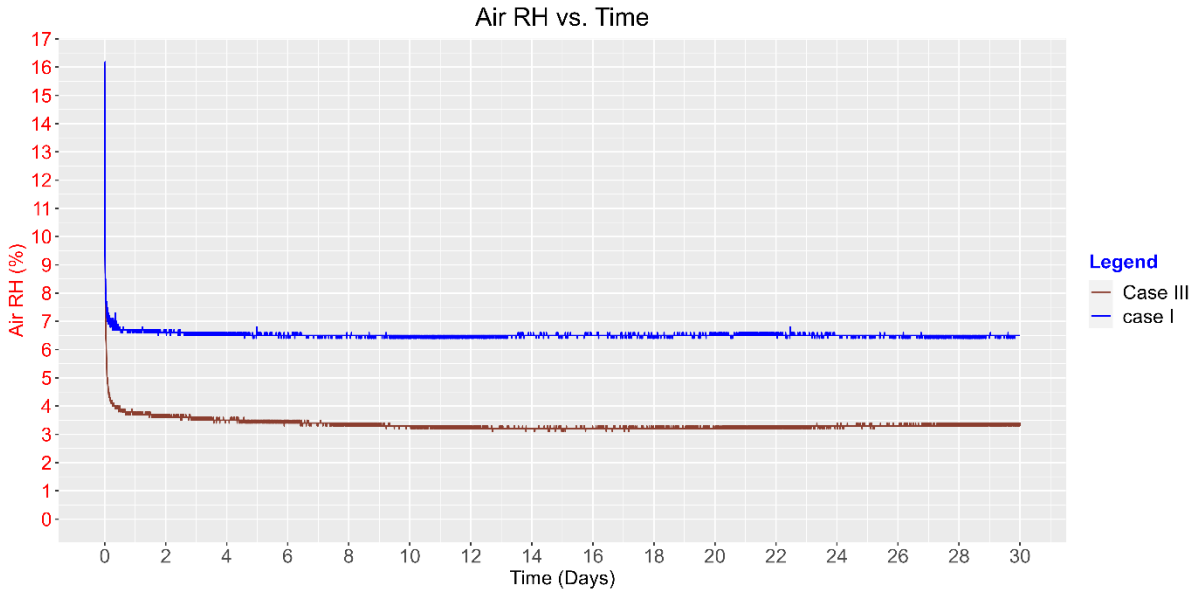

Figure 7-7 Air RH in the drying chamber of AFD apparatus- case III (-15 °C, High adsorbent ratio) & I (-15 °C, Low adsorbent ratio)

The RH of the air for case III is almost the half the value of the RH of air in case I. This can be explained by lower equilibrium moisture content of air as a result of the much higher adsorbent quantity.

7.3.2.3 AFD hops sublimation flux

Figure 7-8 shows the sublimation flux for the case III (brown), I (blue) and II (red). The sublimation flux for case III is higher than the sublimation flux for case II, even though both are at the same process temperature of -15 °C. This can be explained by the increased mass transfer gradient available for mass transfer as the higher adsorbent quantity in case III decreases the equilibrium air moisture content in air thus generating a higher overall mass transfer gradient.

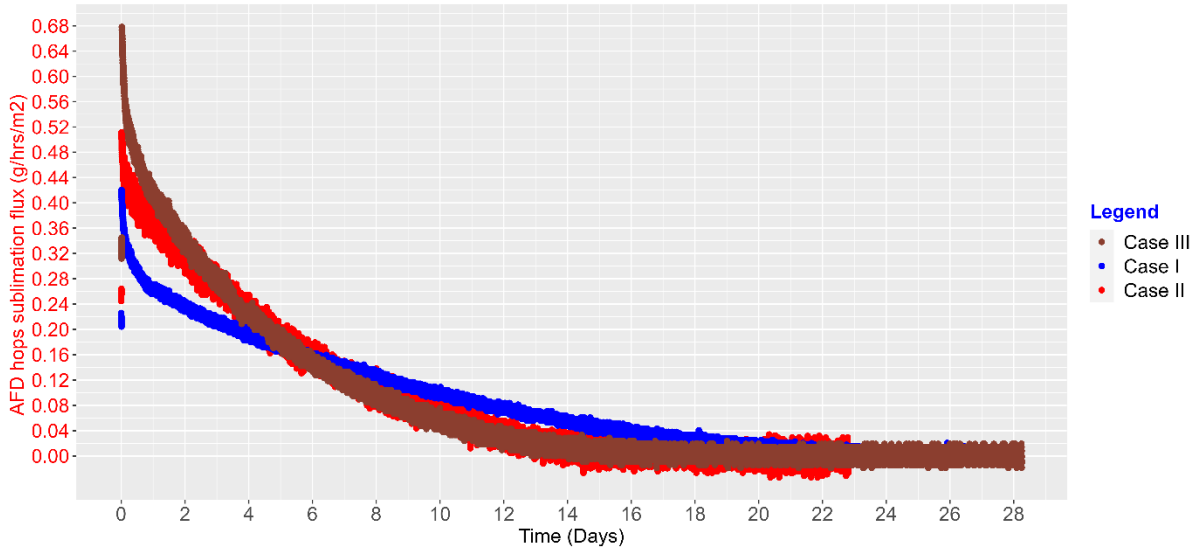

Figure 7-8 AFD hops sublimation flux comparison - case III (-15 °C, High adsorbent ratio), I (-15 °C, Low adsorbent ratio) & II (-12 °C, Low adsorbent ratio)

The sublimation flux for case III can be found to be the same as that of case I which is a at the higher temperature of -12 °C, but with lower adsorbent to hops ratio. The comparison can be seen more clearly in Figure 7-9.

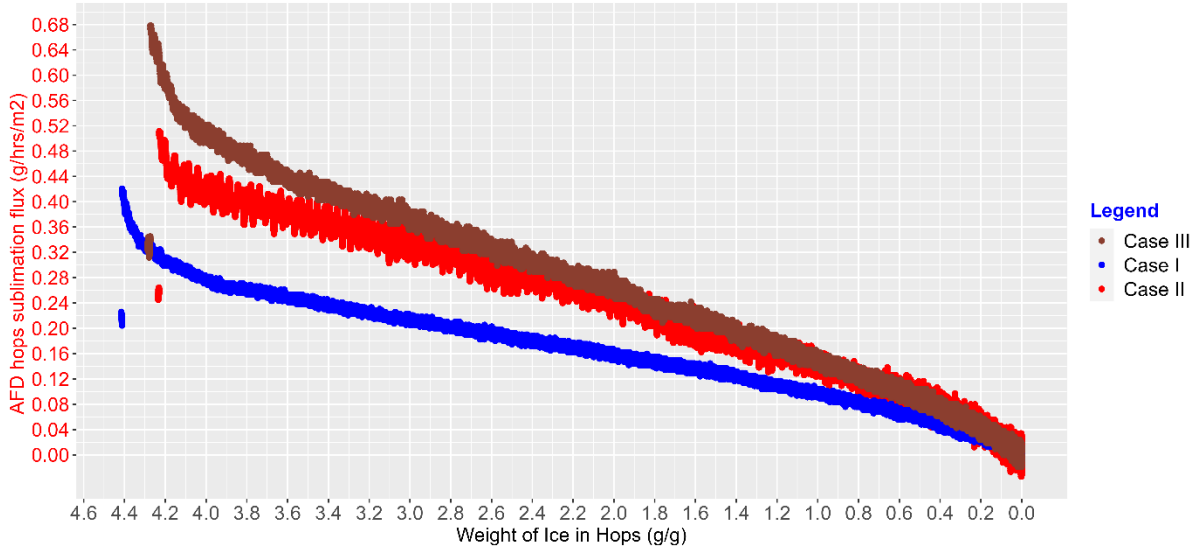

Figure 7-9 AFD hops sublimation flux comparison - case III (-15 °C, High adsorbent ratio), I (-15 °C, Low adsorbent ratio) & II (-12 °C, Low adsorbent ratio)

The effect of lower air RH due to higher adsorbent quantity is significant industrially. The use of a desiccant wheel could result in a very high adsorbent to product ratio and thus a low air RH for higher mass transfer gradient and a faster drying rate.

7.3.3 Effect of air circulation on AFD of hops kinetics

7.3.3.1 Weight loss by sublimation

Figure 7-10 shows the case IV (dark green) weight loss of hops sample during the AFD with air circulation and the drying is completed within 11 days.

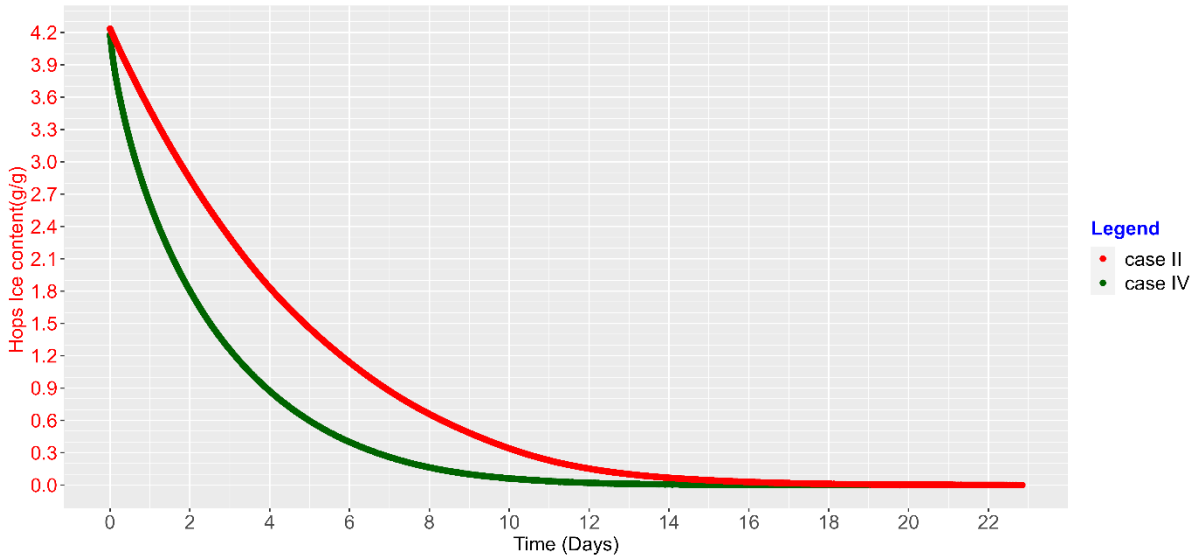

Figure 7-10 Weight loss during AFD of Hops - case IV (-12 °C, Fan ON)& case II (-12 °C, Fan OFF)

On comparing weight loss for case IV with the case II (red), which is for the same temperature and same ratio of adsorbent to hops, it is found that the time required to complete the drying is less. The time required for the end of drying is 11 days in the current experiment with fan and the time required for drying with without fan is 15 days. The air circulation could result in decrease in the mass transfer resistance across the boundary layer near the hops as well as near the adsorbent.

7.3.3.2 Air humidity in the AFD apparatus drying chamber

Figure 7-11 shows the air RH during the AFD of hops experiments case IV (dark green) and II (red) at same temperature. The air RH for case IV can be seen as increasing slowly from a lower initial RH value unlike what is observed in the case II. This initial low value would suggest a faster moisture adsorption rate at the adsorbent side and thus increased mass transfer gradient for the mass transfer and thus a higher rate of drying.

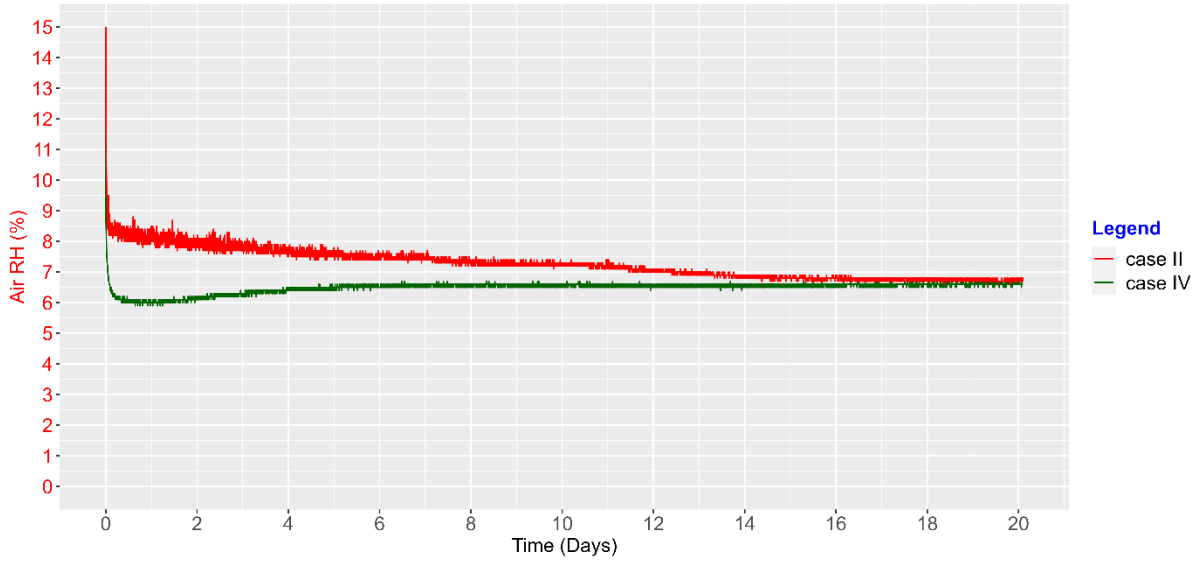

Figure 7-11 Air RH in the drying chamber of AFD apparatus- case IV (-12 °C, Fan ON)& case II (-12 °C, Fan OFF)

7.3.3.3 AFD hops sublimation flux

Figure 7-12 shows the sublimation flux for case IV (dark green) & case II (red). For case IV, there is a high sublimation flux for the first 4-5 days and a lower sublimation flux value with long tail for the rest of the AFD process. When compared with case II, case IV has higher the sublimation flux even though both are at the same process temperature of -12 °C.

The sublimation flux reduces only after the moisture content is reduced to a low value of 0.8 kg ice/kg dry hops (after the initial moisture content is reduced by more than 80%). After that, both the experiments followed the same sublimation flux rates. This experiment shows that the AFD of hops is affected by air circulation throughout most of the moisture loss time course and that this influence is not an initial period phenomenon as reported for some biological non-leafy products in the literature for AFD.

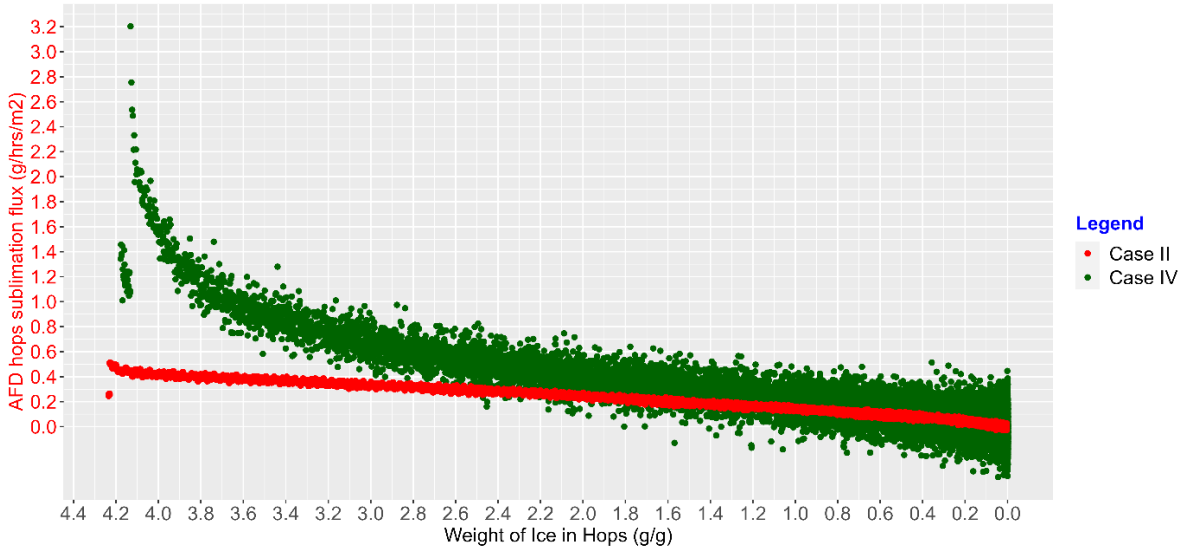

Figure 7-12 AFD hops sublimation flux comparison - case IV & II

7.4 Comparison of experiment results with the model predictions

The results from the experiment were compared with the simulated values from the model developed for AFD in the Chapter 6. Experiments conducted at different process parameter settings are simulated with the model and compared to validate the model based on the mechanism putatively involved in the current AFD process under consideration.

7.4.1 Calculation of fitting parameters – RF_I & RF_II

Data from AFD of hops in case 0 were used to calculate the fitting parameters (fitting procedure shown in appendix). The temperature used for the model was -12 °C. The fitted values for the model parameters are:

RF_I : 1.19×10^{6} (Cell resistance factor)

RF_II : 1.70×10^{5} (Intercellular region resistance factor)

7.4.1.1 Weight loss during sublimation

Figure 7-13 shows the comparison between the experiment data and the simulated data after using the fitted resistance factors.

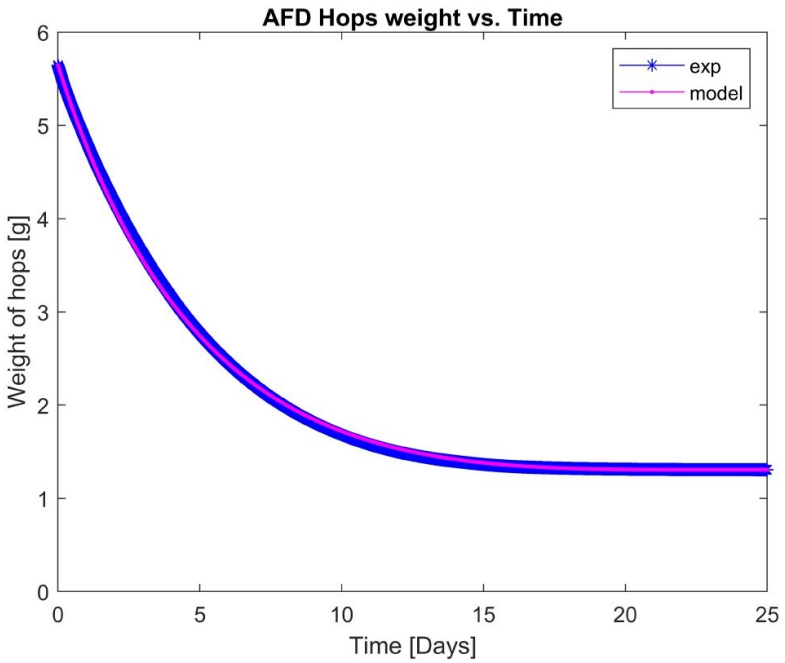

Figure 7-13 Comparison of weight loss during sublimation – AFD Hops case 0 (-12 °C, Fan OFF, Low adsorbent ratio)

7.4.1.2 Air RH during sublimation

Figure 7-14 shows the air RH measured during the experiment and the model-predicted values for same.

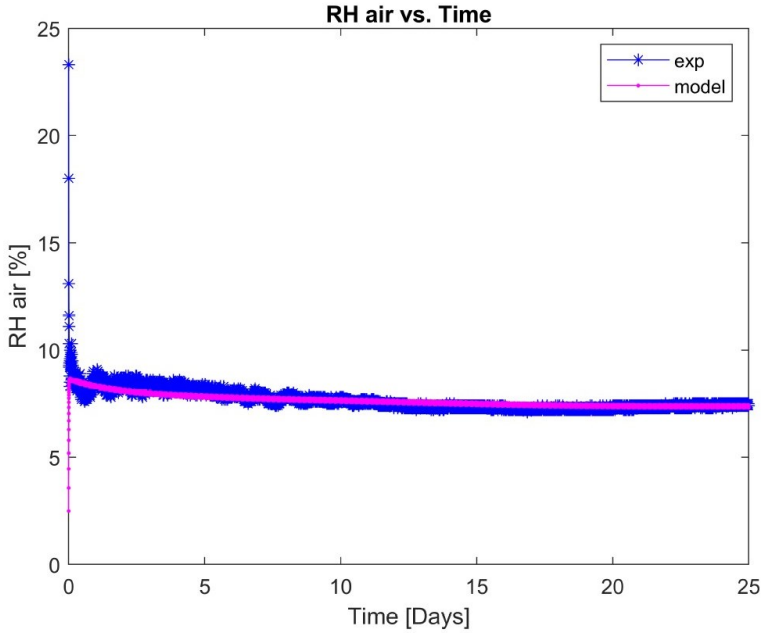

Figure 7-14 Comparison of Air RH (%) - Model vs AFD Hops case 0 (-12 °C, Fan OFF, Low adsorbent ratio)

The parameters used for the model simulations in the following sections are given in the Table 7-2.

Table 7-2 Resistance factor values for model prediction and fitting

		Temp (°C)	RF_I	RF_II
Fitted values				
0	Case 0	-12	1.19×10^{6}	1.70×10^{5}
Effect of temperature				
1	Case II	-12	1.19×10^{6}	1.70×10^{5}
2	Case I	-15	1.19×10^{6}	1.95×10^{5}
Ratio of adsorbent to hops				
3	Case III	-15	1.19×10^{6}	1.20×10^{5}
Air circulation				
4	Case IV	-12	1.19×10^{6}	0.80×10^{5}

Note: RF_I represents the fitting factor for the resistance for mass transfer in the cells when the moisture moves through the porous cell residue and RF_II represent the fitting factor for resistance for mass transfer in the intercellular gas exchange pathways in the leaf-like products (hop petals).

7.4.2 AFD of Hops – Case II

Weight loss during sublimation and RH of the air during the AFD of hops experiment VII are modelled below. The air temperature value used was -12 °C. The values of the fitted parameters RF_I and RF_II calculated from the AFD hops experiment I, 1.19×10^{6} and 1.70×10^{5} respectively, were used here.

7.4.2.1 Weight loss during sublimation

Figure 7-15 shows the comparison between the experiment data and the model-predicted values.

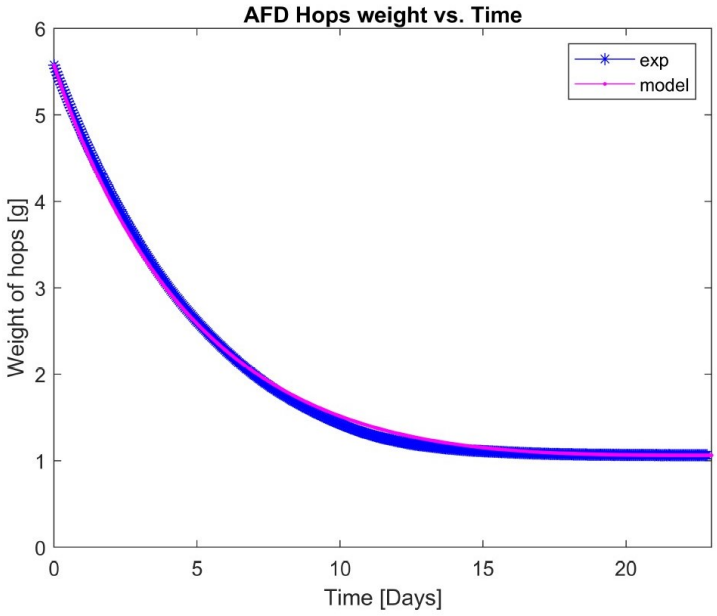

Figure 7-15 Comparison of weight loss during sublimation – AFD Hops case II (-12 °C, Fan OFF, Low adsorbent ratio)

7.4.2.2 Air RH during sublimation

Figure 7-16 shows the air RH measured during the experiment and the model-predicted values for same.

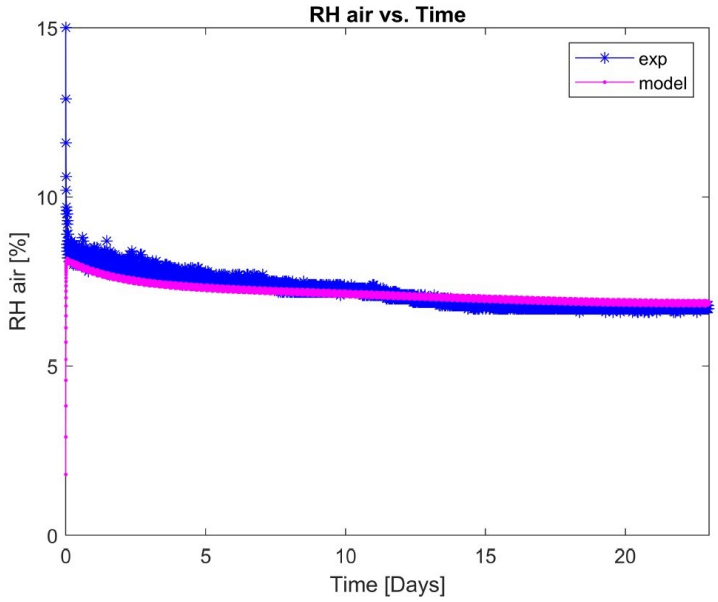

Figure 7-16 Comparison of Air RH (%) - Model vs AFD Hops case II (-12 °C, Fan OFF, Low adsorbent ratio)

7.4.3 AFD of Hops – Case I

Weight loss during sublimation and the RH of the air during the AFD of hops in case I with lower temperature are modelled below. The air temperature value used was -15 °C. The values of the fitted parameters RF_I and RF_II were 1.19×10^{6} and 1.95×10^{5} respectively. The RF_II value had to be increased to fit the data. This could mean that the resistance factor RF_II which relates to the resistance in intercellular region is inversely sensitive to temperature. RF_I which is related to the resistance in the cell, is a structural constant and is independent of the temperature.

7.4.3.1 Weight loss during sublimation

Figure 7-17 shows the comparison between the experiment data and the model-predicted values.

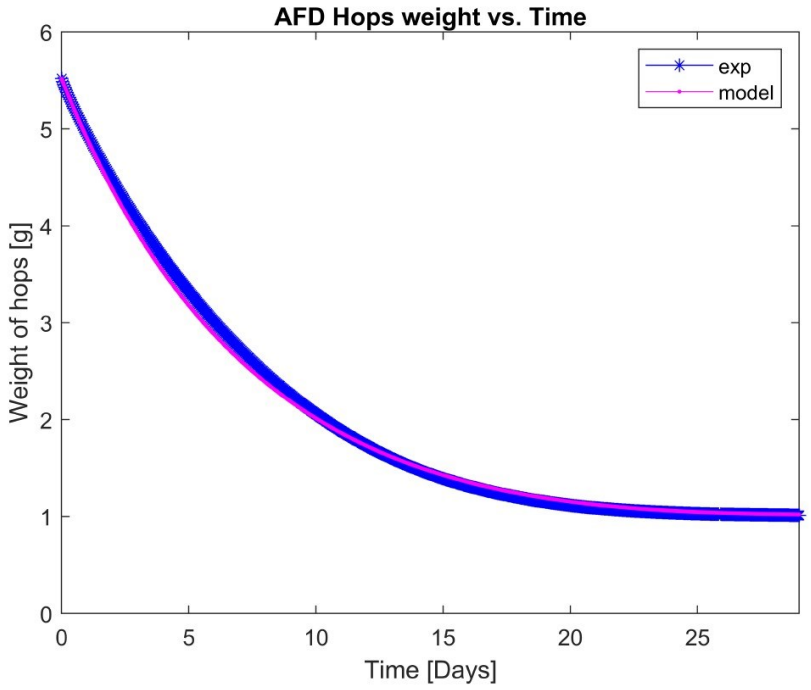

Figure 7-17 Comparison of weight loss during sublimation – AFD Hops case I (-15 °C, Fan OFF, Low adsorbent ratio)

7.4.3.2 Air RH during sublimation

Figure 7-18 shows the air RH measured during the experiment and the model-predicted values for same.

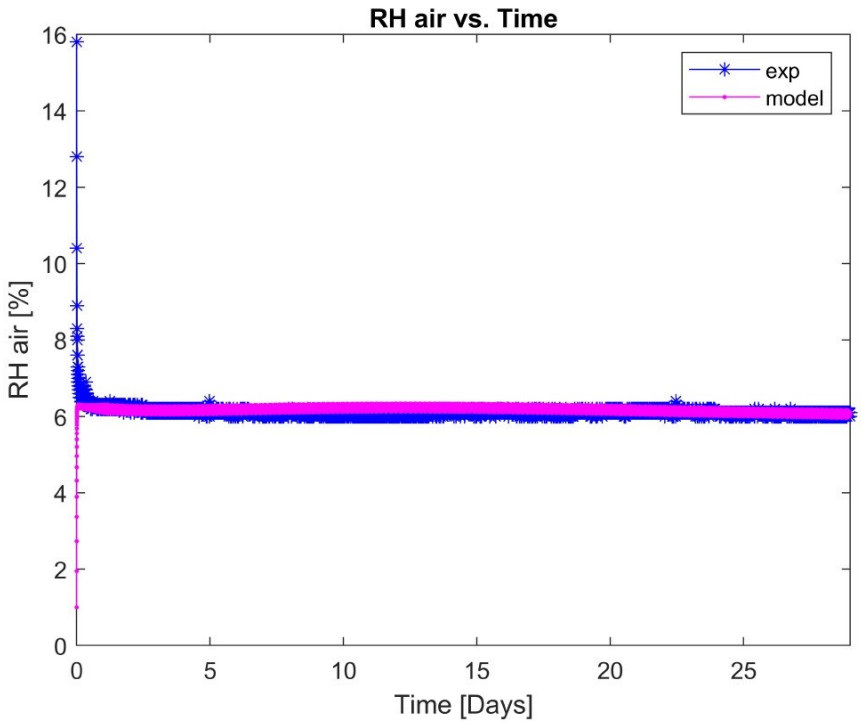

Figure 7-18 Comparison of Air RH (%) - Model vs AFD Hops case I (-15 °C, Fan OFF, Low adsorbent ratio)

7.4.4 AFD of Hops – Case III

Weight loss during sublimation and RH of the air during AFD of hops case III with lower temperature and higher adsorbent to hops ratio are modelled below. The air temperature value used was -15 °C. The values of the fitted parameters RF_I and RF_II were 1.19×10^{6} and 1.20×10^{5} respectively. RF_II had to be decreased to fit the data. The resistance factor RF_II which relates to the resistance in intercellular region is sensitive to the temperature and should have increased as the process temperature is low, as seen in the modelling of AFD hops case I, shown in the section above, but the decrease in the resistance factor value implies a higher dependence of the resistance factor on the mass transfer gradient present. Here, the RF_II decreases with the increase in the mass transfer gradient in the system.

7.4.4.1 Weight loss during sublimation

Figure 7-19 shows the comparison between the experiment data and the model-predicted values.

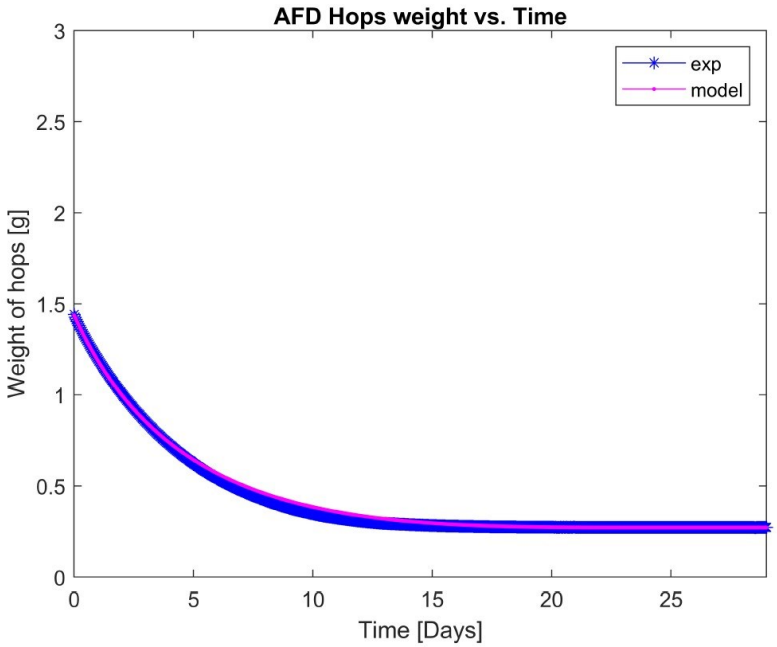

Figure 7-19 Comparison of weight loss during sublimation – AFD Hops case III (-15 °C, Fan OFF, High adsorbent ratio)

7.4.4.2 Air RH during sublimation

Figure 7-20 shows the air RH measured during the experiment and the model predicted values for same.

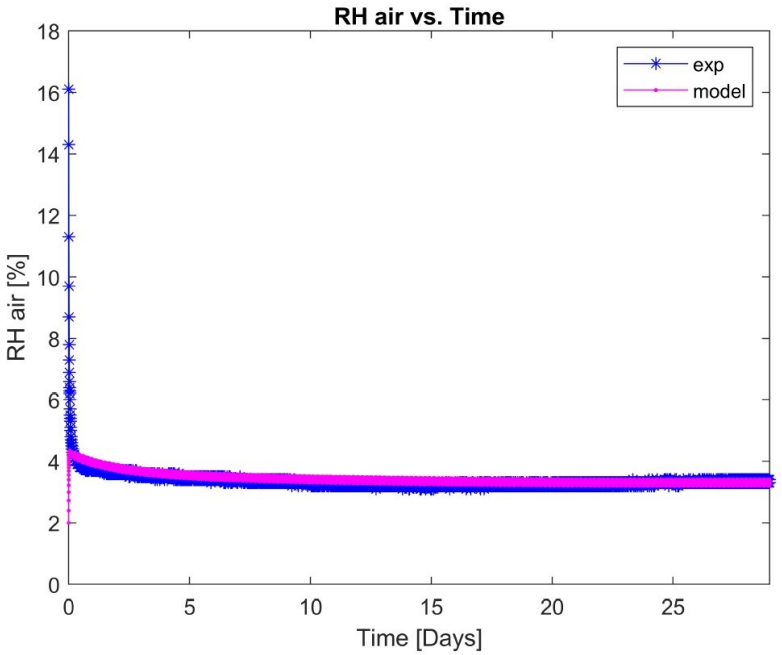

Figure 7-20 Comparison of Air RH (%) - Model vs AFD Hops case III (-15 °C, Fan OFF, High adsorbent ratio)

7.4.5 AFD of Hops – Case IV

Weight loss during sublimation and RH of the air during AFD of hops case IV with air circulation are modelled below. The air temperature value used was -12 °C. The values of the fitted parameters RF_I and RF_II were 1.19×10^{6} and 0.80×10^{5} respectively. The RF_II had to be decreased to fit the data. The resistance factor RF_II which relates to the resistance in intercellular region is found to be sensitive to the temperature and decreases with increasing temperature and decreases with the increase in mass transfer gradient available based on the modelling results in the above sections. The current experiment has both higher temperature and higher mass transfer gradient and thus the larger decrease in the RF_II factor can be explained.

7.4.5.1 Weight loss during sublimation

Figure 7-21 shows the comparison between the experiment data and the model-predicted values.

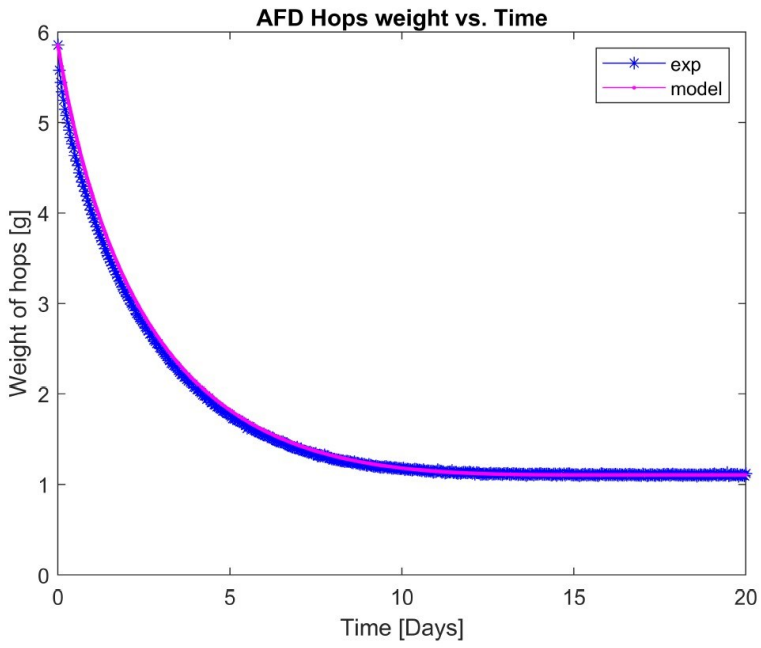

Figure 7-21 Comparison of weight loss during sublimation – AFD Hops case IV (-12 °C, Fan ON, Low adsorbent ratio)

7.4.5.2 Air RH during sublimation

Figure 7-22 below shows the air RH measured during the experiment and the model-predicted values for same.

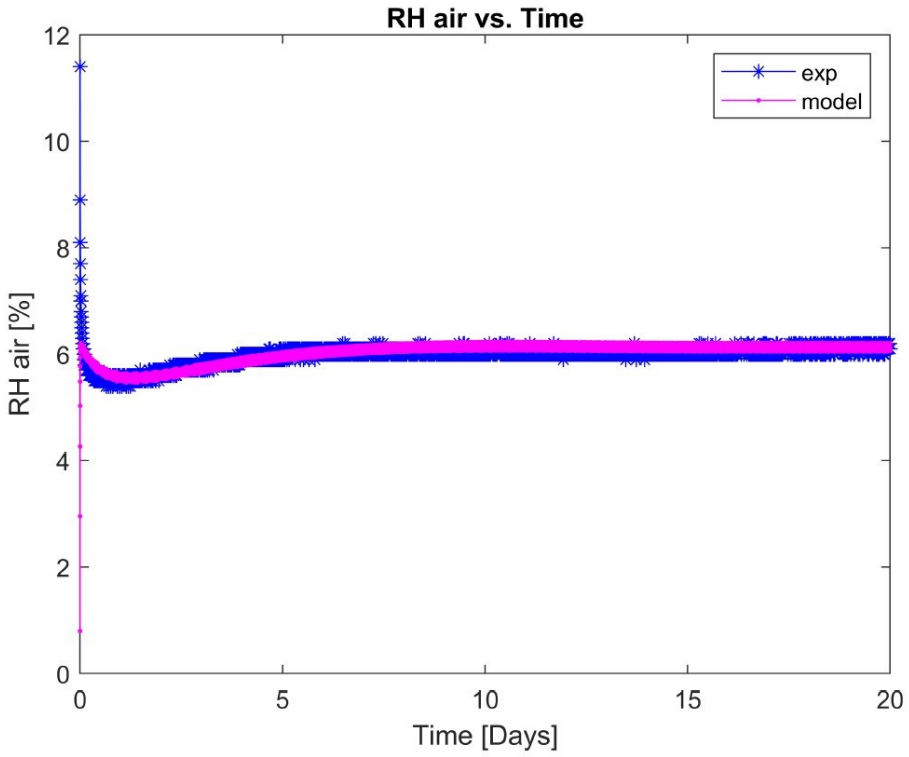

Figure 7-22 Comparison of Air RH (%) - Model vs AFD Hops case IV (-12 °C, Fan ON, Low adsorbent ratio)

7.5 Conclusions

Experiments on AFD of hops under different settings successfully generated data giving insights into the mechanisms involved in the drying kinetics and supporting model development. It was found that, for AFD using adsorbent as the moisture removing mechanism, the drying rate can be improved by increasing the process temperature, using higher adsorbent to drying sample ratio and by having air circulation.

A model was developed and validated for predicting AFD of hops by modifying the model developed for ice sublimation in Chapter 6, to assume that AFD under the current settings is not limited by heat transfer. This model was able to explain all the experiment scenarios very well.

The resistance factor RF_I, describing resistance to mass transfer in the cell remains constant for all the experiments and is independent of temperature or other factors considered and thus can be said to be a function of the composition of the hop's cellular material which would be a constant.

On the other hand, factor RF_II, which is related to the mass transfer resistance in the intercellular gas pathway region is found to depend on temperature, air circulation and mass transfer gradient available. This could mean that the factor RF_II, is not a function of the structure of the hops alone and further studies would be required to differentiate the components for this factor.

Furthermore, drying rate was limited, and the apparent RF_II value restricted, by poor removal of water vapour from the chamber air when air was not circulated or when insufficient adsorbent surface area was provided.

Combining the results of the experiments and the model, it could be concluded that AFD of hops using adsorbent is a mass transfer limited process and the drying rate can thus theoretically be increased by using techniques to enhance the mass transfer processes. Some of these aspects are discussed in the next chapter on overall discussion and future works.

Chapter 8 Overall Discussion and Future Work

8.1 Overall conclusions

The present study was aimed at understanding the rate controlling mechanisms in the atmospheric freeze drying (AFD) of leaf-like products and at developing a model for the process. AFD is a slow process and understanding the rate limiting mechanism would help in introducing appropriate technological interventions to increase rate. One of the goals was also to develop an experimental set-up to capture high quality data to study this process.

The AFD experiment apparatus developed was capable of continuous weight-loss measurement and data logging for the weight loss, drying chamber temperature and air RH. The experiment data obtained using this experimental set-up were used to parameterize a model developed in this study.

The study of the AFD of hops was preceded by the study of ice sublimation in the AFD system under consideration to characterize the different resistances in the system. This study helped quantify the different resistances and maximum sublimation fluxes for ice sublimation in the system. The ice temperature remained constant throughout the sublimation process which meant that the current AFD system was not limited by heat transfer and was limited by mass transfer. The sublimation rate was found to increase with air circulation and depended on the area of ice available for sublimation. A model was developed for the time course of ice sublimation in the current AFD settings and was able to give good predictions for the time course of ice sublimation. The model parameters for the experiment with and without air circulation was then used in the model simulations for the hops, which was taken as the model specimen for leaf-like materials.

During the study of AFD of hops, it was found that the drying rate is limited by mass transfer. The AFD rate was found to increase with process temperature and increase with the adsorbent to hops ratio which is related to an increase in mass transfer gradient for the water vapour movement from the sublimation site inside the product to the adsorbent surface. It was also found that the drying rate increased when the air was circulated which also enhanced the mass transfer. The model, developed based on the hypothesis that the current AFD process is not limited by heat transfer, was able to simulate the process well,

thus leading to the conclusion that the AFD of hops in the AFD with adsorbent system is a mass transfer limited process.

The hypothesis of a uniform retreating ice front model used by other researchers (Claussen, Andresen, et al., 2007; Claussen, Ustad, et al., 2007; Heldman & Hohner, 1974; Wolff & Gibert, 1990) for cubes and spheres was not used here. Instead, it was assumed that all the ice in the leaf-like products is present inside individual cells, and gas exchange pathways used for photosynthesis provide parallel routes for vapour produced by sublimation of ice in all cells simultaneously. The model was able to simulate the experiment results well, providing support for this assumption.

Technological interventions to increase AFD rate should act by increasing the mass transfer rates. From the experiment results, AFD kinetics depends on the temperature and thus to increase the drying rate of the AFD of hops, the process temperature could be increased until the product structural stability is compromised. The adsorbent to the hops ratio could be increased to give a higher mass transfer gradient in the system which would enhance AFD kinetics. The available mass transfer gradient decreases as the adsorbent moisture content increases; this is because the mass transfer gradient depends on the equilibrium air moisture content for the adsorbent and which in turn depends on the moisture content in the silica adsorbent. This can be rectified by either using a large quantity of adsorbent to minimise limitations of moisture adsorption on the adsorbent or by regenerating the adsorbent continuously to remove the adsorbed moisture and thus maintain the gradient. The AFD rate was also found to increase by air circulation and thus a higher air circulation might be maintained to increase AFD rate.

In the literature review, other researchers have used microwave and ultrasound enhanced AFD to increase the drying rate. Use of microwave does not increase the mass transfer directly but would increase the temperature of the ice inside the product and thus increase the mass transfer gradient available and thus the mass transfer rate. This would not be a good option, if the product temperature is very sensitive to any changes in the temperature. On the other hand, use of ultrasound could help in directly increasing the mass transfer with little increase in the heat addition, and since the current AFD system is limited by mass transfer, this would be a good option to look further into.

8.2 Suggested future works

The current works assumes that the results for AFD of hops could be extrapolated to other leaf-like materials. This needs to be validated with further studies on other leaf-like specimens such as herbs or cut flowers. The model developed for the current AFD system, uses two parameters RF_I and RF_II. The intra cellular resistance factor, RF_I remains constant and independent of the processing conditions, and further studies are required to check whether the same value used for hops could be used for all leaf-like products or whether each species would require a different value.

The factor RF_II, linked with the extracellular resistance, was found to be affected by the process parameters. Further studies are required to understand how this factor is affected and to differentiate the effect of structural (pore length, tortuosity, etc.) and non-structural components (temperature, air circulation, mass transfer gradient) on this factor. This can help in estimating the AFD fitting parameter under different settings and thus help to simulate the process for a wide range of process conditions and adsorbent to hops ratios.

Further studies on the maximum limit for the AFD rate that could be achieved individually by increasing the air circulation and adsorbent to hops ratio could help in validating the model further.

In the current study, the maximum process temperature was -12 ^{o}C, and this was limited by the chest freezer used. The industrial AFD processes are expected to work at a higher temperature in the vicinity of -5 ^{o}C, and studies carried out in this temperature could help in getting more realistic data to fit the model parameters for RF_II.

Once the resistance factor, RF_II, is better understood and the model modified accordingly, the model could be used to simulate the various process conditions for maximum AFD rate.

Further studies with ultrasound could be done on the hops system to study its effect on enhancing internal mass transfer within the plant pores. If so, the model may be modified to include the effects of ultrasound use in AFD.

References

Alves-Filho, O., Eikevik, T., Mulet, A., Garau, C., & Rossello, C. (2007). Kinetics and Mass Transfer during Atmospheric Freeze Drying of Red Pepper. *Drying Technology*, *25*(7–8), 1155–1161. https://doi.org/10.1080/07373930701438469

Andrés, R. R., Riera, E., Gallego-Juárez, J. A., Mulet, A., García-Pérez, J. V., & Cárcel, J. A. (2019). Airborne power ultrasound for drying process intensification at low temperatures: Use of a stepped-grooved plate transducer. *Drying Technology*, 1–14. https://doi.org/10.1080/07373937.2019.1677704

Awad, T. S., Moharram, H. A., Shaltout, O. E., Asker, D., & Youssef, M. M. (2012). Applications of ultrasound in analysis, processing and quality control of food: A review. In *Food Research International* (Vol. 48, Issue 2, pp. 410–427). https://doi.org/10.1016/j.foodres.2012.05.004

Bantle, M., Kolsaker, K., & Eikevik, T. M. (2011). Modification of the Weibull Distribution for Modeling Atmospheric Freeze-Drying of Food. *Drying Technology*, *29*(10), 1161–1169. https://doi.org/10.1080/07373937.2011.574242

Bellissent-Funel, M.-C., Teixeira, J., & Teixeira, J. (2016). Structural and Dynamic Properties of Bulk and Confined Water. In L. Rey (Ed.), *Freeze-Drying/Lyophilization of Pharmaceutical and Biological Products* (3rd ed., pp. 43–65). CRC Press. https://doi.org/10.3109/9781439825761

Berk, Z. (2018). Freeze drying (lyophilization) and freeze concentration. In *Food Process Engineering and Technology* (3rd ed., pp. 567–581). Elsevier. https://doi.org/10.1016/B978-0-12-812018-7.00023-3

Bhatta, S., Janezic, T. S., & Ratti, C. (2020). Freeze-drying of plant-based foods. In *Foods* (Vol. 9, Issue 1). MDPI Multidisciplinary Digital Publishing Institute. https://doi.org/10.3390/foods9010087

Bobba, S., Harguindeguy, M., Colucci, D., & Fissore, D. (2020). Diffuse interface model of the freeze-drying process of individually frozen products. *Drying Technology*, *38*(5–6), 758–774. https://doi.org/10.1080/07373937.2019.1710711

Bubnovich, V., Quijada, E., & Reyes, A. (2009). Computer simulation of atmospheric freeze drying of carrot slices in a fluidized bed. *Numerical Heat Transfer; Part A: Applications*. https://doi.org/10.1080/10407780903107386

Bubnovich, V., Reyes, A., Quijada, E., & Mahn, A. (2012). Numerical simulation of lyophilization of carrot slices at atmospheric pressure in a fluidized bed. *Journal of Food Engineering*, *109*(4), 659–667. https://doi.org/10.1016/j.jfoodeng.2011.11.030

Campañone, L. A., Salvadori, V. O., & Mascheroni, R. H. (2005). Food freezing with simultaneous surface dehydration: Approximate prediction of weight loss during freezing and storage. *International Journal of Heat and Mass Transfer*, *48*(6), 1195–

1204. https://doi.org/10.1016/j.ijheatmasstransfer.2004.09.031

Canny, M. J., & Huang, C. X. (2006). Leaf water content and palisade cell size. *New Phytologist*, *170*(1), 75–85. https://doi.org/10.1111/j.1469-8137.2005.01633.x

Capozzi, L. C., Barresi, A. A., & Pisano, R. (2019). A multi-scale computational framework for modeling the freeze-drying of microparticles in packed-beds. *Powder Technology*, *343*, 834–846. https://doi.org/10.1016/j.powtec.2018.11.067

Carrión, C., Mulet, A., García-Pérez, J. V., & Cárcel, J. A. (2018). Ultrasonically assisted atmospheric freeze-drying of button mushroom. Drying kinetics and product quality. *Drying Technology*, *36*(15), 1814–1823. https://doi.org/10.1080/07373937.2017.1417870

Chaplin, M. (2019). *Water structure and science*. http://www1.lsbu.ac.uk/water/water_structure_science.html

Chua, H. T., Ng, K. C., Chakraborty, A., Oo, N. M., & Othman, M. A. (2002). Adsorption Characteristics of Silica Gel + Water Systems. *Journal of Chemical & Engineering Data*, *47*(5), 1177–1181. https://doi.org/10.1021/je0255067

Claussen, I. C., Andresen, T., Eikevik, T., & Strømmen, I. (2007). Atmospheric freeze drying - Modeling and simulation of a tunnel dryer. *Drying Technology*, *25*(12), 1959–1965. https://doi.org/10.1080/07373930701727275

Claussen, I. C., Strømmen, I., Hemmingsen, A. K. T., & Rustad, T. (2007). Relationship of product structure, sorption characteristics, and freezing point of atmospheric freeze-dried foods. *Drying Technology*, *25*(5), 853–865. https://doi.org/10.1080/07373930701370233

Claussen, I. C., Ustad, T. S., Str⊘mmen, I., & Walde, P. M. (2007). Atmospheric Freeze Drying—A Review. *Drying Technology*, *25*(6), 947–957. https://doi.org/10.1080/07373930701394845

Colucci, D., Fissore, D., Rossello, C., & Carcel, J. A. (2018). On the effect of ultrasound-assisted atmospheric freeze-drying on the antioxidant properties of eggplant. *Food Research International*, *106*, 580–588. https://doi.org/10.1016/j.foodres.2018.01.022

Di Matteo, P., Donsì, G., & Ferrari, G. (2003). The role of heat and mass transfer phenomena in atmospheric freeze-drying of foods in a fluidised bed. *Journal of Food Engineering*, *59*(2–3), 267–275. https://doi.org/10.1016/S0260-8774(02)00467-3

Duan, X., Yang, X., Ren, G., Pang, Y., Liu, L., & Liu, Y. (2016). Technical aspects in freeze-drying of foods. *Drying Technology*, *34*(11), 1271–1285. https://doi.org/10.1080/07373937.2015.1099545

Duan, X., Zhang, M., Mujumdar, A. S., & Wang, S. (2010). Microwave freeze drying of sea cucumber (Stichopus japonicus). *Journal of Food Engineering*, *96*(4), 491–497.

https://doi.org/10.1016/j.jfoodeng.2009.08.031

Earles, J. M., Theroux-Rancourt, G., Roddy, A. B., Gilbert, M. E., McElrone, A. J., & Brodersen, C. R. (2018). Beyond Porosity: 3D Leaf Intercellular Airspace Traits That Impact Mesophyll Conductance. *Plant Physiology*, *178*(1), 148–162. https://doi.org/10.1104/pp.18.00550

Eikevik, T. M., Alves-Filho, O., & Bantle, M. (2012). Microwave-Assisted Atmospheric Freeze Drying of Green Peas: A Case Study. *Drying Technology*, *30*(14), 1592–1599. https://doi.org/10.1080/07373937.2012.700671

Farid, M. M. (2010). Mathematical Modeling of Food Processing. In M. M. Farid (Ed.), *Mathematical modeling of food processing* (1st Editio). CRC Press. https://doi.org/10.1201/9781420053548

Garcia-Perez, J. V., Carcel, J. A., Riera, E., Rosselló, C., & Mulet, A. (2012). Intensification of Low-Temperature Drying by Using Ultrasound. *Drying Technology*, *30*(11–12), 1199–1208. https://doi.org/10.1080/07373937.2012.675533

Green, D. W., & Southard, M. Z. (2019). *Perry's Chemical Engineers' Handbook* (D. W. Green & M. Z. Southard (eds.); 9th Editio). McGraw-Hill Education. https://www.accessengineeringlibrary.com/content/book/9780071834087

Halder, A., Datta, A. K., & Spanswick, R. M. (2011). Water transport in cellular tissues during thermal processing. *AIChE Journal*, *57*(9), 2574–2588. https://doi.org/10.1002/aic.12465

Haseley, P., & Oetjen, G.-W. (2018). *Freeze-Drying 3e*. Wiley-VCH Verlag GmbH & Co. KGaA. https://doi.org/10.1002/9783527808946

Heldman, D. R., & Hohner, G. A. (1974). An analysis of atmospheric freeze drying. *Journal of Food Science*, *39*(1), 147–155. https://doi.org/10.1111/j.1365-2621.1974.tb01010.x

Horwitz, W. (2010). *Official methods of analysis of AOAC International. Volume I, agricultural chemicals, contaminants, drugs* (W. Horwitz (ed.)). Gaithersburg (Maryland): AOAC International, 1997.

Hua, T.-C., Liu, B.-L., & Zhang, H. (2010a). Fundamentals of Freeze Drying. In *Freeze-Drying of Pharmaceutical and Food Products* (pp. 18–67). Elsevier. https://doi.org/10.1533/9781845697471.18

Hua, T.-C., Liu, B.-L., & Zhang, H. (2010b). Heat-Mass Transfer Analyses and Modeling of the Drying Process. In *Freeze-Drying of Pharmaceutical and Food Products* (pp. 68–110). Elsevier. https://doi.org/10.1533/9781845697471.68

Huang, J. (2018). A simple accurate formula for calculating saturation vapor pressure of water and ice. *Journal of Applied Meteorology and Climatology*, *57*(6), 1265–1272.

https://doi.org/10.1175/JAMC-D-17-0334.1

Jambon-Puillet, E., Shahidzadeh, N., & Bonn, D. (2018). Singular sublimation of ice and snow crystals. *Nature Communications*, *9*(1), 4191. https://doi.org/10.1038/s41467-018-06689-x

Janssen, S., Verboven, P., Nugraha, B., Wang, Z., Boone, M., Josipovic, I., & Nicolaï, B. M. (2020). 3D pore structure analysis of intact 'Braeburn' apples using X-ray micro-CT. *Postharvest Biology and Technology*, *159*, 111014. https://doi.org/10.1016/J.POSTHARVBIO.2019.111014

Jones, F. E. (1978). AIR DENSITY EQUATION AND THE TRANSFER OF THE MASS UNIT. *J Res Natl Bur Stand (US)*, *83*(5), 419–428. https://doi.org/10.6028/jres.083.028

Kiani, H., & Sun, D.-W. (2011). Water crystallization and its importance to freezing of foods: A review. *Trends in Food Science & Technology*, *22*(8), 407–426. https://doi.org/10.1016/j.tifs.2011.04.011

Kim, J. H., Lee, C. H., Kim, W. S., Lee, J. S., Kim, J. T., Suh, J. K., & Lee, J. M. (2003). Adsorption equilibria of water vapor on alumina, zeolite 13X, and a zeolite X/activated carbon composite. *Journal of Chemical and Engineering Data*, *48*(1), 137–141. https://doi.org/10.1021/je0201267

Kochs, M., Körber, C., Heschel, I., & Nunner, B. (1993). The influence of the freezing process on vapour transport during sublimation in vacuum-freeze-drying of macroscopic samples. *International Journal of Heat and Mass Transfer*, *36*(7), 1727–1738. https://doi.org/10.1016/S0017-9310(05)80159-0

Kochs, M., Körber, C., Nunner, B., & Heschel, I. (1991). The influence of the freezing process on vapour transport during sublimation in vacuum-freeze-drying. *International Journal of Heat and Mass Transfer*, *34*(9), 2395–2408. https://doi.org/10.1016/0017-9310(91)90064-L

Li, S., Stawczyk, J., & Zbicinski, I. (2007). CFD Model of Apple Atmospheric Freeze Drying at Low Temperature. *Drying Technology*, *25*(7–8), 1331–1339. https://doi.org/10.1080/07373930701438907

Liapis, A. I., & Bruttini, R. (1995). Freeze-Drying of Pharmaceutical Crystalline and Amorphous Solutes in Vials: Dynamic Multi-Dimensional Models of the Primary and Secondary Drying Stages and Qualitative Features of the Moving Interface. *Drying Technology*, *13*(1–2), 43–72. https://doi.org/10.1080/07373939508916942

MacKenzie, A. P. (2006). FACTORS AFFECTING THE MECHANISM OF TRANSFORMATION OF ICE INTO WATER VAPOR IN THE FREEZE-DRYING PROCESS*. *Annals of the New York Academy of Sciences*, *125*(2), 522–547. https://doi.org/10.1111/j.1749-6632.1965.tb45412.x

Mathers, A. W., Hepworth, C., Baillie, A. L., Sloan, J., Jones, H., Lundgren, M., Fleming,

A. J., Mooney, S. J., & Sturrock, C. J. (2018). Investigating the microstructure of plant leaves in 3D with lab-based X-ray computed tomography. *Plant Methods*, *14*(1). https://doi.org/10.1186/s13007-018-0367-7

Mello, R. E., Fontana, A., Mulet, A., Correa, J. L. G., & Cárcel, J. A. (2020). Ultrasound-assisted drying of orange peel in atmospheric freeze-dryer and convective dryer operated at moderate temperature. *Drying Technology*, *38*(1–2), 259–267. https://doi.org/10.1080/07373937.2019.1645685

Merone, D., Colucci, D., Fissore, D., Sanjuan, N., & Carcel, J. A. (2020). Energy and environmental analysis of ultrasound-assisted atmospheric freeze-drying of food. *Journal of Food Engineering*, *283*, 110031. https://doi.org/10.1016/j.jfoodeng.2020.110031

Meryman, H. T. (1959). Sublimation Freeze-Drying without Vacuum. *Science*, *130*(3376), 628–629. https://doi.org/10.1126/science.130.3376.628

Moreno, C., Brines, C., Mulet, A., Rosselló, C., & Cárcel, J. A. (2017). Antioxidant potential of atmospheric freeze-dried apples as affected by ultrasound application and sample surface. *Drying Technology*, *35*(8), 957–968. https://doi.org/10.1080/07373937.2016.1256890

Nakagawa, K. (2018). Food drying at sub-zero temperature: Importance of glassy phase on product quality. *Science, Engineering and Health Studies*, *12*(3), 125–137. https://doi.org/10.14456/sehs.2018.12

Nakagawa, K., Horie, A., & Nakabayashi, M. (2020). Modeling atmospheric freeze-drying of food products operated above glass transition temperature. *Chemical Engineering Research and Design*, *163*, 12–20. https://doi.org/10.1016/j.cherd.2020.08.017

Nugraha, B., Verboven, P., Janssen, S., Wang, Z., & Nicolaï, B. M. (2019). Non-destructive porosity mapping of fruit and vegetables using X-ray CT. *Postharvest Biology and Technology*, *150*, 80–88. https://doi.org/10.1016/J.POSTHARVBIO.2018.12.016

Oetjen, G.-W. (2000). DISTILLATION | Freeze-Drying. In *Encyclopedia of Separation Science* (pp. 1023–1034). Elsevier. https://doi.org/10.1016/B0-12-226770-2/05591-5

Ouchi, T., HAMAMOTO, Y., & MORI, H. (2019). Measurement of Adsorption/Desorption Rate of Water Vapor to a Silica gel Thin Film Coated on a Surface of a Cross-fin Tube Heat Exchanger (特集 デシカント空調に関わる最新技術). *日本冷凍空調学会論文集 = Transactions of the Japan Society of Refrigerating and Air Conditioning Engineers*, *36*(3), 157–163. https://doi.org/https://doi.org/10.11322/tjsrae.19-10DC_OA

Pesaran, A. A., & Mills, A. F. (1987). Moisture transport in silica gel packed beds—I.Theoretical study. *International Journal of Heat and Mass Transfer*, *30*(6), 1037–

1049. https://doi.org/10.1016/0017-9310(87)90034-2

Petzold, G., & Aguilera, J. M. (2009). Ice Morphology: Fundamentals and Technological Applications in Foods. *Food Biophysics*, *4*(4), 378–396. https://doi.org/10.1007/s11483-009-9136-5

Phimolsiripol, Y., Siripatrawan, U., & Cleland, D. J. (2011). Weight loss of frozen bread dough under isothermal and fluctuating temperature storage conditions. *Journal of Food Engineering*, *106*(2), 134–143. https://doi.org/10.1016/j.jfoodeng.2011.04.020

Pikal, M. J., Shah, S., Senior, D., & Lang, J. E. (1983). Physical Chemistry of Freeze-drying: Measurement of Sublimation Rates for Frozen Aqueous Solutions by a Microbalance Technique. *Journal of Pharmaceutical Sciences*, *72*(6), 635–650. https://doi.org/10.1002/jps.2600720614

Rahman, S. M. A., & Mujumdar, A. S. (2012). Atmospheric Freeze Drying. In *Progress in Food Preservation* (pp. 143–160). Wiley-Blackwell. https://doi.org/10.1002/9781119962045.ch7

Roth, C., Winter, G., & Lee, G. (2001). Continuous measurement of drying rate of crystalline and amorphous systems during freeze-drying using an in situ microbalance technique. *Journal of Pharmaceutical Sciences*, *90*(9), 1345–1355. https://doi.org/10.1002/jps.1087

Sandall, O. C., King, C. J., & Wilke, C. R. (1967). The relationship between transport properties and rates of freeze-drying of poultry meat. *AIChE Journal*, *13*(3), 428–438. https://doi.org/10.1002/aic.690130309

Santacatalina, J. V., Fissore, D., Cárcel, J. A., Mulet, A., & García-Pérez, J. V. (2015). Model-based investigation into atmospheric freeze drying assisted by power ultrasound. *Journal of Food Engineering*, *151*, 7–15. https://doi.org/10.1016/j.jfoodeng.2014.11.013

Santacatalina, J. V, Cárcel, J. A., Simal, S., Garcia-Perez, J. V, & Mulet, A. (2012). Atmospheric freeze drying assisted by power ultrasound. *IOP Conference Series: Materials Science and Engineering*, *42*(1), 012021. https://doi.org/10.1088/1757-899X/42/1/012021

Sheehan, P., & Liapis, A. I. (1998). Modeling of the primary and secondary drying stages of the freeze drying of pharmaceutical products in vials: Numerical results obtained from the solution of a dynamic and spatially multi-dimensional lyophilization model for different operational policies. *Biotechnology and Bioengineering*, *60*(6), 712–728. https://doi.org/10.1002/(SICI)1097-0290(19981220)60:6<712::AID-BIT8>3.0.CO;2-4

Slaton, M. R., & Smith, W. K. (2002). Mesophyll architecture and cell exposure to intercellular air space in alpine, desert, and forest species. *International Journal of Plant Sciences*, *163*(6), 937–948. https://doi.org/10.1086/342517

Stawczyk, J., Li, S., & Modrzejewska, Z. (2007). Chitosan stuffs atmospheric freeze-drying kinetics. *Asia-Pacific Journal of Chemical Engineering*, *2*(2), 124–129. https://doi.org/10.1002/apj.54

Stawczyk, J., Li, S., Witrowa-Rajchert, D., & Fabisiak, A. (2007). Kinetics of Atmospheric Freeze-drying of Apple. *Transport in Porous Media*, *66*(1–2), 159–172. https://doi.org/10.1007/s11242-006-9012-4

Stigter, E. E., Litt, M., Steiner, J. F., Bonekamp, P. N. J., Shea, J. M., Bierkens, M. F. P., & Immerzeel, W. W. (2018). The Importance of Snow Sublimation on a Himalayan Glacier. *Frontiers in Earth Science*, *6*. https://doi.org/10.3389/feart.2018.00108

Sun, D.-W., & Li, B. (2003). Microstructural change of potato tissues frozen by ultrasound-assisted immersion freezing. *Journal of Food Engineering*, *57*(4), 337–345. https://doi.org/10.1016/S0260-8774(02)00354-0

Tétreault, J., & Bégin, P. (2018). Silica gel : passive control of relative humidity. *CCI Technical Bulletin No. 33*, 22. https://www.canada.ca/en/conservation-institute/services/conservation-preservation-publications/technical-bulletins/silica-gel-relative-humidity.html#a6d

Tolstorebrov, I., Eikevik, T. M., Petrova, I., Shokina, Y., & Bantle, M. (2018). Description of atmospheric freeze-drying process of organic apples using thermo-physical properties. *Proceedings of 21th International Drying Symposium*, *17*(September), 11–14. https://doi.org/10.4995/IDS2018.2018.7697

Veraverbeke, E. A., Verboven, P., Scheerlinck, N., Lan Hoang, M., & Nicolaï, B. M. (2003). Determination of the diffusion coefficient of tissue, cuticle, cutin and wax of apple. *Journal of Food Engineering*, *58*(3), 285–294. https://doi.org/10.1016/S0260-8774(02)00387-4

Verboven, P., Kerckhofs, G., Mebatsion, H. K., Ho, Q. T., Temst, K., Wevers, M., Cloetens, P., & Nicolaï, B. M. (2008). Three-dimensional gas exchange pathways in pome fruit characterized by synchrotron x-ray computed tomography. *Plant Physiology*, *147*(2), 518–527. https://doi.org/10.1104/pp.108.118935

Vicent, V., Ndoye, F.-T., Verboven, P., Nicolaï, B., & Alvarez, G. (2019). Effect of dynamic storage temperatures on the microstructure of frozen carrot imaged using X-ray micro-CT. *Journal of Food Engineering*, *246*, 232–241. https://doi.org/10.1016/J.JFOODENG.2018.11.015

Warning, A. D., Arquiza, J. M. R., & Datta, A. K. (2015). A multiphase porous medium transport model with distributed sublimation front to simulate vacuum freeze drying. *Food and Bioproducts Processing*, *94*, 637–648. https://doi.org/10.1016/J.FBP.2014.08.011

Warning, A., Verboven, P., Nicolaï, B., van Dalen, G., & Datta, A. K. (2014). Computation of mass transport properties of apple and rice from X-ray microtomography images. *Innovative Food Science & Emerging Technologies*, *24*,

14–27. https://doi.org/10.1016/j.ifset.2013.12.017

Wolff, E., & Gibert, H. (1990). Atmospheric freeze-drying part 2 : Modelling drying kinetics using adsorption isotherms. *Drying Technology*, *8*(2), 405–428. https://doi.org/10.1080/07373939008959891

Xu, D., Wei, L., Guangyue, R., Wenchao, L., & Yunhong, L. (2015). Comparative study on the effects and efficiencies of three sublimation drying methods for mushrooms. *International Journal of Agricultural and Biological Engineering*, *8*(1), 91–97. https://doi.org/10.3965/j.ijabe.20150801.012

A. Appendices

I. Derivation for the ODE for heat balance in Ice

ODE for temperature of ice – T_{ice}

Unsteady state heat balance in product

rate of accumulation of heat in ice	=	*rate of heat entering ice from air*	-	*rate of heat leaving ice by sublimation*

$$\frac{d(M_{ice}\ Cp_{ice}\ T_{ice})}{dt} = 2A_{ice}\ h_{air}\ [T_{air} - T_{ice}] - \lambda_{sub}\ D_{H2O\_air}\ A_{ice}\ \frac{[X_{ice\_surf} - X_{air}]}{l_{ice\_air}}\ \rho_{air}$$

$$T_{ice}Cp_{ice}\frac{dM_{ice}}{dt} + M_{ice}Cp_{ice}\frac{dT_{ice}}{dt} = 2A_{ice}\ h_{air}\ [T_{air} - T_{ice}] - \lambda_{sub}\ D_{H2O\_air}\ A_{ice}\ \frac{[X_{ice\_surf} - X_{air}]}{l_{ice\_air}}\ \rho_{air}$$

The term of $T_{ice} \times Cp_{ice} \times \frac{dM_{ice}}{dt}$ is brought to the RHS

$$M_{ice}Cp_{ice}\frac{dT_{ice}}{dt} = 2A_{ice}\ h_{air}\ [T_{air} - T_{ice}] - \lambda_{sub}\ D_{H2O_{air}}\ A_{ice}\ \frac{[X_{ice_{surf}} - X_{air}]}{l_{ice_{air}}}\ \rho_{air} - T_{ice}Cp_{ice}\frac{dM_{ice}}{dt}$$

The term $\frac{dM_{ice}}{dt}$ is substituted for the ODE for rate of change of mass of ice (Eqn. 5.1). Note that the substitution has a negative sign thus the overall term becomes +ve.

$$M_{ice}Cp_{ice}\frac{dT_{ice}}{dt} = 2A_{ice}\ h_{air}\ [T_{air} - T_{ice}]$$

$$- \lambda_{sub}\ D_{H2O_{air}}\ A_{ice}\ \frac{[X_{ice\_surf} - X_{air}]}{l_{ice_{air}}}\ \rho_{air}$$

$$+\ T_{ice} Cp_{ice} D_{H2O\_air}\ A_{ice}\ \frac{[X_{ice\_surf} - X_{air}]}{l_{ice\_air}}\ \rho_{air}$$

$$M_{ice}\ Cp_{ice} \frac{dT_{ice}}{dt} = 2A_{ice}\ h_{air}\ [T_{air} - T_{ice}]$$

$$- [\lambda_{sub} - T_{ice} Cp_{ice}] \times D_{H2O\_air}\ A_{ice} \frac{[X_{ice\_surf} - X_{air}]}{l_{ice\_air}}\ \rho_{air}$$

II. Fitting of constants for the model

The model constants are fitted visually to get the best fit in terms of following the experiment data as well as the trend.

Fitting of the initial boundary layer thickness for the ice sublimation – case I

The best fit was observed for a value of $l_{ice\text{-}air,o}$ (initial effective path length for diffusion in ice sublimation) at 0.0197 m as shown in the Figure A-1. The sensitivity of fit to excursions of $l_{ice\text{-}air,o}$ value was tested at ±2% of 0.0197 m as shown in Figure A-2 & Figure A-3. The boundary layer thickness was then calculated as the difference between the path length (0.0139 m) and the effective path length (0.0197 m) giving a value of 0.0058 m. This is used as the boundary layer value for AFD of hops.

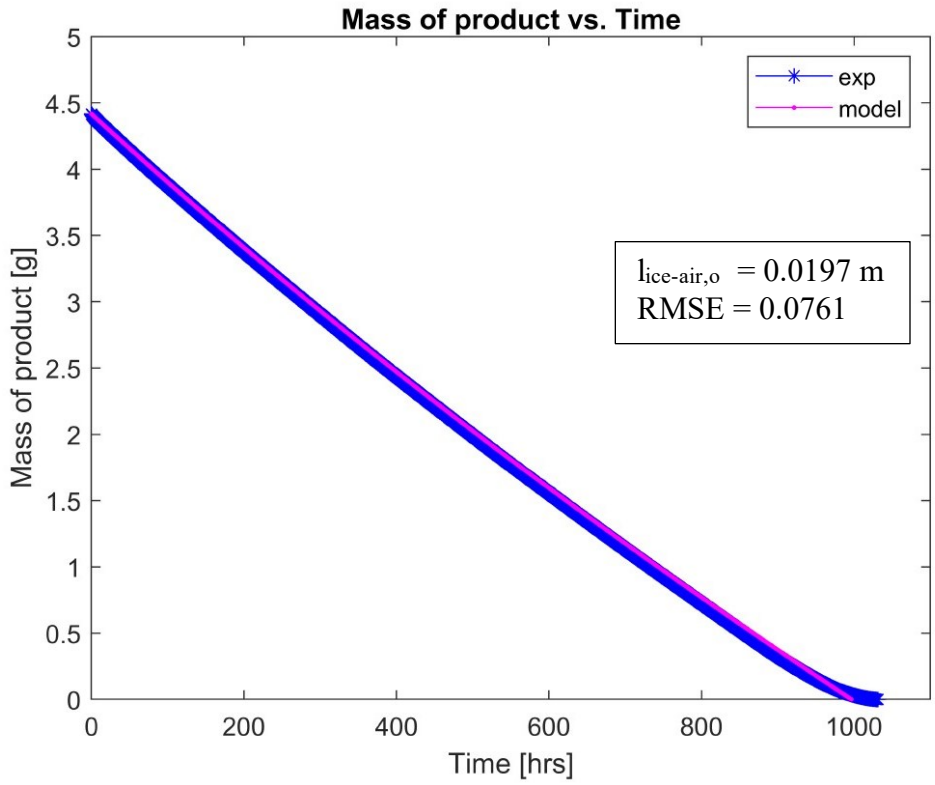

Figure A-1 Fitted value for the boundary layer thickness – case I

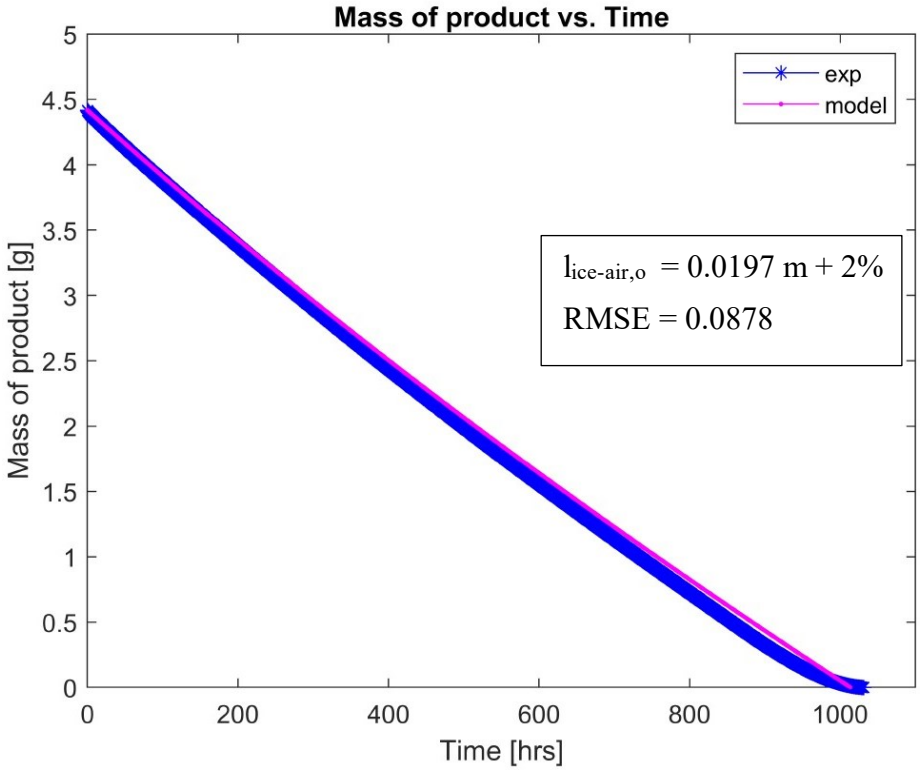

Figure A-2 Fitted value for the boundary layer thickness – case I (+2%)

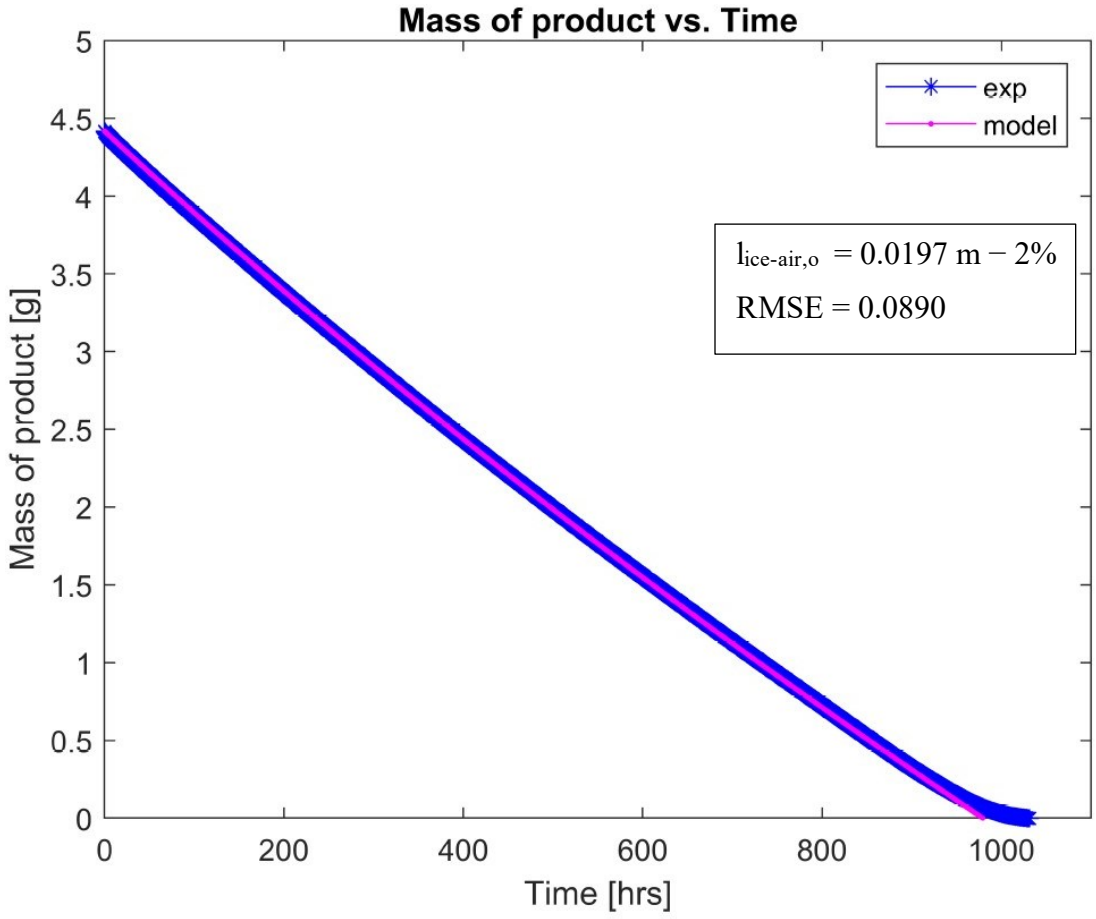

Figure A-3 Fitted value for the boundary layer thickness – case I (-2%)

Fitting of the RF_I and RF_II for the AFD of hops – case 0

The best fit was observed for RF_I at 1.19×10^{6} and RF_II at 1.7×10^{5} as shown in the Figure A-4. Figure A-5 & Figure A-6 show the fit at ±2% of the fitted value.

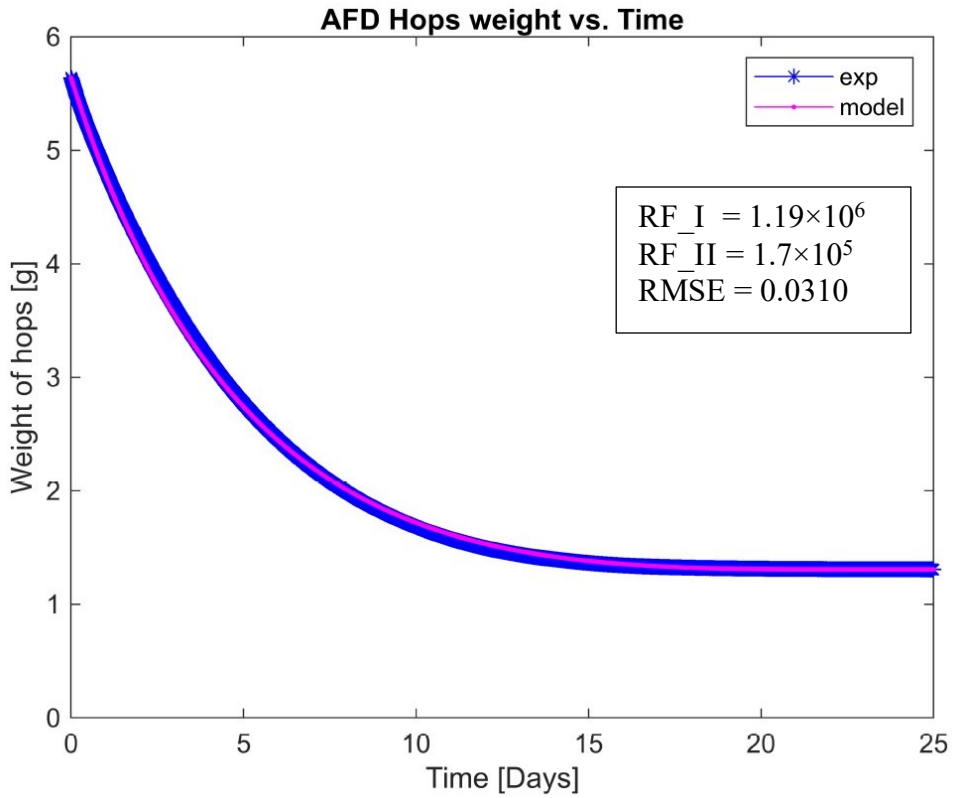

Figure A-4 Fitted value for RF_I and RF_II – case 0

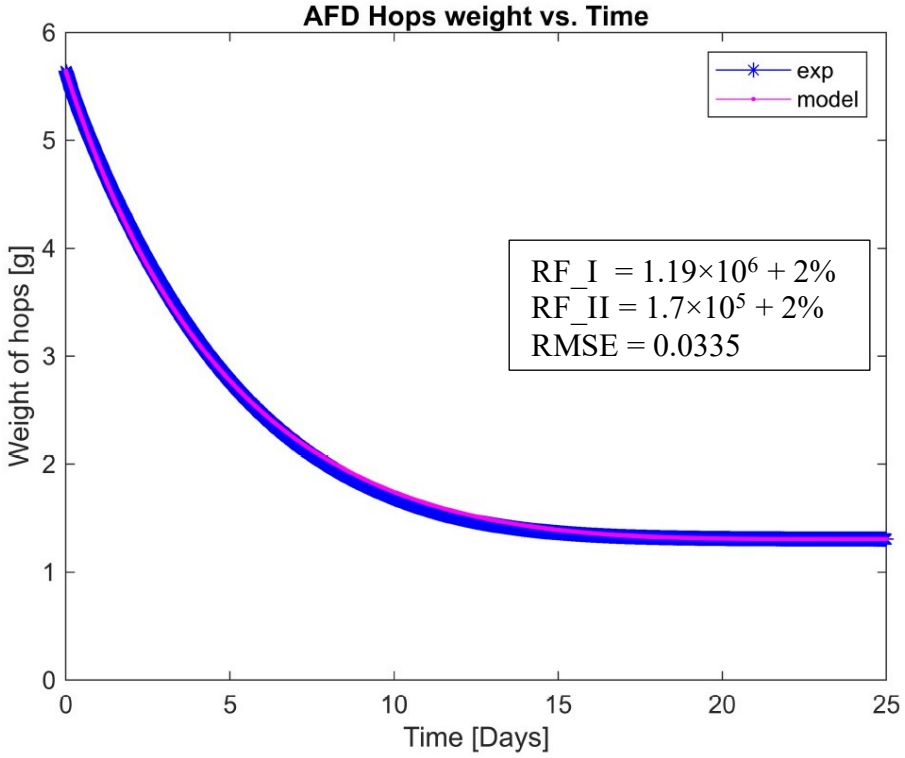

Figure A-5 Fitted value for RF_I and RF_II – case 0 (+2%)

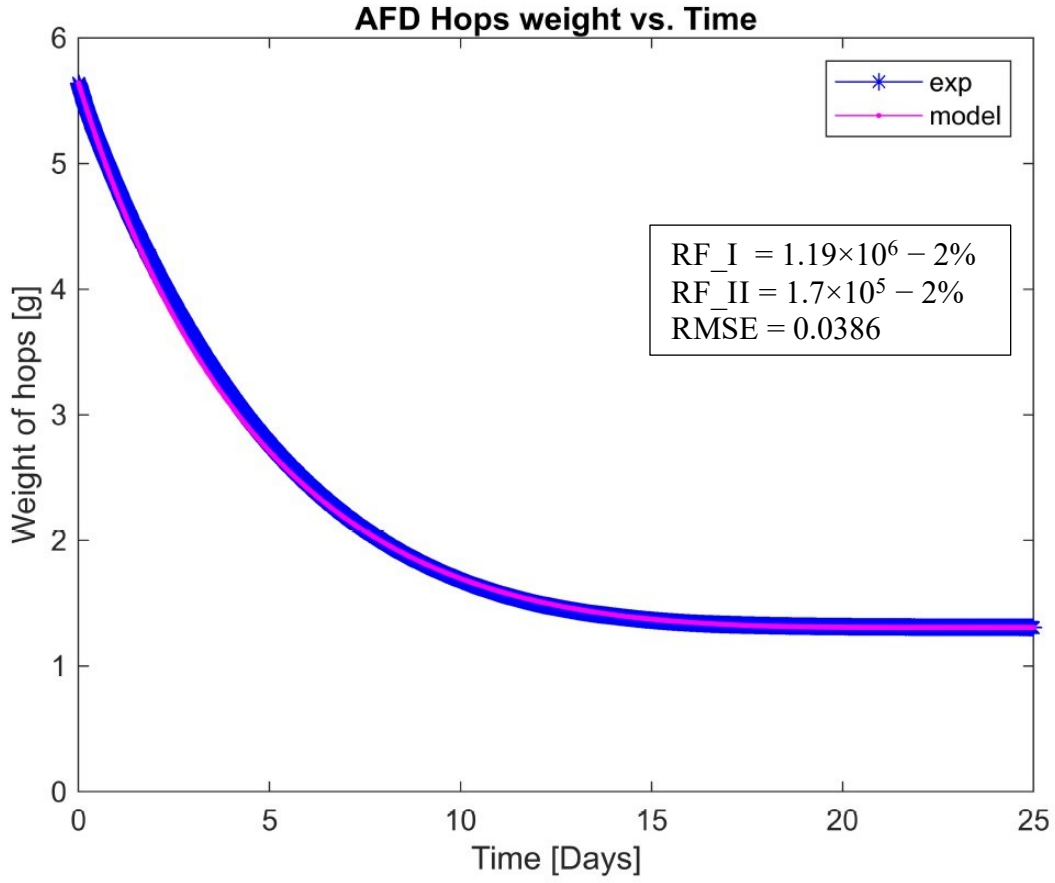

Figure A-6 Fitted value for RF_I and RF_II – case 0 (-2%)

III. Biot Number calculation

The Biot number for the ice and hops are calculated as shown in Table A-1.

$$B_i = \frac{h\,L}{k}$$

Table A-1 Biot number for ice and hops

	Unit	Ice	Air	Hops
Thickness, L	m	0.006		5.00E-05
Thermal Conductivity, k	W/mK	2.125		0.37
Heat Transfer coefficient, h	W/m^2K		25	
Biot No.		0.0706		0.0034

IV. MATLAB codes -Pure ice sublimation – Case II

The sample MATLAB code for the models of the ice sublimation is given here.

```
%Script to solve AFD ODES
clc;
clf;
clear all;
global     T_air %     Temperature of air (     K     )
global     A_ice %     Area of Ice  (     m2    )
global     M_silicagel %     Mass of Silica gel (dry) (     kg    )
global     r_silicagel %     Average radius of silica gel   (     m
     )
global     V_ice_i     %     Volume of ice      (     m3    )
global     V_box %     Volume of air in box     (     m3    )
global     rho_ice     %     density of ice     (     kg/m3 )
global     l_ice_air_i %     Initial boundary layer thickness for ice
     (     m     )
global     P_total     %     Total system pressure    (     Pa    )
global     u_air %     Air velocity (     m/s   )
global     T_silicagel %     Temperature of silica gel      (     K
     )

% System Input
T_air          = 261.15;     %     Temperature of air (     K     )
T_silicagel      =     T_air ;     %     Temperature of silica gel
     (     K     )
A_ice          = 0.000784    ;     %     Area of Ice  (     m2    )
M_silicagel      =     0.2   ;     %     Mass of Silica gel (dry) (
     kg    )
r_silicagel      =     0.002 ;     %     Average radius of silica gel
     (     m     )
l_box          = 0.48  ;     %     Length of box      (     m     )
b_box          = 0.28  ;     %     width of box (     m     )
z_box          = 0.25  ;     %     height of box      (     m     )
rho_ice        = 920   ;     %     density of ice     (     kg/m3 )
P_total        = 101325;     %     Total system pressure    (     Pa
     )
u_air          = 0     ;     %     Air velocity (     m/s   )
V_box          = l_box*b_box*z_box  ;     %     Volume of air in box
     (     m3    )

P_air_sat=exp(43.494-6545.8/(T_air+4.85))/(T_air+594.85)^2;
RH_air_i=0.008;
P_air_i=RH_air_i*P_air_sat;

% Initial conditions
M_ice_i            =    0.0126669    ;     %     Initial mass of ice
     (     kg    )
X_silicagel_i    =     0.445*RH_air_i     ;     %     Initial moisture
content Silica gel (dry) (     kg/kg )
T_ice_i            =    T_air ;     %     Initial temperature of ice
     (     K     )
```

```
X_air_i            =    0.018*P_air_i/0.029./(P_total-P_air_i);     %
     Initial moisture content in air (dry) (      kg/kg )

V_ice_i            =    M_ice_i/rho_ice    ;     %     Volume of ice
     (     m3    )
l_ice_air_i          = 0.0058;     %     Initial boundary layer
thickness for ice (      m     )

ICs=[M_ice_i X_silicagel_i T_ice_i X_air_i ];

% Solving the ODEs
options=odeset('RelTol',1e-5);
[t,Ds]=ode45(@AFD_ODES,0:60:330*3600, ICs,options);
M_ice           =Ds(:,1);
X_silicagel     =Ds(:,2);
T_ice           =Ds(:,3);
X_air           =Ds(:,4);

%subplot(4,1,1)
plot(t/3600,M_ice,'k.')
title('Mass of Ice vs. Time')
xlabel('Time [hrs]')
ylabel('Mass of Ice [kg]')
%subplot(4,1,2)
plot(t/3600,X_silicagel,'c.')
title('Moisture content in Silica gel(dry) vs. Time')
xlabel('Time [hrs]')
ylabel('Moisture Content [kg/kg]')

%subplot(4,1,3)
plot(t/3600,T_ice,'k.')title('Temperature of Ice vs. Time')
xlabel('Time [hrs]')
ylabel('Temp [degC]')

%subplot(4,1,4)
plot(t/3600,X_air,'c.')
title('Moisture content in air (dry) vs. Time')
xlabel('Time [hrs]')
ylabel('Moisture Content [kg/kg]')
% Experiment data Import
opts = delimitedTextImportOptions("NumVariables", 3);
% Specify range and delimiter
opts.DataLines = [2, Inf];
opts.Delimiter = ",";
% Specify column names and types
opts.VariableNames = ["Var1", "Time", "Weight"];
opts.SelectedVariableNames = ["Time", "Weight"];
opts.VariableTypes = ["string", "double", "double"];
% Specify file level properties
```

```
opts.ExtraColumnsRule = "ignore";
opts.EmptyLineRule = "read";
% Specify variable properties
opts = setvaropts(opts, "Var1", "WhitespaceRule", "preserve");
opts = setvaropts(opts, "Var1", "EmptyFieldRule", "auto");
% Import the data
M_product_exp = readmatrix("C:\Users\mmathew\OneDrive - Massey
University\Merit\Research\Models\AFD ODE Model\Model - thesis chapter\AFD
ICE\AFD ICE Matlab\R_Trial_ice_VII_1_hrs.txt", opts);

figure
plot (M_product_exp(:,1), M_product_exp(:,2),'b-*')
hold on
plot (t/3600, M_ice*1000,'m.-')
title('AFD Ice weight vs. Time')
legend('exp data','model','Location','northeast')
xlabel('Time [hrs]')
ylabel('Weight of Ice Exp VII [g]')

xlim([0 340])
ylim([0 13])
P_air=X_air*P_total./(X_air+0.622);
P_air_sat=exp(43.494-6545.8/(T_air+4.85))/(T_air+594.85)^2;
RH_air=P_air/P_air_sat;

figure
plot (t/3600, RH_air*100,'k.')
title('RH air vs. Time')
xlabel('Time [hrs]')
ylabel('RH - Air [%]')
% RH Exp data import
opts = spreadsheetImportOptions("NumVariables", 2);

% Specify sheet and range
opts.Sheet = "Sheet1";
opts.DataRange = "B2:C3725";

% Specify column names and types
opts.VariableNames = ["TimeHrs", "RH"];
opts.VariableTypes = ["double", "double"];

% Import the data
RH_Exp = readmatrix("C:\Users\mmathew\OneDrive - Massey
University\Merit\Research\Models\AFD ODE Model\Model - thesis chapter\AFD
ICE\AFD ICE Matlab\AFD ICE Exp
VII_27_07_22_12_00_PM_to_10_08_22_09_20_AM_RH_I.xlsx", opts, "UseExcel",
false);

figure
```

```
plot (RH_Exp(:,1), RH_Exp(:,2),'b-*')
hold on
plot (t/3600, RH_air*100,'m.-')
title('RH air vs. Time')
legend('exp','model','Location','northeast')
xlabel('Time [hrs]')
ylabel('RH air [%]')

P_ice=exp(43.494-6545.8./(T_ice+4.85))./(T_ice+594.85).^2;
X_ice=0.018*P_ice/0.029./(P_total-P_ice);
figure
plot (t/3600, X_ice,'k.')
title('Moisture content near Ice(dry) vs. Time')
xlabel('Time [hrs]')
ylabel('Moisture Content [kg/kg]')

xlim([0 340])
ylim([0.0013 0.00135])
```

```
function dD_dt= AFD_ODES(t,D)
% function for odes for Atmospheric freeze drying - Ice Sublimation

global     T_air %     Temperature of air (     K     )
global     A_ice %     Area of Ice  (     m2    )
global     M_silicagel %     Mass of Silica gel (dry) (     kg    )
global     r_silicagel %     Average radius of silicagel    (     m
     )
global     V_ice_i     %     Volume of ice      (     m3    )
global     V_box %     Volume of air in box     (     m3    )
global     rho_ice     %     density of ice     (     kg/m3 )
global     l_ice_air_i %     Initial boundary layer thickness for ice
     (     m     )
global     P_total     %     Total system pressure    (     Pa    )
global     u_air %     Air velocity (     m/s   )
global     T_silicagel %     Temperature of silica gel      (     K
     )


M_ice          =D(1);
X_silicagel    =D(2);
T_ice          =D(3);
X_air          =D(4);


P_ice=exp(43.494-6545.8/(T_ice+4.85))/(T_ice+594.85)^2;
```

```
 X_ice=0.018*P_ice/0.029/(P_total-P_ice);
 V_ice=M_ice/rho_ice;
 if  t>=119.84*3600
     l_ice_air=0.003;
     u_air=0.23;
 else
     l_ice_air=l_ice_air_i+(V_ice_i-V_ice)/A_ice;
     u_air=0;
 end
 P_air=X_air*P_total/(X_air+0.622);
 P_air_sat=exp(43.494-6545.8/(T_air+4.85))/(T_air+594.85)^2;
 RH_air=P_air/P_air_sat;
 X_silicagel_air=0.445*RH_air;
 K_MT_silicagel=1.09*exp(-42000/8.314/T_air)+1.80*(10^-8)*(u_air)^0.5;
 D_H2O_silicagel= 5.58*10^(-8)*exp(-0.45*42000/8.314/T_silicagel);
 D_H2O_eff_silicagel=r_silicagel/15/(r_silicagel/15/D_H2O_silicagel+1/K_M
T_silicagel);
 D_H2O_air=1.735*(10^-9)*T_air^1.685;
 rho_air=0.0034848*(101325-0.003796*RH_air*1.7526*(10^11)*exp(-
5315.76/T_air))/T_air;

 dD_dt=zeros(4,1); % start the matlab from here
 dD_dt(1)=-D_H2O_air*A_ice*(X_ice - X_air)*rho_air/l_ice_air;
 dD_dt(2)=(M_silicagel*15*D_H2O_eff_silicagel*(X_silicagel_air-
X_silicagel)/r_silicagel^2)/M_silicagel;
 dD_dt(3)=0;
 % (for non constant ice temp) dD_dt(3)=(2*A_ice*h_air*(T_air-T_ice)-
(lamb_sub-T_ice*Cp_ice)*D_H2O_air*A_ice*(X_ice-
X_air)*rho_air/l_ice_air)/M_ice/Cp_ice;
 dD_dt(4)=(D_H2O_air*A_ice*(X_ice-X_air)*rho_air/l_ice_air-
M_silicagel*15*D_H2O_eff_silicagel*(X_silicagel_air-
X_silicagel)/r_silicagel^2)/V_box/rho_air;

 end
```

V. MATLAB codes -AFD Hops – Case II

The sample MATLAB codes for the model of the AFD of hops is given here.

```
 %Script to solve AFD Hops ODES
 clc;
 clf;
 clearvars;
 tic
 global     T_hops%     Temperature of hops      (     K     )
```

```
global     T_air %     Temperature of air (     K     )
global     T_silicagel %     Temperature of silica gel      (     K
     )
global     M_silicagel %     Mass of Silica gel (dry) (     kg    )
global     r_silicagel %     Average radius of silica gel   (     m
     )
global     d_ice_i     %     Initial diameter of ice crystal(     m
     )
global     V_box %     Volume of air in box     (     m3    )
global     rho_ice     %     density of ice     (     kg/m3 )
global     l_hops_air  %     Boundary layer thickness for hops     (
     m     )
global     l_hops_inter%     Average intercellular path length     (
     m     )
global     P_total     %     Total system pressure    (     Pa    )
global     u_air %     Air velocity (     m/s   )
global     M_hops_dry  %     Mass of hops dry (dry)   (     kg    )
global     RF_1  %     Resistance factor for resistance in cell    (
          )
global     RF_2  %     Resistance factor for resistance in
intercellular region     (           )
global     N_ice %     Number of Ice crystals   (           )

% System Input
T_air              =    261.15;     %     Temperature of air (     K
     )
T_hops             =    T_air ;     %     Temperature of hops      (
     K     )
T_silicagel          = T_air ;     %     Temperature of silica gel
     (     K     )
M_silicagel          = 0.2   ;     %     Mass of Silica gel (dry) (
     kg    )
r_silicagel          = 0.002 ;     %     Average radius of silica gel
     (     m     )
l_box              =    0.48  ;     %     Length of box      (     m
     )
b_box              =    0.28  ;     %     width of box (     m     )
z_box              =    0.25  ;     %     height of box      (     m
     )
V_box              =    l_box*b_box*z_box  ;     %     Volume of air in
box   (     m3    )
rho_ice            =    918.207     ;     %     density of ice     (
     kg/m3 )
l_hops_air     = 0.0058;     %     Boundary layer thickness for hops
     (     m     )
l_hops_inter     =     0.00005     ;     %     Average intercellular
path length (     m     )
P_total            =    101325;     %     Total system pressure    (
     Pa    )
```

```
u_air              =    0      ;      %      Air velocity (      m/s    )
M_hops_dry      = 0.0010641    ;      %      Mass of hops dry (dry)    (
     kg    )
RF_2          =    170000;      %      Resistance factor for resistance in
intercellular region     (            )
RF_1          =    1190000      ;      %      Resistance factor for
resistance in cell(            )
rho_hops_dry      =      1486.868     ;      %      Density of dry hops
     (      kg/m3 )
d_cell             =    0.0000107    ;      %      Average diameter of a
cell  (      m      )
V_cell             =    3.14*(d_cell^3)/6  ;      %      Volume of a cell
     (      m3     )

P_air_sat=exp(43.494-6545.8/(T_air+4.85))/(T_air+594.85)^2;
RH_air_i=0.018;
P_air_i=RH_air_i*P_air_sat;

% Initial conditions
X_hops_i        = 4.2393;      %      Initial Moisture content in hops
(dry) (      kg/kg )
X_silicagel_i     =      0.445*RH_air_i     ;      %      Initial moisture
content Silica gel (dry) (      kg/kg )
X_air_i            =    0.018*P_air_i/0.029./(P_total-P_air_i);      %
     Initial moisture content in air (dry) (      kg/kg )

M_ice_i            =    X_hops_i*M_hops_dry      ;      %      Initial
mass of ice in hops      (      kg     )
V_ice_i            =    M_ice_i/rho_ice    ;      %      Volume of ice
     (      m3     )
V_hops             =    M_ice_i/rho_ice + M_hops_dry/rho_hops_dry   ;
     %      Volume of hops      (      m3     )
N_ice              =    V_hops/V_cell      ;      %      Number of Ice
crystals    (            )
d_ice_i            =    (6*V_ice_i/N_ice/3.14)^(1/3)    ;      %
     Initial diameter of ice crystal(      m      )


ICs=[X_hops_i X_silicagel_i X_air_i];

% Solving the ODEs
options=odeset('RelTol',1e-5);
[t,Ds]=ode45(@AFD_ODES,0:60:700*3600, ICs,options);
X_hops          =Ds(:,1);
X_silicagel     =Ds(:,2);
X_air           =Ds(:,3);

%subplot(4,1,1)
plot(t/3600,X_hops,'k.')
```

```
title('Moisture content in hops vs. Time')
xlabel('Time [hrs]')
ylabel('Moisture content [kg/kg]')

M_hops= M_hops_dry*(1+X_hops);

%subplot(4,1,2)
plot(t/3600,M_hops*1000,'k.')
title('Mass of hops vs. Time')
xlabel('Time [hrs]')
ylabel('Mass of hops [g]')
%subplot(4,1,3)
plot(t/3600,X_silicagel,'c.')
title('Moisture content in Silica gel(dry) vs. Time')
xlabel('Time [hrs]')
ylabel('Moisture Content [kg/kg]')
%subplot(4,1,4)
plot(t/3600,X_air,'c.')
title('Moisture content in air (dry) vs. Time')
xlabel('Time [hrs]')
ylabel('Moisture Content [kg/kg]')

% Experiment data Import
opts = delimitedTextImportOptions("NumVariables", 3);
% Specify range and delimiter
opts.DataLines = [2, Inf];
opts.Delimiter = ",";
% Specify column names and types
opts.VariableNames = ["Var1", "Time", "Weight"];
opts.SelectedVariableNames = ["Time", "Weight"];
opts.VariableTypes = ["string", "double", "double"];
% Specify file level properties
opts.ExtraColumnsRule = "ignore";
opts.EmptyLineRule = "read";
% Specify variable properties
opts = setvaropts(opts, "Var1", "WhitespaceRule", "preserve");
opts = setvaropts(opts, "Var1", "EmptyFieldRule", "auto");
% Import the data
M_product_exp = readmatrix("R_Trial_hops_Exp VII_1_hrs.txt", opts);

figure
plot (M_product_exp(:,1)/24, M_product_exp(:,2),'b-*')
hold on
plot (t/3600/24, M_hops*1000,'m.-')
title('AFD Hops weight vs. Time')
legend('exp','model','Location','northeast')
xlabel('Time [Days]')
ylabel('Weight of hops [g]')
```

```
xlim([0 23])
ylim([0 6])

P_air=X_air*P_total./(X_air+0.622);
P_air_sat=exp(43.494-6545.8/(T_air+4.85))/(T_air+594.85)^2;
RH_air=P_air/P_air_sat;

figure
plot (t/3600, RH_air*100,'k.')
title('RH air vs. Time')
xlabel('Time [hrs]')
ylabel('RH - Air [%]')

% RH Exp data import
opts = spreadsheetImportOptions("NumVariables", 2);

% Specify sheet and range
opts.Sheet = "Sheet1";
opts.DataRange = "B2:C6620";

% Specify column names and types
opts.VariableNames = ["TimeHrs", "RH"];
opts.VariableTypes = ["double", "double"];

% Import the data
RH_Exp = readmatrix("AFD Hops Exp
VII_02_07_22_05_12_PM_to_25_07_22_04_59_PM_RH_I.xlsx", opts, "UseExcel",
false);

figure
plot (RH_Exp(:,1)/24, RH_Exp(:,2),'b-*')
hold on
plot (t/3600/24, RH_air*100,'m.-')
title('RH air vs. Time')
legend('exp','model','Location','northeast')
xlabel('Time [Days]')
ylabel('RH air [%]')
xlim([0 23])

P_ice=exp(43.494-6545.8./(T_hops+4.85))./(T_hops+594.85).^2;
X_ice=0.018*P_ice/0.029./(P_total-P_ice);
figure
plot (t/3600, X_ice,'k.')
title('Moisture content near Ice(dry) vs. Time')
xlabel('Time [hrs]')
ylabel('Moisture Content [kg/kg]')

xlim([0 560])
toc
```

```
function dD_dt= AFD_ODES(t,D)
% function for odes for Atmospheric freeze drying - AFD Hops

global     T_hops%     Temperature of hops      (     K     )
global     T_air %     Temperature of air (     K     )
global     T_silicagel %     Temperature of silica gel      (     K
     )
global     M_silicagel %     Mass of Silica gel (dry) (     kg    )
global     r_silicagel %     Average radius of silica gel   (     m
     )
global     d_ice_i     %     Initial diameter of ice crystal(     m
     )
global     V_box %     Volume of air in box     (     m3    )
global     rho_ice     %     density of ice     (     kg/m3 )
global     l_hops_air  %     Boundary layer thickness for hops    (
     m     )
global     l_hops_inter%     Average intercellular path length    (
     m     )
global     P_total     %     Total system pressure    (     Pa    )
global     u_air %     Air velocity (     m/s    )
global     M_hops_dry  %     Mass of hops dry (dry)   (     kg    )
global     RF_1  %     Resistance factor for resistance in cell    (
           )
global     RF_2  %     Resistance factor for resistance in
intercellular region     (           )
global     N_ice %     Number of Ice crystals   (           )

X_hops          =D(1);
X_silicagel     =D(2);
X_air           =D(3);


P_ice=exp(43.494-6545.8/(T_hops+4.85))/(T_hops+594.85)^2;
X_ice=0.018*P_ice/0.029/(P_total-P_ice);
M_ice=X_hops*M_hops_dry;
V_ice=M_ice/rho_ice;
d_ice=(6*V_ice/N_ice/3.14)^(1/3);
A_ice=N_ice*3.14*d_ice^2;
l_hops_cell=d_ice_i-d_ice;
P_air=X_air*P_total/(X_air+0.622);
P_air_sat=exp(43.494-6545.8/(T_air+4.85))/(T_air+594.85)^2;
RH_air=P_air/P_air_sat;
X_silicagel_air=0.445*RH_air;
K_MT_silicagel=1.09*exp(-42000/8.314/T_air)+1.80*(10^-6)*(u_air)^0.5;
D_H2O_silicagel= 5.58*10^(-8)*exp(-0.45*42000/8.314/T_silicagel);
D_H2O_eff_silicagel=r_silicagel/15/(r_silicagel/15/D_H2O_silicagel+1/K_M
T_silicagel);
```

```
 D_H2O_air=1.735*(10^-9)*T_air^1.685;
 rho_air=0.0034848*(101325-0.003796*RH_air*1.7526*(10^11)*exp(-
5315.76/T_air))/T_air;

 dD_dt=zeros(3,1); % start the matlab from here
 dD_dt(1)=-A_ice*(X_ice-
X_air)*rho_air/(l_hops_air/D_H2O_air+RF_2*l_hops_inter/D_H2O_air+RF_1*l_h
ops_cell/D_H2O_air)/M_hops_dry;
 dD_dt(2)=(M_silicagel*15*D_H2O_eff_silicagel*(X_silicagel_air-
X_silicagel)/r_silicagel^2)/M_silicagel;
 dD_dt(3)=(A_ice*(X_ice-
X_air)*rho_air/(l_hops_air/D_H2O_air+RF_2*l_hops_inter/D_H2O_air+RF_1*l_h
ops_cell/D_H2O_air)-M_silicagel*15*D_H2O_eff_silicagel*(X_silicagel_air-
X_silicagel)/r_silicagel^2)/V_box/rho_air;

 end
```